REDUCED GABA SIGNALING DURING ZEBRAFISH BRAIN DEVELOPMENT INCREASES NEURAL ACTIVITY, DECREASES THE EXCITATORY-TO-INHIBITORY CELL RATIO, AND ALTERS VISUALLY EVOKED BEHAVIOR

by

CARLY ROSE DUFFY

(Under the Direction of James D Lauderdale)

ABSTRACT

Gama-aminobutyric acid (GABA) is the key inhibitory transmitter in the central nervous system of adults. It has a crucial role in maintaining the proper balance of excitation to inhibition and is therefore key in the regulation of brain development and neural circuitry. GABA is formed by the decarboxylation of glutamate by the enzyme glutamic acid decarboxylase (GAD). In humans, GAD has two isoforms, GAD65 and GAD67, which arise from Gad2 and Gad1, respectively. Issues with GAD1 have been associated with multiple neurological disorders, such as epilepsy, schizophrenia, and autism spectrum disorder (ASD). While the exact mechanisms behind the cause of these neurological disorders are not well known, it is believed that mutations in a GAD gene would lead to decreased GABA signaling, which in turn would alter the excitatory to inhibitory balance. Disruptions in this balance are thought to cause dysregulation of synaptic pruning resulting in decreased circuitry refinement. However, studying the effects of decreased GABA levels throughout development has been challenging due to a lack of viable GAD mutants in most model organisms, particularly mice. In zebrafish, a genome duplication event gave rise to paralogs of GAD, *gad1a* and *gad1b*. Our lab was able to generate CRISPR

mutants of *gad1a* null larvae and *gad1b* null larvae that are viable. Characterization of these animals has identified the *gad1b* mutants as candidates for studying the effects chronic decreased GABA signaling has on brain development, particularly on neural circuitry refinement and sensory processing by using light sheet calcium imaging, light sheet volumetric imaging, and an optomotor response behavioral assay. Through these studies, evidence of altered neural circuitry, a decreased excitatory-to-inhibitory cell ratio in a subset of cells essential for visual processing, and impairments in visual processing have been elucidated.

INDEX WORDS: GABA, GAD, OMR, synaptic pruning, excitatory to inhibitory balance balance, visual processing, calcium imaging, lightsheet imaging,

REDUCED GABA SIGNALING DURING ZEBRAFISH BRAIN DEVELOPMENT INCREASES NEURAL ACTIVITY, DECREASES THE EXCITATORY-TO-INHIBITORY CELL RATIO, AND ALTERS VISUALLY EVOKED BEHAVIOR

by

CARLY ROSE DUFFY

BS, Middle Tennessee State University, 2014

A Dissertation Submitted to the Graduate Faculty of The University of Georgia in Partial Fulfillment of the Requirements for the Degree

DOCTOR OF PHILOSOPHY

ATHENS, GEORGIA

2023

REDUCED GABA SIGNALING DURING ZEBRAFISH BRAIN DEVELOPMENT INCREASES NEURAL ACTIVITY, DECREASES THE EXCITATORY-TO-INHIBITORY CELL RATIO, AND ALTERS VISUALLY EVOKED BEHAVIOR

by

CARLY ROSE DUFFY

Major Professor:	James D. Lauderdale
Committee:	Scott Dougan
	Karl Lechtreck
	Doug Menke
	Cordula Schulz

Electronic Version Approved:

Ron Walcott
Vice Provost for Graduate Education and Dean of the Graduate School
The University of Georgia
December 2023

DEDICATION

I dedicate this body of work to my family. Firstly, to my parents, Terrence Duffy and Claudia Duffy, who have always been my greatest supporters, without whom I never would have finished my studies. They were always there to offer reassurance during my toughest and lowest points of my graduate career, and they have been invaluable as I stayed with them while I finished writing. Secondly, to my sister, Julianne Duffy, who never fails to let me know how proud she is of me for all that I've accomplished. Thirdly, to my nephews, Cole McDonald and Ryland Eidson, who I believe I've convinced to think, even if just a little bit, that being a scientist is the coolest. Fourthly, to my beloved cats, Vulcan and Andoria, who I believe deserve an honorary PhD for the time they've spent sitting with me (or trying to sit directly on my keyboard) while I work. They were always there to welcome me home after long hours in the lab with gleeful excitement, and they've kept me company through hours of writing and reading at home.

And lastly, I dedicate this work to those I love who are no longer here with me. Those I lost during my time in graduate school, my Opa, Raymond Whitworth, my grandma, Shirley Duffy, my grandpa, Jim Duffy, and my aunt, Sandra Vines, and those I lost prior, my Oma, Angela Whitworth, and my brother, Luke Duffy. I miss them all terribly and wish so much they were all still here to see me reach this milestone. Particularly to my brother, who I believe is in heaven watching over me. I know he would be so proud.

ACKNOWLEDGEMENTS

I first wish to acknowledge my advisor, Dr. Jim Lauderdale. He has been an excellent mentor, and he has taught me an abundance about the brain, zebrafish, designing experiments, and critically analyzing my results. Secondly, I wish to thank my committee members Dr. Scott Dougan, Dr. Karl Lechtreck, Dr. Doug Menke, and Dr. Cordula Schulz who have been able to provide excellent advice to keep my project on track.

Next, I wish to acknowledge my lab mates and collaborators. I thank my lab mates, Dr. Heike Kroger, Christina Sabin, Sneha Mohan, and Rida Osman, who were always able to offer me advice on my work in the lab. I also thank my collaborators, Peter Kner and his students, Yang Liu and Bingxi Liu, for all their help in light sheet imaging, as well as, Delia Shelton, who was invaluable in teaching me the skills for running the behavioral assays for these studies.

I also wish to acknowledge the assistance of the Biomedical Microscopy Core at the University of Georgia with imaging using the Zeiss LSM 710 confocal microscope, Zeiss LSM 880, and the IMARIS software workstation.

TABLE OF CONTENTS

LIST OF TABLES

Page

LIST OF FIGURES

Page

CHAPTER 1

INTRODUCTION AND LITERATURE REVIEW

Purpose of this Study

Maintaining the fine balance of excitation to inhibition (E/I) is crucial for the brain to form proper neural circuitry. Various neurological disorders are associated with an interrupted balance of excitation and inhibition such as altered seizure disorders, autism spectrum disorder, and schizophrenia (Ademuwagun et al., 2021; Arevian et al., 2008; Beck & Hallett, 2011; Blatt & Fatemi, 2011; Coghlan et al., 2012; Hortopan et al., 2010; Kaila et al., 2014; Lynex et al., 2004; Solimena et al., 1990; Wu & Sun, 2015). In this study, I aim to use zebrafish as a model to study the effects of decreased inhibition on brain development and resulting neural processing issues.

Significance

Studying the developmental effects of an interrupted balance of excitation to inhibition has been challenging due to the lack of viable null mutants. In mice, these types of studies rely upon knockdowns or conditional knockouts (Duan et al., 2020; Kash et al., 1997). Zebrafish make a great model for studying developmental defects caused by an interrupted E/I balance since their paralogs of genes are often viable (Brenet et al., 2019; Grone et al., 2017). Our lab has a null *gad1b* zebrafish that leads to decreased γ-amino butyric acid (GABA) levels, causing decreased inhibition, and consequently increased neural excitability. We use this model to study how neural propagation, neural circuitry, and sensory processing have been affected.

Expected Results

We expect to see an increase in neural activity with a change in the pattern of spontaneous neural events in the *gad1b* mutant larvae due to their impaired ability to inhibit neural signals and, therefore, an inability to maintain clear paths of neural signaling. We also predict that because these fish developed with an interrupted E/I balance, there will be alterations in their numbers of soma accompanying unrefined neural circuitry resulting from dysregulated synaptic pruning. Lastly, we expect these larvae will have visually evoked behavioral deficits due to their lowered ability of neural inhibition.

Roles of GABA in the brain

γ-amino butyric acid (GABA) is one of the main inhibitory neurotransmitters in the adult central nervous system, and it has a crucial role in regulating brain function by inhibiting neuronal activity (Martin & Rimvall, 1993; Tillakaratne et al., 1995). GABA is formed by the α-decarboxylation of L-glutamate by glutamic acid decarboxylase (GAD) (Erlander et al., 1991; Roberts & Frankel, 1950, 1951a, 1951b). As GABA functions in neural signaling, most of the protein resides at the synaptic terminals where it is packaged into synaptic vessels and released into the synaptic left as an action potential arrives. It can then bind to one of three receptors on the post-synaptic cell: GABA-$_A$, GABA-$_B$, or GABA-$_C$. GABA-$_A$ and GABA-$_B$ are the two main receptors of these three receptors (Bowery, 1989; Enz et al., 1996). The $GABA_A$ receptor is a ligand-gated ion channel. When GABA binds to the receptor, the channel opens which allows Cl^- to enter the postsynaptic neuron, causing hyperpolarization of the membrane which inhibits signaling, therefore reducing its excitability (Enz et al., 1996). $GABA_B$ receptors are G protein-coupled metabotropic receptors. They also function in inhibiting neuronal excitability but in two different ways. They can either open a G-protein gated inwardly rectifying K^+ (GIRK) channel

leading to K^+ outflux, or they can shut a Voltage-gated Ca_2^+ channel (VGCC), stopping the influx of Ca_2^+ (Bowery, 1989; Enz et al., 1996).

Interestingly, GABA is also found in the cell body which is suggestive that GABA has roles besides neurotransmission such as metabolism (Martin & Rimvall, 1993; Tillakaratne et al., 1995). It is believed to be involved in the Tricarboxylic Acid (TCA) cycle that involves a GABA shunt pathway, where GABA is broken down and used for metabolism (Hassel et al., 1998).

Along with playing a role in neural inhibition and metabolism, GABA signaling is also involved in neuronal proliferation, synaptogenesis, and cell migration (Cobos et al., 2007; Le et al., 2017; Schmidt et al., 2013). In early development, GABA acts as an excitatory neurotransmitter, therefore, it causes depolarization instead of hyperpolarization, which can stimulate the proliferation of neural precursor cells (Yehezkel Ben-Ari et al., 2007; Cherubini et al., 1991; Wu & Sun, 2015). This is due to the high levels of chloride ions in young neurons (Rivera et al., 1999; Yamada et al., 2004). Therefore, in early development when these GABAergic progenitor cells release GABA, promoting excitation, proliferation is stimulated in neighboring cells. As the CNS matures, GABAergic signaling switches from excitatory to inhibitory as intracellular Cl^- levels decrease, leading to the hyperpolarizing effects of GABA. After this switch, GABA primarily functions to dampen neuronal activity and maintain network stability (Ganguly et al., 2001; Zhang et al., 2010). GABA signaling has been implicated in the migration of neural stem cells in the brain during early development. GABA receptors have been found on migrating neuroblasts, and activation of those neurons can affect the migration of those cells.

GAD genes

In humans and most vertebrates, there are two GAD genes, GAD 1 and GAD2, which likely arose from an ancestral GAD gene that duplicated early in the vertebrate lineage, before the divergence of teleost and cartilaginous fish (Bosma et al., 1999; Erlander et al., 1991). GAD1 and GAD2 code for the proteins GAD67 and GAD65 respectively(Erlander et al., 1991; Feldblum et al., 1993; Legay et al., 1986).

GAD 67, named after its molecular weight of 67kdaltons, is found at the synapses, throughout the cell body, and in the dendrites (Bosma et al., 1999; Erlander et al., 1991; Kaufman et al., 1991). Meanwhile, GAD65, also named after its molecular weight, is found only at the synapses (Bosma et al., 1999; Erlander et al., 1991) which could suggest that there is a slightly different function of each enzyme. Possibly, GAD67 could have a role in generating the GABA which is used for cell metabolism.

Zebrafish and other teleost fish experienced a whole genome duplication event that gave rise to the paralogous, many of which remained functional (Bosma et al., 1999). Understanding the roles of the two paralogs in the zebrafish has been an area of interest as it appears *gad1a* and *gad1b* may have slightly different functions due to their differing expression patterns (VanLeuven, 2018).

During early development, *gad2* and *gad1b* transcripts are expressed in the ventral spinal cord close to the floor plate in neurons that are likely Kolmer-Agduhr (KA) or Ventral Longitudinal Descending (VeLD) neurons (VanLeuven, 2018). Meanwhile, *gad1a* transcripts are expressed in some of those same ventral spinal neurons expressing *gad1b* and *gad2*, but also in dorsal spinal neurons, which are possibly Dorsal Longitudinal Ascending (DoLA) and Commissural Secondary Ascending (CoSA) neurons. (Bernhardt et al., 1992; VanLeuven, 2018)

As development progresses to 3dpf, all three *gad* genes are still expressed in the zebrafish brain. *gad1b* and *gad2* have similar expression patterns at this stage and are primarily coexpressed in the forebrain, midbrain, and hindbrain. *gad1a* however shows a different pattern of expression (VanLeuven, 2018). The exact coexpression of the three *gad* genes at later developmental ages has yet to be elucidated as fluorescent labeling with a more sensitive detection method, such as HCR, is required.

In mice, the mutation in the *Gad1* gene causes a severe cleft palate and is neonatal lethal, which makes it challenging to study the effects of mutations in this gene on development and health (Asada et al., 1997; Condie et al., 1997; Kakizaki et al., 2015). Therefore, current studies of decreased GABA signaling due to issues with GAD in mice rely upon conditional knockouts. Thus, the paralogs of *gad1a* and *gad1b* mentioned earlier make zebrafish a unique model as *gad1b* null mutants and *gad1a* null mutants are viable (VanLeuven, 2018).

Since GABA works primarily to inhibit neurons, it leaves the brain in an easily excitable state when GABA signaling is interrupted which can lead to spontaneous activity and seizures. Some epileptic conditions can be linked to a deficiency in GABA levels or an interruption in GABA signaling (Abreu et al., 2020). Due to the role of GAD in regulating GABA, any issue in it's expression could lead to similar issues. In fact, in humans, issues such as schizophrenia, epilepsy, and anxiety have been found to be associated with mutations in the GAD1 genes (Cotter et al., 2017; Egerton et al., 2017; Fatemi et al., 2005; Gonzalez-Burgos et al., 2011; Lynex et al., 2004; Magri et al., 2018). GAD2 has not been as well studied as GAD1, but it is thought that issues with this enzyme could also be related to neurological disorders as well (Pan, 2012).

Regulation of GABAergic precursor production by DLX TFs

The cluster of the Distal-less homeobox (DLX) transcription factor (TF) gene family consists of 6 DLX genes, all of which are involved in embryonic development (Le et al., 2017; MacDonald et al., 2010; Mendes et al., 2020; Zerucha et al., 2000). Particularly, these TFs are involved in the development of certain tissues, one of which is the nervous system. DLX3/4/5/6 are also involved in craniofacial development and craniofacial structure formation. The DLX TFs help specify GABAergic neurons as they regulate genes for proteins involved in GABA signaling such as GAD and GABA receptors (Le et al., 2017; MacDonald et al., 2010). This regulation makes the DLX-expressing interneurons another key player in maintaining the excitatory inhibitory balance, which is essential for normal brain functioning. Therefore, mutations in the *dlx* genes can cause neurodevelopmental conditions.

In zebrafish, *dlx5a* expression begins early at 1-4 somite stage in the forebrain, and it remains on even into adulthood (Mendes et al., 2020; Thisse & Thisse, 2005). At early developmental ages, *dlx5a* can be detected in the optic tectum, however, at later developmental stages it is no longer detected(Thisse & Thisse, 2005). The reporter transgene, Tg(*1.4dlx5a-dlx6a:GFP*) consists of the genomic region containing *dlx5a* and *dlx6a* (Zerucha et al., 2000). This transgene is sparsely expressed and remains on in the optic tectum, making it great for imaging experiments studying GABAergic precursors in the optic tectum.

Interrupting the excitatory-inhibitory balance and regulation of synaptic pruning

During early development, there is a high level of neuroplasticity, meaning the brain can form new connections between neurons rapidly (Ganguly & Poo, 2013; L. M. Nevin et al., 2008). There is rapid synaptogenesis leaving an overabundance of excitatory and inhibitory

neurons, mny of which are not needed and are later eliminated through synaptic pruning. The pruning process is crucial for the finetuning of neural circuits, and the process is selective on which synapses are eliminated (Ganguly & Poo, 2013). This is determined by the activation and contribution of the neuron to efficient neural communication. Neurons that are frequently activated are kept, while neurons that are not are labeled for elimination. This idea is referred to as "use it or lose it."

If the balance of excitatory to inhibitory is affected, this can alter the pruning process, leading to inaccurate circuits and synapses (Chechik et al., 1998; Jill, 2020). Deviations in the E/I balance, and dysregulation of synaptic pruning are implicated in various neurological disorders (Y. Ben-Ari, 2014; Duan et al., 2020; Hortopan et al., 2010; Le et al., 2017; Sohal & Rubenstein, 2019; Zhao et al., 2022; Zhubi et al., 2017). One such is autism spectrum disorder (ASD). The cause of ASD is still unknown, but an interrupted E/I balance through development is one assumed cause (Coghlan et al., 2012; Dakin & Frith, 2005; Horder et al., 2018; Pensado-López et al., 2020; Sohal & Rubenstein, 2019; Zaidel et al., 2015; Zhao et al., 2022).

Methods of studying the effects of an altered E/I balance are still limited but recent technologies have been helpful in revealing the lasting effects of this developmental issue. Due to the nature of multiple paralogs, zebrafish make a good model for studying altered E/I balance and its effect on the developing brain. In fact, zebrafish is emerging as a model to study ASD (Rea & Raay, 2020; Tayanloo-Beik et al., 2022).

The optic tectum

The optic tectum (TeO) is a structure found in the midbrain of vertebrate animals (DeMarco et al., 2020; L. M. Nevin et al., 2008; Pietri et al., 2017). It plays a crucial role in

processing visual information and coordinating eye and head movements, therefore helping them to make rapid and coordinated responses to the visual stimuli in their environment. The optic tectum is particularly well-developed in animals that rely heavily on vision for their survival, such as birds, reptiles, fish, and certain mammals. In humans, the optic tectum is equivalent to the superior colliculus. It plays a role in visual processing though it is not as complex or as prominent as the optic tectum. The optic tectum provides a great canvas for studying neural circuitry as it is very well studied, easily imaged, and functionally significant to visual processing (Baraban et al., 2005; Bene et al., 2010; L. Nevin et al., 2010; L. M. Nevin et al., 2008)

The neuropil of the optic tectum is primarily composed of layers of dendritic projections and some cell bodies. The dendritic layers are classified into 6 different layers (Förster et al., 2020; Scott & Baier, 2009): The stratum Marginal (SM), the stratum Opticum (SO), the Stratum Fibroseum et Griseum Superficiale (SFGS), the Stratum Album Central (SAC), and the Stratum Griseum Centrale (SGC) The SM is the outermost layer, adjacent to the neuropil surface. It contains many axons from retinal ganglion cells and other sources, which provide visual input to the tectum. The SO is situated just below the SM and consists of processes from retinal ganglion cells. It serves as the initial site of visual input processing. SFGS is a layer deeper than SO and contains neurons, dendrites, and axons that are involved in the processing of visual information and the integration of sensory inputs. The SAC is a central white matter layer containing axons that project to and from various brain regions, helping to transmit information to and from the optic tectum. The SGC is an important layer for multisensory integration and sensorimotor processing. It receives input from various sensory modalities, including vision and audition, and plays a role in generating appropriate motor responses. The optic tectum also consists of a cell

body layer. This is called the Stratum Album Periventricular (SPV). It contains axons and processes involved in various aspects of tectal function, including motor control and feedback processing (Förster et al., 2020; L. Nevin et al., 2010; Robles et al., 2011; Scott & Baier, 2009).

Interneurons act as intermediaries between sensory and motor neurons and maintain network coordination meaning they play a role in critical coordination and synchronization (Bene et al., 2010; DeMarco et al., 2020; Lucas & Clem, 2017; Tremblay et al., 2016). Interneurons are also involved in feedback and feedforward processing. Feedback inhibition involves providing inhibitory signals to neurons that are part of the same circuit, helping control the timing and strength of neural signals, and feedforward inhibition involves inhibiting neurons in anticipation of an impending excitation to maintain a balance in neural activity (Ferrante et al., 2009; Kee et al., 2015). Therefore, in sensory processing, interneurons can filter or modulate sensory input (DeMarco et al., 2020).

In zebrafish, superficial interneurons (SINs) are found in the outer layer of the neuropil of the optic tectum (Barker et al., 2017, 2021). They are found within the SO and communicate with synapses of the SFGS, which are composed of dendrites of interneurons from the SPV. SINs have inhibitory and excitatory functions as some are GABAergic and others or glutamatergic. While they can receive input from many regions in the brain, their processing is local due to their short dendrites. They receive sensory input and therefore have an important role in cognition and motor control based on the sensory information perceived (Barker et al., 2017, 2021).

Pyramidal neurons (PYRN) are crucial for integrating and processing information from multiple sources (DeMarco et al., 2020, 2021). They receive input from other neurons, including sensory input and input from other brain regions, and they integrate this information to generate output signals. Pyramidal neurons are highly plastic, meaning their synaptic connections can

change in response to experience and learning (DeMarco et al., 2021). This synaptic plasticity is a key in adaptation to changing environments (Ganguly & Poo, 2013; L. M. Nevin et al., 2008)

OMR and visually processing behavioral responses

The optomotor response is a reflexive movement found in many flying and swimming animals such as insects, birds, and fish (Huang & Neuhauss, 2008; Masseck & Hoffmann, 2009). It is a way for animals to stabilize their receptive field when there is a perceived motion in the environment around them (Matsuda & Kubo, 2021; Thompson et al., 2016). This perceived motion is known as optic flow which they experience as they are displaced in the environment, either due to their own self-movement or in the case of fish, the movement of the environment around them (Roeser & Baier, 2003). Optic flow has been found to be processed through the optic tectum, and it leads to consistent eye and body movement. The movement of the eye in response to optic flow is known as the optokinetic response (Huang & Neuhauss, 2008).

The optomotor response assay is a well-established assay that tests the behavior of animals, and their ability to perceive the visual stimulus. Therefore, it can be used to measure visual acuity and visual processing in animals. It has been a popular assay for forward genetics screening to identify mutants with visual deficits, and it is also often used to study the effects of drugs or toxins in the environment (Muto et al., 2005; Naumann et al., 2016; Neuhauss et al., 1999). In zebrafish, the optomotor response can be performed on adults and larvae (Matsuda & Kubo, 2021; Muto et al., 2005; Rinner et al., 2005). In adults, the fish are placed individually in a container with a pining drum with black and white markings (Roeser & Baier, 2003). Their eyes will follow the motion of the markings in one direction and then snap back to their initial position. Larvae will be placed in a horizontal container with a display beneath them showing

one directional moving bars. The fish will swim in the same direction as the moving bars (Roeser & Baier, 2003).

The OMR is initially perceived at the retina, where the signal is processed through DSRGs (Direction Selective Ganglion Cells) are direction-specific and have a strong response depending on the direction of motion. This is fundamental for having the proper OMR. (Matsuda & Kubo, 2021). DSGCs are in direct communication with amacrine cells as they receive information from them. Their axons form arborization fields, which are numbered 1-10 currently. AF5 is believed to be the arborization field that is involved in OKR and the OMR (Baier & Wullimann, 2021; Matsuda & Kubo, 2021). The AF5 innervates the optic tectum, likely at the SFGS layer. However, this signal is not required for the OMR as other studies have shown that larvae can still have an OMR response even after tectal ablation (Roeser & Baier, 2003). The AF5 also innervates the pretectum, which is part of the diencephalon and is found ventral to the optic tectum (Baier & Wullimann, 2021; Matsuda & Kubo, 2021). The pretectum is where the OMR response is processed, as well as the OKR response. The signal is integrated at the pretectum and sent to the cerebellum, which controls motor coordination, and the nucleus of the medial longitudinal fasciculus (nMLF) and reticulospinal neurons which both regulate OMR swimming (Matsuda & Kubo, 2021)

Amacrine cells are a type of interneuron in the retinas making them intermediate neurons between photoreceptors and ganglion cells (Lagnado, 1998; Marshak, 2016; L. M. Nevin et al., 2008). They are also GABAergic, therefore, they can inhibit or dampen the signal from neighboring cells, which helps shape the receptive fields of ganglion cells, allowing for more complex and selective responses to visual stimuli. (Lagnado, 1998; Marshak, 2016; L. M. Nevin et al., 2008). They help create a complex network of neural circuits in the retina, and they help

process visual information by combining multiple photoreceptor cell signals and modulating the strength and timing of the signals they send to the ganglion cells. They are essential to certain aspects of visual processing, particularly in contrast enhancement and motion detection.(Almeida et al., 2014; Förster et al., 2020; Robles et al., 2014). With all their roles and their communication with ganglion cells, they would be an integral part of an OMR.

As mentioned earlier, the OMR assay is popular for use in forward genetic screens (Muto et al., 2005; Naumann et al., 2016; Neuhauss et al., 1999; Severi et al., 2014). It has not been used as widely in reverse genetics for the characterization of sensory processing in genetic mutants. By modulating the activity of various retinal neurons, GABAergic signaling helps enhance contrast, sharpen visual acuity, and contribute to other aspects of visual perception. Dysregulation of GABAergic signaling in the retina can lead to visual disorders and impairments (Arevian et al., 2008; Connaughton et al., 2008; L. M. Nevin et al., 2008; Niell & Smith, 2005; Rinner et al., 2005; Zhang et al., 2010). GABA signaling plays an important role in sensory processing, including visual perception and so we should be able to use the OMR assay to test for deficits in visual processing in the zebrafish mutants that could be due to lowered GABA signaling.

References

Abreu, M. S. de, Genario, R., Giacomini, A. C. V. V., Demin, K. A., Lakstygal, A. M., Amstislavskaya, T. G., Fontana, B. D., Parker, M. O. & Kalueff, A. V. (2020). Zebrafish as a Model of Neurodevelopmental Disorders. *Neuroscience*, *445*, 3–11. https://doi.org/10.1016/j.neuroscience.2019.08.034

Ademuwagun, I. A., Rotimi, S. O., Syrbe, S., Ajamma, Y. U. & Adebiyi, E. (2021). Voltage Gated Sodium Channel Genes in Epilepsy: Mutations, Functional Studies, and Treatment Dimensions. *Frontiers in Neurology*, *12*, 600050. https://doi.org/10.3389/fneur.2021.600050

Almeida, A. D., Boije, H., Chow, R. W., He, J., Tham, J., Suzuki, S. C. & Harris, W. A. (2014). Spectrum of Fates: a new approach to the study of the developing zebrafish retina. *Development*, *141*(14), 2912–2912. https://doi.org/10.1242/dev.114108

Arevian, A. C., Kapoor, V. & Urban, N. N. (2008). Activity-dependent gating of lateral inhibition in the mouse olfactory bulb. *Nature Neuroscience*, *11*(1), 80–87. https://doi.org/10.1038/nn2030

Asada, H., Kawamura, Y., Maruyama, K., Kume, H., Ding, R.-G., Kanbara, N., Kuzume, H., Sanbo, M., Yagi, T. & Obata, K. (1997). Cleft palate and decreased brain γ-aminobutyric acid in mice lacking the 67-kDa isoform of glutamic acid decarboxylase. *Proceedings of the National Academy of Sciences*, *94*(12), 6496–6499. https://doi.org/10.1073/pnas.94.12.6496

Baier, H. & Wullimann, M. F. (2021). Anatomy and function of retinorecipient arborization fields in zebrafish. *Journal of Comparative Neurology*, *529*(15), 3454–3476. https://doi.org/10.1002/cne.25204

Baraban, S. C., Taylor, M. R., Castro, P. A. & Baier, H. (2005). Pentylenetetrazole induced changes in zebrafish behavior, neural activity and c-fos expression. *Neuroscience*, *131*(3), 759–768. https://doi.org/10.1016/j.neuroscience.2004.11.031

Barker, A. J., Helmbrecht, T. O., Grob, A. A. & Baier, H. (2017). Detection of whole-field luminance changes by superficial interneurons in the zebrafish tectum. *BioRxiv*, 178970. https://doi.org/10.1101/178970

Barker, A. J., Helmbrecht, T. O., Grob, A. A. & Baier, H. (2021). Functional, molecular and morphological heterogeneity of superficial interneurons in the larval zebrafish tectum. *Journal of Comparative Neurology*, *529*(9), 2159–2175. https://doi.org/10.1002/cne.25082

Beck, S. & Hallett, M. (2011). Surround inhibition in the motor system. *Experimental Brain Research*, *210*(2), 165–172. https://doi.org/10.1007/s00221-011-2610-6

Ben-Ari, Y. (2014). The GABA excitatory/inhibitory developmental sequence: A personal journey. *Neuroscience*, *279*, 187–219. https://doi.org/10.1016/j.neuroscience.2014.08.001

Ben-Ari, Yehezkel, Gaiarsa, J.-L., Tyzio, R. & Khazipov, R. (2007). GABA: A Pioneer Transmitter That Excites Immature Neurons and Generates Primitive Oscillations. *Physiological Reviews*, *87*(4), 1215–1284. https://doi.org/10.1152/physrev.00017.2006

Bene, F. D., Wyart, C., Robles, E., Tran, A., Looger, L., Scott, E. K., Isacoff, E. Y. & Baier, H. (2010). Filtering of Visual Information in the Tectum by an Identified Neural Circuit. *Science*, *330*(6004), 669–673. https://doi.org/10.1126/science.1192949

Bernhardt, R. P., Patel, C. K., Wilson, S. W. & Kuwada, J. Y. (1992). Axonal Trajectories and Distribution of GABAergic Spinal Neurons in Wildtype and Mutant Zebrafish LackingFloor Plate Cells. *The Journal of Comparative Neurology*.

Blatt, G. J. & Fatemi, S. H. (2011). Alterations in GABAergic Biomarkers in the Autism Brain: Research Findings and Clinical Implications. *The Anatomical Record*, *294*(10), 1646–1652. https://doi.org/10.1002/ar.21252

Bosma, P. T., Blázquez, M., Collins, M. A., Bishop, J. D., Drouin, G., Priede, I. G., Docherty, K. & Trudeau, V. L. (1999). Multiplicity of glutamic acid decarboxylases (GAD) in vertebrates: molecular phylogeny and evidence for a new GAD paralog. *Molecular Biology and Evolution*, *16*(3), 397–404. https://doi.org/10.1093/oxfordjournals.molbev.a026120

Bowery, N. (1989). GABAB receptors and their significance in mammalian pharmacology. *Trends in Pharmacological Sciences*, *10*(10), 401–407. https://doi.org/10.1016/0165-6147(89)90188-0

Brenet, A., Hassan-Abdi, R., Somkhit, J., Yanicostas, C. & Soussi-Yanicostas, N. (2019). Defective excitatory/inhibitory synaptic balance and increased neuron apoptosis in a zebrafish model of Dravet syndrome. *BioRxiv*, 781393. https://doi.org/10.1101/781393

Chechik, G., Meilijson, I. & Ruppin, E. (1998). Synaptic Pruning in Development: A Computational Account. *Neural Computation*, *10*(7), 1759–1777. https://doi.org/10.1162/089976698300017124

Cherubini, E., Gaiarsa, J. L. & Ben-Ari, Y. (1991). GABA: an excitatory transmitter in early postnatal life. *Trends in Neurosciences*, *14*(12), 515–519. https://doi.org/10.1016/0166-2236(91)90003-d

Cobos, I., Borello, U. & Rubenstein, J. L. R. (2007). Dlx Transcription Factors Promote Migration through Repression of Axon and Dendrite Growth. *Neuron*, *54*(6), 873–888. https://doi.org/10.1016/j.neuron.2007.05.024

Coghlan, S., Horder, J., Inkster, B., Mendez, M. A., Murphy, D. G. & Nutt, D. J. (2012). GABA system dysfunction in autism and related disorders: From synapse to symptoms. *Neuroscience & Biobehavioral Reviews*, *36*(9), 2044–2055. https://doi.org/10.1016/j.neubiorev.2012.07.005

Condie, B. G., Bain, G., Gottlieb, D. I. & Capecchi, M. R. (1997). Cleft palate in mice with a targeted mutation in the γ-aminobutyric acid-producing enzyme glutamic acid decarboxylase 67. *Proceedings of the National Academy of Sciences*, *94*(21), 11451–11455. https://doi.org/10.1073/pnas.94.21.11451

Connaughton, V. P., Nelson, R. & Bender, A. M. (2008). Electrophysiological evidence of GABAA and GABAC receptors on zebrafish retinal bipolar cells. *Visual Neuroscience*, *25*(2), 139–153. https://doi.org/10.1017/s0952523808080322

Cotter, D., Kelso, A. & Neligan, A. (2017). Genetic biomarkers of posttraumatic epilepsy: A systematic review. *Seizure*, *46*, 53–58. https://doi.org/10.1016/j.seizure.2017.02.002

Dakin, S. & Frith, U. (2005). Vagaries of Visual Perception in Autism. *Neuron*, *48*(3), 497–507. https://doi.org/10.1016/j.neuron.2005.10.018

DeMarco, E., Tesmer, A. L., Hech, B., Kawakami, K. & Robles, E. (2021). Pyramidal Neurons of the Zebrafish Tectum Receive Highly Convergent Input From Torus Longitudinalis. *Frontiers in Neuroanatomy*, *15*, 636683. https://doi.org/10.3389/fnana.2021.636683

DeMarco, E., Xu, N., Baier, H. & Robles, E. (2020). Neuron types in the zebrafish optic tectum labeled by an id2b transgene. *Journal of Comparative Neurology*, *528*(7), 1173–1188. https://doi.org/10.1002/cne.24815

Duan, Z. R. S., Che, A., Chu, P., Modol, L., Bollmann, Y., Babij, R., Fetcho, R. N., Otsuka, T., Fuccillo, M. V., Liston, C., Pisapia, D. J., Cossart, R. & García, N. V. D. M. (2020). GABAergic Restriction of Network Dynamics Regulates Interneuron Survival in the Developing Cortex. *Neuron*, *105*(1), 75-92.e5. https://doi.org/10.1016/j.neuron.2019.10.008

Egerton, A., Modinos, G., Ferrera, D. & McGuire, P. (2017). Neuroimaging studies of GABA in schizophrenia: a systematic review with meta-analysis. *Translational Psychiatry*, *7*(6), e1147–e1147. https://doi.org/10.1038/tp.2017.124

Enz, R., Brandstätter, J. H., Wässle, H. & Bormann, J. (1996). Immunocytochemical Localization of the GABACReceptor ρ Subunits in the Mammalian Retina. *The Journal of Neuroscience*, *16*(14), 4479–4490. https://doi.org/10.1523/jneurosci.16-14-04479.1996

Erlander, M. G., Tillakaratne, N. J. K., Feldblum, S., Patel, N. & Tobin, A. J. (1991). Two genes encode distinct glutamate decarboxylases. *Neuron*, *7*(1), 91–100. https://doi.org/10.1016/0896-6273(91)90077-d

Fatemi, S. H., Fatemi, S. H., Stary, J. M., Earle, J. A., Araghi-Niknam, M. & Eagan, E. (2005). GABAergic dysfunction in schizophrenia and mood disorders as reflected by decreased levels of glutamic acid decarboxylase 65 and 67 kDa and Reelin proteins in cerebellum. *Schizophrenia Research*, *72*(2–3), 109–122. https://doi.org/10.1016/j.schres.2004.02.017

Feldblum, S., Erlander, M. G. & Tobin, A. J. (1993). Different distributions of GAD65 and GAD67 mRNAS suggest that the two glutamate decarboxylases play distinctive functional roles. *Journal of Neuroscience Research*, *34*(6), 689–706. https://doi.org/10.1002/jnr.490340612

Ferrante, M., Migliore, M. & Ascoli, G. A. (2009). Feed-forward inhibition as a buffer of the neuronal input-output relation. *Proceedings of the National Academy of Sciences*, *106*(42), 18004–18009. https://doi.org/10.1073/pnas.0904784106

Förster, D., Helmbrecht, T. O., Mearns, D. S., Jordan, L., Mokayes, N. & Baier, H. (2020). Retinotectal circuitry of larval zebrafish is adapted to detection and pursuit of prey. *ELife*, *9*, e58596. https://doi.org/10.7554/elife.58596

Ganguly, K. & Poo, M. (2013). Activity-Dependent Neural Plasticity from Bench to Bedside. *Neuron*, *80*(3), 729–741. https://doi.org/10.1016/j.neuron.2013.10.028

Ganguly, K., Schinder, A. F., Wong, S. T. & Poo, M. (2001). GABA Itself Promotes the Developmental Switch of Neuronal GABAergic Responses from Excitation to Inhibition. *Cell*, *105*(4), 521–532. https://doi.org/10.1016/s0092-8674(01)00341-5

Gonzalez-Burgos, G., Fish, K. N. & Lewis, D. A. (2011). GABA Neuron Alterations, Cortical Circuit Dysfunction and Cognitive Deficits in Schizophrenia. *Neural Plasticity*, *2011*, 723184. https://doi.org/10.1155/2011/723184

Grone, B. P., Qu, T. & Baraban, S. C. (2017). Behavioral Comorbidities and Drug Treatments in a Zebrafish scn1lab Model of Dravet Syndrome. *ENeuro*, *4*(4), ENEURO.0066-17.2017. https://doi.org/10.1523/eneuro.0066-17.2017

Hassel, B., Johannessen, C. U., Sonnewald, U. & Fonnum, F. (1998). Quantification of the GABA Shunt and the Importance of the GABA Shunt Versus the 2-Oxoglutarate Dehydrogenase Pathway in GABAergic Neurons. *Journal of Neurochemistry*, *71*(4), 1511–1518. https://doi.org/10.1046/j.1471-4159.1998.71041511.x

Horder, J., Petrinovic, M. M., Mendez, M. A., Bruns, A., Takumi, T., Spooren, W., Barker, G. J., Künnecke, B. & Murphy, D. G. (2018). Glutamate and GABA in autism spectrum disorder—a translational magnetic resonance spectroscopy study in man and rodent models. *Translational Psychiatry*, *8*(1), 106. https://doi.org/10.1038/s41398-018-0155-1

Hortopan, G. A., Dinday, M. T. & Baraban, S. C. (2010). Spontaneous Seizures and Altered Gene Expression in GABA Signaling Pathways in a mind bomb Mutant Zebrafish. *The Journal of Neuroscience*, *30*(41), 13718–13728. https://doi.org/10.1523/jneurosci.1887-10.2010

Huang, Y.-Y. & Neuhauss, S. C. F. (2008). The optokinetic response in zebrafish and its applications. *Frontiers in Bioscience*.

Jill, S. (2020). Core Concept: How synaptic pruning shapes neural wiring during development and, possibly, in disease. *Proceedings of the National Academy of Sciences*, *117*(28), 16096. https://doi.org/10.1073/pnas.2010281117

Kaila, K., Ruusuvuori, E., Seja, P., Voipio, J. & Puskarjov, M. (2014). GABA actions and ionic plasticity in epilepsy. *Current Opinion in Neurobiology*, *26*, 34–41. https://doi.org/10.1016/j.conb.2013.11.004

Kakizaki, T., Oriuchi, N. & Yanagawa, Y. (2015). GAD65/GAD67 double knockout mice exhibit intermediate severity in both cleft palate and omphalocele compared with GAD67 knockout and VGAT knockout mice. *Neuroscience*, *288*, 86–93. https://doi.org/10.1016/j.neuroscience.2014.12.030

Kash, S. F., Johnson, R. S., Tecott, L. H., Noebels, J. L., Mayfield, R. D., Hanahan, D. & Baekkeskov, S. (1997). Epilepsy in mice deficient in the 65-kDa isoform of glutamic acid decarboxylase. *Proceedings of the National Academy of Sciences*, *94*(25), 14060–14065. https://doi.org/10.1073/pnas.94.25.14060

Kaufman, D. L., Houser, C. R. & Tobin, A. J. (1991). Two Forms of the γ-Aminobutyric Acid Synthetic Enzyme Glutamate Decarboxylase Have Distinct Intraneuronal Distributions and Cofactor Interactions. *Journal of Neurochemistry*, *56*(2), 720–723. https://doi.org/10.1111/j.1471-4159.1991.tb08211.x

Kee, T., Sanda, P., Gupta, N., Stopfer, M. & Bazhenov, M. (2015). Feed-Forward versus Feedback Inhibition in a Basic Olfactory Circuit. *PLoS Computational Biology*, *11*(10), e1004531. https://doi.org/10.1371/journal.pcbi.1004531

Lagnado, L. (1998). Retinal processing: Amacrine cells keep it short and sweet. *Current Biology*, *8*(17), R598–R600. https://doi.org/10.1016/s0960-9822(98)70385-9

Le, T. N., Zhou, Q.-P., Cobos, I., Zhang, S., Zagozewski, J., Japoni, S., Vriend, J., Parkinson, T., Du, G., Rubenstein, J. L. & Eisenstat, D. D. (2017). GABAergic Interneuron Differentiation in the Basal Forebrain Is Mediated through Direct Regulation of Glutamic Acid Decarboxylase Isoforms by Dlx Homeobox Transcription Factors. *Journal of Neuroscience*, *37*(36), 8816–8829. https://doi.org/10.1523/jneurosci.2125-16.2017

Legay, F., Pelhate, S. & Tappaz, M. L. (1986). Phylogenesis of Brain Glutamic Acid Decarboxylase from Vertebrates: Immunochemical Studies. *Journal of Neurochemistry*, *46*(5), 1478–1486. https://doi.org/10.1111/j.1471-4159.1986.tb01765.x

Lucas, E. K. & Clem, R. L. (2017). GABAergic interneurons: The orchestra or the conductor in fear learning and memory? *Brain Research Bulletin*, *141*, 13–19. https://doi.org/10.1016/j.brainresbull.2017.11.016

Lynex, C. N., Carr, I. M., Leek, J. P., Achuthan, R., Mitchell, S., Maher, E. R., Woods, C. G., Bonthon, D. T. & Markham, A. F. (2004). Homozygosity for a missense mutation in the 67

kDa isoform of glutamate decarboxylase in a family with autosomal recessive spastic cerebral palsy: parallels with Stiff-Person Syndrome and other movement disorders. *BMC Neurology*, *4*(1), 20. https://doi.org/10.1186/1471-2377-4-20

MacDonald, R. B., Debiais-Thibaud, M., Talbot, J. C. & Ekker, M. (2010). The relationship between dlx and gad1 expression indicates highly conserved genetic pathways in the zebrafish forebrain. *Developmental Dynamics*, *239*(8), 2298–2306. https://doi.org/10.1002/dvdy.22365

Magri, C., Giacopuzzi, E., Via, L. L., Bonini, D., Ravasio, V., Elhussiny, M. E. A., Orizio, F., Gangemi, F., Valsecchi, P., Bresciani, R., Barbon, A., Vita, A. & Gennarelli, M. (2018). A novel homozygous mutation in GAD1 gene described in a schizophrenic patient impairs activity and dimerization of GAD67 enzyme. *Scientific Reports*, *8*(1), 15470. https://doi.org/10.1038/s41598-018-33924-8

Marshak, D. W. (2016). A tale of two neurotransmitters. *Visual Neuroscience*, *33*, E017. https://doi.org/10.1017/s0952523816000146

Martin, D. L. & Rimvall, K. (1993). Regulation of γ-Aminobutyric Acid Synthesis in the Brain. *Journal of Neurochemistry*, *60*(2), 395–407. https://doi.org/10.1111/j.1471-4159.1993.tb03165.x

Masseck, O. A. & Hoffmann, K. (2009). Comparative Neurobiology of the Optokinetic Reflex. *Annals of the New York Academy of Sciences*, *1164*(1), 430–439. https://doi.org/10.1111/j.1749-6632.2009.03854.x

Matsuda, K. & Kubo, F. (2021). Circuit Organization Underlying Optic Flow Processing in Zebrafish. *Frontiers in Neural Circuits*, *15*, 709048. https://doi.org/10.3389/fncir.2021.709048

Mendes, H. W., Taktek, M., Duret, T. & Ekker, M. (2020). Expression of dlx genes in the normal and regenerating brain of adult zebrafish. *PLoS ONE*, *15*(6), e0229549. https://doi.org/10.1371/journal.pone.0229549

Muto, A., Orger, M. B., Wehman, A. M., Smear, M. C., Kay, J. N., Page-McCaw, P. S., Gahtan, E., Xiao, T., Nevin, L. M., Gosse, N. J., Staub, W., Finger-Baier, K. & Baier, H. (2005). Forward Genetic Analysis of Visual Behavior in Zebrafish. *PLoS Genetics*, *1*(5), e66. https://doi.org/10.1371/journal.pgen.0010066

Naumann, E. A., Fitzgerald, J. E., Dunn, T. W., Rihel, J., Sompolinsky, H. & Engert, F. (2016). From Whole-Brain Data to Functional Circuit Models: The Zebrafish Optomotor Response. *Cell*, *167*(4), 947-960.e20. https://doi.org/10.1016/j.cell.2016.10.019

Neuhauss, S. C. F., Biehlmaier, O., Seeliger, M. W., Das, T., Kohler, K., Harris, W. A. & Baier, H. (1999). Genetic Disorders of Vision Revealed by a Behavioral Screen of 400 Essential

Loci in Zebrafish. *The Journal of Neuroscience*, *19*(19), 8603–8615. https://doi.org/10.1523/jneurosci.19-19-08603.1999

Nevin, L. M., Taylor, M. R. & Baier, H. (2008). Hardwiring of fine synaptic layers in the zebrafish visual pathway. *Neural Development*, *3*(1), 36. https://doi.org/10.1186/1749-8104-3-36

Nevin, L., Robles, E., Baier, H. & Scott, E. K. (2010). Focusing on optic tectum circuitry through the lens of genetics. *BMC Biology*.

Niell, C. M. & Smith, S. J. (2005). Functional Imaging Reveals Rapid Development of Visual Response Properties in the Zebrafish Tectum. *Neuron*, *45*(6), 941–951. https://doi.org/10.1016/j.neuron.2005.01.047

Pan, Z. Z. (2012). Transcriptional control of Gad2. *Transcription*, *3*(2), 68–72. https://doi.org/10.4161/trns.19511

Pensado-López, A., Veiga-Rúa, S., Carracedo, Á., Allegue, C. & Sánchez, L. (2020). Experimental Models to Study Autism Spectrum Disorders: hiPSCs, Rodents and Zebrafish. *Genes*, *11*(11), 1376. https://doi.org/10.3390/genes11111376

Pietri, T., Romano, S. A., Pérez-Schuster, V., Boulanger-Weill, J., Candat, V. & Sumbre, G. (2017). The Emergence of the Spatial Structure of Tectal Spontaneous Activity Is Independent of Visual Inputs. *Cell Reports*, *19*(5), 939–948. https://doi.org/10.1016/j.celrep.2017.04.015

Rea, V. & Raay, T. J. V. (2020). Using Zebrafish to Model Autism Spectrum Disorder: A Comparison of ASD Risk Genes Between Zebrafish and Their Mammalian Counterparts. *Frontiers in Molecular Neuroscience*, *13*, 575575. https://doi.org/10.3389/fnmol.2020.575575

Rinner, O., Rick, J. M. & Neuhauss, S. C. F. (2005). Contrast Sensitivity, Spatial and Temporal Tuning of the Larval Zebrafish Optokinetic Response. *Investigative Opthalmology & Visual Science*, *46*(1), 137. https://doi.org/10.1167/iovs.04-0682

Rivera, C., Voipio, J., Payne, J. A., Ruusuvuori, E., Lahtinen, H., Lamsa, K., Pirvola, U., Saarma, M. & Kaila, K. (1999). The K+/Cl− co-transporter KCC2 renders GABA hyperpolarizing during neuronal maturation. *Nature*, *397*(6716), 251–255. https://doi.org/10.1038/16697

Roberts, E. & Frankel, S. (1950). γ-AMINOBUTYRIC ACID IN BRAIN: ITS FORMATION FROM GLUTAMIC ACID. *Journal of Biological Chemistry*, *187*(1), 55–63. https://doi.org/10.1016/s0021-9258(19)50929-2

Roberts, Eugene. & Frankel, Sam. (1951a). FURTHER STUDIES OF GLUTAMIC ACID DECARBOXYLASE IN BRAIN. *Journal of Biological Chemistry*, *190*(2), 505–512. https://doi.org/10.1016/s0021-9258(18)55998-6

Roberts, Eugene. & Frankel, Sam. (1951b). GLUTAMIC ACID DECARBOXYLASE IN BRAIN. *Journal of Biological Chemistry*, *188*(2), 789–795. https://doi.org/10.1016/s0021-9258(19)77753-9

Robles, E., Laurell, E. & Baier, H. (2014). The Retinal Projectome Reveals Brain-Area-Specific Visual Representations Generated by Ganglion Cell Diversity. *Current Biology*, *24*(18), 2085–2096. https://doi.org/10.1016/j.cub.2014.07.080

Robles, E., Smith, S. J. & Baier, H. (2011). Characterization of Genetically Targeted Neuron Types in the Zebrafish Optic Tectum. *Frontiers in Neural Circuits*, *5*, 1. https://doi.org/10.3389/fncir.2011.00001

Roeser, T. & Baier, H. (2003). Visuomotor Behaviors in Larval Zebrafish after GFP-Guided Laser Ablation of the Optic Tectum. *The Journal of Neuroscience*, *23*(9), 3726–3734. https://doi.org/10.1523/jneurosci.23-09-03726.2003

Schmidt, R., Strähle, U. & Scholpp, S. (2013). Neurogenesis in zebrafish – from embryo to adult. *Neural Development*, *8*(1), 3. https://doi.org/10.1186/1749-8104-8-3

Scott, E. K. & Baier, H. (2009). The Cellular Architecture of the Larval Zebrafish Tectum, as Revealed by Gal4 Enhancer Trap Lines. *Frontiers in Neural Circuits*, *3*, 13. https://doi.org/10.3389/neuro.04.013.2009

Severi, K. E., Portugues, R., Marques, J. C., O'Malley, D. M., Orger, M. B. & Engert, F. (2014). Neural Control and Modulation of Swimming Speed in the Larval Zebrafish. *Neuron*, *83*(3), 692–707. https://doi.org/10.1016/j.neuron.2014.06.032

Sohal, V. S. & Rubenstein, J. L. R. (2019). Excitation-inhibition balance as a framework for investigating mechanisms in neuropsychiatric disorders. *Molecular Psychiatry*, *24*(9), 1248–1257. https://doi.org/10.1038/s41380-019-0426-0

Solimena, M., Folli, F., Aparisi, R., Pozza, G. & Camilli, P. (1990). Autoantibodies to GABA-ergic Neurons and Pancreatic Beta Cells in Stiff-Man Syndrome. *The New England Journal of Medicine*.

Tayanloo-Beik, A., Hamidpour, S. K., Abedi, M., Shojaei, H., Tavirani, M. R., Namazi, N., Larijani, B. & Arjmand, B. (2022). Zebrafish Modeling of Autism Spectrum Disorders, Current Status and Future Prospective. *Frontiers in Psychiatry*, *13*, 911770. https://doi.org/10.3389/fpsyt.2022.911770

Thisse, C. & Thisse, B. (2005). *High Throughput Expression Analysis of ZF-Models Consortium Clones. ZFIN Direct Data Submission*. http://zfin.org

Thompson, A. W., Vanwalleghem, G. C., Heap, L. A. & Scott, E. K. (2016). Functional Profiles of Visual-, Auditory-, and Water Flow-Responsive Neurons in the Zebrafish Tectum. *Current Biology*, *26*(6), 743–754. https://doi.org/10.1016/j.cub.2016.01.041

Tillakaratne, N. J. K., Medina-Kauwe, L. & Gibson, K. M. (1995). Gamma-aminobutyric acid (GABA) metabolism in mammalian neural and nonneural tissues. *Comparative Biochemistry and Physiology Part A: Physiology*, *112*(2), 247–263. https://doi.org/10.1016/0300-9629(95)00099-2

Tremblay, R., Lee, S. & Rudy, B. (2016). GABAergic Interneurons in the Neocortex: From Cellular Properties to Circuits. *Neuron*, *91*(2), 260–292. https://doi.org/10.1016/j.neuron.2016.06.033

VanLeuven, A. J. (2018). *UNDERSTANDING THE ROLE OF THE GAD GENES IN NEURAL DEVELOPMENT AND NERVOUS SYSTEM FUNCTION IN ZEBRAFISH*.

Wu, C. & Sun, D. (2015). GABA receptors in brain development, function, and injury. *Metabolic Brain Disease*, *30*(2), 367–379. https://doi.org/10.1007/s11011-014-9560-1

Yamada, J., Okabe, A., Toyoda, H., Kilb, W., Luhmann, H. J. & Fukuda, A. (2004). Cl− uptake promoting depolarizing GABA actions in immature rat neocortical neurones is mediated by NKCC1. *The Journal of Physiology*, *557*(3), 829–841. https://doi.org/10.1113/jphysiol.2004.062471

Zaidel, A., Goin-Kochel, R. P. & Angelaki, D. E. (2015). Self-motion perception in autism is compromised by visual noise but integrated optimally across multiple senses. *Proceedings of the National Academy of Sciences*, *112*(20), 6461–6466. https://doi.org/10.1073/pnas.1506582112

Zerucha, T., Stühmer, T., Hatch, G., Park, B. K., Long, Q., Yu, G., Gambarotta, A., Schultz, J. R., Rubenstein, J. L. R. & Ekker, M. (2000). A Highly Conserved Enhancer in the Dlx5/Dlx6Intergenic Region is the Site of Cross-Regulatory Interactions betweenDlx Genes in the Embryonic Forebrain. *The Journal of Neuroscience*, *20*(2), 709–721. https://doi.org/10.1523/jneurosci.20-02-00709.2000

Zhang, R., Wei, H., Xia, Y. & Du, J. (2010). Development of light response and GABAergic excitation-to-inhibition switch in zebrafish retinal ganglion cells. *The Journal of Physiology*, *588*(14), 2557–2569. https://doi.org/10.1113/jphysiol.2010.187088

Zhao, H., Mao, X., Zhu, C., Zou, X., Peng, F., Yang, W., Li, B., Li, G., Ge, T. & Cui, R. (2022). GABAergic System Dysfunction in Autism Spectrum Disorders. *Frontiers in Cell and Developmental Biology*, *9*, 781327. https://doi.org/10.3389/fcell.2021.781327

Zhubi, A., Chen, Y., Guidotti, A. & Grayson, D. R. (2017). Epigenetic regulation of RELN and GAD1 in the frontal cortex (FC) of autism spectrum disorder (ASD) subjects. *International Journal of Developmental Neuroscience*, *62*(J. Psychiatr. Res. 45 11 2011), 63–72. https://doi.org/10.1016/j.ijdevneu.2017.02.003

CHAPTER 2

DECREASED GABA LEVELS DURING DEVELOPMENT RESULT IN INCREASED CONNECTIVITY IN LARVAL ZEBRAFISH TECTUM

Yang Liu[1†], Yongkai Chen[2†], Carly R. Duffy[3†], Ariel J VanLeuven[3*], John Branson Byers[3], Hannah C. Schriever[3], Rebecca E. Ball[3], Jessica M. Carpenter[4,5], Chelsea E. Gunderson[3], Nikolay M. Filipov[4], Ping Ma[2], Peter A. Kner[1], and James D. Lauderdale[3,5], To be submitted to Molecular Neurobiology

Abstract

γ-aminobutyric acid (GABA) is an abundant neurotransmitter that plays multiple roles in the vertebrate central nervous system (CNS). In the early developing CNS, GABAergic signaling acts to depolarize cells. It mediates several aspects of neural development, including cell proliferation, neuronal migration, neurite growth, and synapse formation, as well as the development of critical periods. Later in CNS development, GABAergic signaling acts in an inhibitory manner when it becomes the predominant inhibitory neurotransmitter in the brain. This behavior switch occurs due to changes in chloride/cation transporter expression. Abnormalities of GABAergic signaling appear to underlie several human neurological conditions, including epilepsy. However, the impact of reduced GABAergic signaling on brain development has been challenging to study in mammals. Here we take advantage of zebrafish and light sheet imaging to assess the impact of reduced GABAergic signaling on the functional circuitry in the larval zebrafish optic tectum. Zebrafish have three gad genes: two *gad1* paralogs known as *gad1a* and *gad1b*, and *gad2.* The *gad1b* and *gad2* genes are expressed in the developing optic tectum. Null mutations in *gad1b* significantly reduce GABA levels in the brain and increase electrophysiological activity in the optic tectum. Fast light sheet imaging of genetically encoded calcium indicator (GCaMP)--expressing *gab1b* null larval zebrafish revealed patterns of neural activity that were different than either *gad1b*-normal larvae or *gad1b*-normal larvae acutely exposed to pentylenetetrazol (PTZ). These results demonstrate that reduced GABAergic signaling during development increases functional connectivity and concomitantly hyper-synchronization of neuronal networks.

Introduction

In the functionally mature brain, GABAergic interneurons gate information flow and mediate network dynamics in a variety of contexts, including the processing of sensory information (Yokoi et al., 1995; Isaacson and Strowbridge, 1998; Flores-Herr et al., 2001; Schoppa and Urban, 2003; Lee and Zhou, 2006; Arevian et al., 2008; Popova, 2015), motor control (Beck and Hallett, 2011), and cognition (Tepper et al., 2008; Tremblay et al., 2016; Koyama and Pujala, 2018; Swanson and Maffei, 2019). In humans, reduction in GABAergic signaling is implicated in several pathologies of the central nervous system, including altered sensory processing (Vucinic et al., 2006; Arevian et al., 2008; Puts et al., 2015), aberrant motor control (Solimena et al., 1990; Kim et al., 1994; Levy et al., 1999; Lynex et al., 2004; Beck and Hallett, 2011; Puts et al., 2015), seizure disorders (Ben-Ari, 2006; Glykys et al., 2009; Galanopoulou, 2010; de Curtis and Avoli, 2016; Wang et al., 2017), Tourette syndrome (Puts et al., 2015), autism spectrum disorder (Abrahams and Geschwind, 2008; Geschwind, 2009; Gaetz et al., 2014; Robertson et al., 2016), and schizophrenia (Wu and Sun, 2015). Despite the impact on human health, the effects of reduced GABAergic signaling on the development and function of inhibitory circuits in a live brain are poorly understood.

Genetics offers an unbiased approach to investigating neural function; however, it has been challenging to establish a model system to study the developmental and physiological effects associated with the genetic reduction of GABA synthesis. In vertebrates, GABA is synthesized from glutamic acid by the enzyme glutamic acid decarboxylase (GAD, IUBMB Enzyme Nomenclature EC 4.1.1.15) (Erlander et al., 1991). In mammals and most vertebrates, the majority of GAD protein exists as two molecularly distinct forms, known as GAD67 and GAD65, encoded by the *GAD1* and *GAD2* genes, respectively (Legay et al., 1986; Erlander and

Tobin, 1991). In humans, homozygous mutations in the *GAD1* gene are associated with seizures and hypertonia, presumably due to reduced synaptic GABA (Lynex et al., 2004; Chatron et al., 2020); however, high-resolution cellular imaging and developmental studies are not feasible in people. No mutations have been reported for the human *GAD2* gene.

Although mice are an excellent genetic model for studying mammalian neural development and function, the role of the *Gad1* gene has been difficult to study as animals homozygous null for *Gad1* die at birth due to cleft palate (Asada et al., 1997; Condie et al., 1997), likely caused by central nervous system (CNS) dysfunction (Oh et al., 2010). While transgenic and conditional workarounds have been developed to study *Gad1* gene function in the pancreas (Yoon et al., 1999), these approaches have not been widely used to perturb GABA synthesis in the brain. Recently, a conditional approach has been used to effect global knockdown of GAD67 in adult mice, which resulted in increased motor activity and impairment of acoustic startle responses as assessed by behavioral assays (Miyata et al., 2021). Mice homozygous mutant for *Gad2* are viable, maintain normal levels of GAD67 and GABA in their brains, and exhibit normal general behavior, including locomotor activity (Asada et al., 1996).

Here we use larval zebrafish homozygous null for *gad1b* and calcium imaging to assess the impact of reduced GABAergic signaling on the function of intrinsic circuits in the optic tectum of the larval zebrafish. The optic tectum of the larval zebrafish is well suited for experiments investigating the functional behavior of circuits. The zebrafish larval tectum integrates and processes visual information for export to premotor targets (Nevin et al., 2010). The tectum is accessible to electrophysiological recordings, and the entirety of the tectum can be imaged at cellular resolution for many hours in the live, intact, non-anesthetized larva (Niell and Smith, 2005; Del Bene et al., 2010; Tao et al., 2011; Gabriel et al., 2012; Nikolaou et al., 2012; Hunter

et al., 2013; Muto et al., 2013; Naumann et al., 2016; Vanwalleghem et al., 2018; Burgstaller et al., 2019; Kramer et al., 2019; Liu et al., 2019b; Forster et al., 2020; Wu et al., 2020), which permits assessment of the dynamics of large neuronal populations in response to different challenges. Owing to work by several labs over the last 30 years, including efforts to generate zebrafish brain atlases (Ronneberger et al., 2012; Randlett et al., 2015; Marquart et al., 2017; Kunst et al., 2019a), much is known about cell type diversity and functional connectivity in the zebrafish optic tectum (Nevin et al., 2010; Thompson et al., 2016; Hildebrand et al., 2017; Helmbrecht et al., 2018; Kunst et al., 2019a), which facilitates cell type identification in imaging data. Additionally, recent work has established that spontaneous activity in the optic tectum of the zebrafish larva reveals significant features of the functional connectivity of different circuits (Marachlian et al., 2018). Although the patterns of spontaneous activity are similar to those of visually evoked responses and are organized according to the tectum's retinotopic map, the formation of the basic circuits does not require visual input or intrinsic retinal activity (Niell and Smith, 2005; Ramdya and Engert, 2008; Grama and Engert, 2012; Avitan et al., 2017; Pietri et al., 2017).

Unlike mice and humans, zebrafish have three gad genes that encode glutamic acid decarboxylase. In addition to *gad2*, zebrafish have two copies of the *gad1* gene, which are *gad1a* and *gad1b* (Grone and Maruska, 2016; Lai et al., 2016; Lai et al., 2017). While it is known that *gad1b* is expressed by neurons in the larval zebrafish optic tectum (Higashijima et al., 2004; Yu et al., 2011; Barker and Baier, 2015; Forster et al., 2017), *gad1a* expression has not been assessed.

In this study, we test the hypothesis that *gad1b*-null mutations result in a localized expansion of the activity in tectal micro-circuits involving *gad1b*-expressing neurons. We imaged *gad1b*-

null mutant larvae expressing a calcium reporter with a light-sheet microscope and quantified the activity level and connectivity between different regions by measuring the correlations in activity. We then compared the connectivity to wild-type larvae and wild-type larvae treated with PTZ. We see an altered pattern of activity in the optic tectum of the *gad1b*-null mutants. Compared to wild-type larvae, the *gad1b*-null mutants show increased connectivity between regions on the same side of the brain and regions on opposite sides.

Materials and Methods

Genetic nomenclature

Specific references to genes for humans, mice and zebrafish follow gene nomenclature conventions appropriate for each organism (Mullins, 1995; Bult et al., 2019; Bruford et al., 2020). Human gene symbols are in upper-case italicized characters. Mouse gene symbols are italicized, with only the first letter in upper-case. Zebrafish gene symbols are in lower-case italicized characters. Protein symbols for human and mouse are denoted by upper-case letters not italicized. Protein symbols for zebrafish are not italicized, and the first letter is in upper-case.

Zebrafish care and maintenance

Adult and larval zebrafish (*Danio rerio*) were obtained from lines maintained in the University of Georgia Zebrafish Facility following standard procedures (Westerfield, 2007). Embryos and larvae were staged using standard staging criteria (Kimmel et al., 1995; Westerfield, 2007). Wild-type fish of the WIK strain and *nacre(mitf)*$^{w2/w2}$ were originally obtained from the Zebrafish International Research Center (ZIRC). Crystal zebrafish (*nacre*$^{w2/w2}$, *alb*$^{b4/b4}$, *roy*$^{a9/a9}$) (Antinucci and Hindges, 2016) were obtained from Dr. Hindges. Fish mutant for

scn1lab (Baraban et al., 2013; Grone et al., 2017) were obtained from Dr. Scott Baraban. Fish transgenic for TgBAC[*gad1b*: loxP-DsRed-loxP-GFP] (Satou et al., 2013) were obtained from Dr.Shin-ichi Higashijima. Fish transgenic for Tg[*elavl3:GCaMP5g*] (Ahrens et al., 2013b; Ahrens et al., 2013a) were obtained from Dr. Ahrens. All adult fish were maintained in an Aquatic Habitats (Apopka, FL) multi-rack system. Habitat water consisted of reverse osmosis filtered/sterilized water to which sodium bicarbonate and other salts (Instant Ocean, Aquarium Systems, Inc., Mentor, OH, USA) were added to maintain pH from 7.0-7.4 and conductivity between 400 and 430 μS. All experimental procedures were conducted in accordance with National Institutes of Health guidelines for use of zebrafish in research under protocols approved and overseen by the University of Georgia Institutional Animal Care and Use Committee.

Generation of zebrafish mutant for *gad1a* and *gad1b*

sgRNA design: The sequences for CRISPR target sites in the *gad1a* and *gad1b* genes were designed using the ZiFiT Targeter program website (http://zifit.partners.org/ZiFiT/ChoiceMenu.aspx) (Hwang et al., 2013a; Hwang et al., 2013b). The resultant target sequences for each gene used in this study can be found in Supplemental Table 1. These target sequences were evaluated for the probability of causing off-target effects using the ZiFiT program. These sequences were confirmed via nucleotide BLAST searches against the zebrafish genome to contain at least three or more mismatches at any other loci thereby limiting the possibility of off-target effects.

sgRNA, Cas9 and RNP construction: The sgRNA for targeting *gad1b* (*ga2303* allele) was made from a PCR-amplified template as described in (Nakayama et al., 2013) and transcribed using the MEGAshortscriptTM T7 Kit (AM1354, Thermo Fischer Scientific, Inc., Waltham,

MA) following the manufacturer protocol. The Cas9 mRNA was transcribed from an optimized expression vector as described in (Jao et al., 2013) using the mMessage mMACHINE Sp6 Kit (AM1340, Thermo Fischer Scientific, Inc., Waltham, MA) following the manufacturer protocol. Both the sgRNA and the Cas9 mRNA were purified by LiCl precipitation and re-dissolved in **DEPC-treated water.**

The *gad1a (ga2404)* allele was made using a ribonucleoprotein (RNP) complex (Burger et al., 2016). To synthesize this sgRNA, we ordered gene-specific crRNA targeting *gad1a* exon5 as well as trRNA which can be used with any crRNA. Both RNA oligonucleotides were purchased from Integrated DNA Technologies (IDT, Skokie, IL) following the online ordering protocol and upon arrival were resuspended to a concentration of 100 μM in the provided Nuclease Free Duplex Buffer. Purified Cas9 nuclease was also purchased from IDT (1074181). Immediately before performing embryonic microinjections, we made a working dilution of Cas9 nuclease in Cas9 working buffer (20 mM HEPES, 150 mM KCl, pH 7.5). The sgRNA duplex was made by combining equimolar amounts (3.4 μL each) of crRNA and trRNA plus 3.2 μL of Nuclease Free Duplex Buffer, incubating at 95°C for 5 minutes, and cooling to room temperature on the benchtop. The RNP complex is assembled by combining 1 μL each of the sgRNA duplex and the Cas9 protein dilution, 0.5 μL DEPC-treated water and 2.5 μL 0.4M KCl with phenol red and incubating at 37°C for 10 minutes.

Microinjections

sgRNA for *gad1b* exon4 plus Cas9 mRNA were co-injected into 1-2 cell stage zebrafish embryos in an approximately 1 nL solution that contained 100 ng/μL of sgRNA and 600 ng/μL of Cas9 mRNA. The RNP complex for gad1a was injected into 1-2 cell stage zebrafish embryos in

an approximately 1 nL solution such that the concentration of the sgRNA duplex is 234 pg (156 pg trRNA, 78 pg crRNA) and the concentration of the Cas9 enzyme is 736 pg. In all cases, only animals that exhibited normal development post-injection were grown to adulthood as potential F0 founders.

Identification and description of *gad1a*$^{-/-}$ and *gad1b*$^{-/-}$ mutant zebrafish

Potential founders that were injected with CRISPR-Cas9 material were crossed with wild-type fish and the F1 progeny were genotyped via PCR and PAGE analyses (VanLeuven et al., 2018). Animals that showed evidence of a mutation from this initial screening were then sequenced via Sanger sequencing to determine the nature of the mutation (Figure 2.1). (Table X for primer sequencea) Animals with the same mutation were housed together and bred to identify fish with homozygous mutations for each allele. F2 generations were sequence-verified before being established as secured homozygous mutant lines (Figure S2.1). Progeny of the F2 generation were grown to adulthood and were used for all behavioral and molecular aspects of this study.

Casper, tg(*elavl3:gcamp5G*) and *gad1b*$^{-/-}$, tg(*elavl3:gcamp5G*) generation and genotyping

nacre$^{w2/w2}$, e*lavl3*:gCaMP5G were crossed to crystal fish (*nacre*$^{w2/w2}$, *alb*$^{b4/b4}$, *roy*$^{a9/a9}$) and the progeny were grown to adults. Progeny were then in crossed to generate casper and crystal fish expressing e*lavl3*:gCaMP5G. However, crystal fish were never obtained, therefore, only casper or nacre fish were used. Crispr generated *gad1b*$^{-/-}$ fish, as previously mentioned, were crossed to *nacre*$^{w2/w2}$, tg(e*lavl3*:gCaMP5G) fish to generate *gad1b*$^{+/-}$, *elavl3*:gCaMP5G $^{tg/o}$ fish. The progenies were grown to adulthood and in-crossed to generate *gad1b*$^{-/-}$, *elavl3*:gCaMP5G

fish. In this process, it was realized that *gad1b* and *nacre* reside on the same chromosome, so no *gad1b*$^{-/-}$, *nacre*$^{w2/w2}$ fish were ever obtained. Mutants were identified by screening through PCR and PAGE as previously mentioned.

Fish rearing for calcium imaging

Larvae from a cross of Casper (*nacre*$^{w2/w2,}$ *roy*$^{a9/a9}$) fish crossed to Casper (*nacre*$^{w2/w2,}$ *roy*$^{a9/a9}$), e*lavl3*:gCaMP5G$^{tg/o}$ were used for the WT larvae and WT larvae treated with 15mM PTZ groups. For the mutants, larvae were used from a cross of *gad1b* $^{-/-}$, e*lavl3*:gCaMP5G $^{tg/o}$ larvae crossed to *gad1b* $^{-/-}$. *gad1b*$^{-/-}$ larvae were treated with 0.003% PTU in egg water starting at 18 hpf. The solution was changed once daily until 5dpf.

In Situ Hybridization probe construction

Probes were constructed for *gad1b* by PCR amplification from whole-embryo cDNA, and probes for *gad1a* and *gad2* were constructed from gBlock Gene Fragments whose sequences (Table S1) DIG-labeled riboprobes for all genes were synthesized with a DIG Labeling Kit (Roche 11175025910) per the manufacturer's protocol. Antisense probes were generated using the T7 promoter and sense probes were generated using the Sp6 promoter.

Colorimetric whole mount in situ hybridization

Whole-mount in situ hybridizations were performed as previously described on 3dpf and 5dpf WIK zebrafish treated with 0.003% PTU (Thisse and Thisse, 2008). Hybridizations were done overnight at 68°C. Color development was performed using NBT/BCIP (Roche) substrate.

Colorimetric sectioned in situ hybridization

5dpf WIK zebrafish fixed in 4%PFA were prepared for cryosection and sliced into 10 µm sections. The in situ was performed as previously described with modifications (Thisse and Thisse, 2008). An antigen retrieval step was added as described in James et al (2016). Color development was done using NBT/BCIP substrate. Color was purposefully overdeveloped in the SPV to capture signal within the SINs of the neuropil.

HCR in situ hybridization

HCR in situ hybridization is performed according to the protocol from the manufacturers at Molecular Probes (Citation). 5 dpf whole zebrafish are fixed in 4% PFA at room temperature for 2 hours, and then dehydrated in methanol to be stored at -20°C until use. On day one, the fish to be used for the experiment are transferred into a fresh 1.5 mL and rehydrated into PBS-tween. The samples are treated with 20µg/ml proteinase K for 30 minutes and then washed with PBST two times without rocking. Samples are then post-fixed with 4% PFA for 20 minutes. Samples are then washed further in PBST. Pre-hybridization of the samples is performed at 37°C for 30 minutes in 500µL of probe hybridization mixture (Molecular Probes). During this time, the probe mixture is prepared. For multiplexed HCR, probes are added into the same mixture. 2µl of a 1 µM stock is added to 500 µL of probe hybridization mixture and warmed at 37°C. After the prehybridization, the probe mixture is added to the samples and incubated at 37°C in a water bath overnight. In the morning, the probe mixture is removed, and samples go through 4 washes at 37°C in probe wash buffer (Molecular Probes). This is followed by 2 washes in 5X SSC at room temperature. Samples are prepared for amplification by incubation at room temperature in an amplification buffer (Molecular Probes). 10 µL of each hairpin is transferred into individual

tubes, heated at 95°C for 90 seconds, and then allowed to cool to room temperature for 30 minutes. All hairpin sets needed for each probe are combined into one tube along with 500μL of amplification buffer. The hairpin mixture is then added to the sample and left for amplification overnight at room temperature in a dark drawer. In the morning, a series of SSC washes are performed to remove excess hairpins. Samples are then washed into PBST and stained with 1X DAPI. Background autofluorescence is suppressed by treatment with a 10 mM CuSO4, and 50 mM Ammonium acetate solution, which will block fluorescein autofluorescence from blood cells. Samples are prepared for imaging by clearing in 70% glycerol in PBST. Fish are mounted in glycerol onto a glass microscope slide with a wall of Vaseline to prevent the flattening of the fish by the coverslip. See Supplemental Table 2 for probe and hairpin sets. A Zeiss LSM880 was used to image at 20X and 40X using a lambda scan to capture the multiple wavelengths.

HPLC-ECD sample preparation

Adult and 7 dpf larval zebrafish were anesthetized in 0.4% Tricaine-S (MS 222; tricaine; pH 7.4) (Westerfield, 1993) and then placed on a pre-chilled metal block. For larval samples, single heads were removed, rinsed with 40 μL of Hank's Final solution (Westerfield, 1993) and then placed in a pre-weighed 1.5 mL microcentrifuge tube to record the wet mass in milligrams (mg). For adult samples, the heads were removed, and brains were dissected out with forceps and rinsed with ~40 μL of Hank's Final solution. Adult brains were briefly blotted on a piece of filter paper and then placed in a pre-weighed 1.5 mL microcentrifuge tube to record the wet mass in mg. For these preparations, we either added 200 μL of 0.2 N perchloric acid to detect catecholamine neurotransmitters or 200 μL of 18.2 Ω Milli-Q Water to detect amino acid neurotransmitters. Once the solution is added to the tube and samples are fully immersed into the

solution, the tubes are immediately frozen on dry ice and stored at -80°C until they were run in HPLC with electrochemical detection (HPLC-ECD). Samples were normalized and run as described previously (Ross and Filipov, 2006; Coban and Filipov, 2007).

High Performance Liquid Chromatography with Electrochemical Detection (HPLC-ECD)

Concentrations of brain amino acids were determined using high performance liquid chromatography with electrochemical detection (HPLC-ECD; Waters Alliance equipment e2695 and 2465, Milford, MA). Brains were removed, homogenized in 200 ml of MilliQ water, and centrifuged (13,200 x G at 4° C for 10 min) prior to sample supernatant collection. Sample supernatants were made electrochemically active with a derivatizing agent 10 min before sample injection (20 ml) into the HPLC-ECD for detection of glutamine, glutamate, and GABA (Monge-Acuña and Fornaguera-Trías, 2009). The analytes were separated on a C_{18}, 5 µm base deactivated reverse-phase column (4.6 µm × 250 mm; Xterra Shield RP18, Waters) using an isocratic flow rate of 0.5 mL/min. The mobile phase with a final pH of 4.5 (adjusted with 1 M phosphoric acid) consisted of 0.1 M monosodium phosphate and 0.5 mM EDTA with 25% methanol (v/v) water (Monge-Acuña and Fornaguera-Trías, 2009). Prior to statistical analysis, amino acid levels were normalized to tissue weight.

PTZ dose response assay

For assays with wild-type, *gad1b* $^{+/-}$, *gad1b* $^{-/-}$, gad1a$^{-/-}$, we either performed a *gad1b* $^{+/-}$ incross and post-hoc genotyped each fish from each treatment group or we crossed several zebrafish of known genotype (wild-type incross, *gad1b* $^{-/-}$ incross or *gad1b* $^{-/-}$ x wild-type). Each experimental replicate was performed on separate occasions. For assays with *gav2404* $^{+/-}$ and

gav2404 $^{-/-}$, we crossed several zebrafish of known genotype (*gad1a* $^{-/-}$ incross or *gad1a* $^{-/-}$ x wild-type) and performed the experiment on three rounds of larvae from these crosses on one day. Embryos were grown in standard egg water (Westerfield, 1993).

To perform the assay, we divided 7 dpf larvae of the desired genotype into six petri dishes each with 15-20 fish and labeled each dish corresponding to the dose that would be assayed. Larvae were allowed to acclimate for 30 min. We remove as much egg water as possible and pour 15 mL of pre-measured pentylenetetrazol (PTZ), a known $GABA_A$ receptor antagonist, diluted in standard egg water at the following concentrations into the appropriately labeled dish: 0 mM (egg water only control), 1 mM, 2.5 mM, 5 mM, 10 mM and 15 mM (positive control). Once the solution is bath applied to the dishes, we began a timer for 10 minutes and monitored all dishes for abnormal behavior as defined by stage II and stage III seizure-like behavior (Baraban et al., 2005). To control for double counting of responding fish, when we saw a fish that exhibited abnormal behavior, we removed that fish and placed it in a separate dish. At the end of 10 minutes, we counted how many fish responded with stage II or stage III behavior and how many fish did not respond at each treatment group.

Extracellular Electrophysiology

Zebrafish of the desired genotype were grown to 7 dpf and immobilized with 250 μM of α-bungarotoxin in 1X E3 media with 1 mM HEPES (Westerfield, 1993). Once paralyzed, we moved single larvae to the lid of a 35 mm non-TC-treated petri dish (Corning Inc., Tewksbury, MA) and oriented the fish laterally. Once properly positioned, we added warm, but not hot, 0.4% agarose in 1X E3 media onto the fish and let it cool for ~2 minutes. We added ~3.5 mL of 1X E3 media to the lid and then inserted a sharp glass pipet microelectrode (15-20 MΩ impedance),

loaded with 2-3 μL of normal Ringer's solution (116 mM NaCl, 2.9 mM KCl, 1.8 mM $CaCl_2$, 5.0 mM HEPES, pH 7.2) into the optic tectum (TeO). The optic tectum was chosen to facilitate comparison with previously published data obtained from larval zebrafish (Baraban et al., 2005). A chloride-coated silver wire (0.010" A-M Systems, Inc., Sequim, WA) reference electrode was placed touching the surrounding solution. Field recordings were collected using Molecular Devices' Axoclamp software and data were digitized at 10 kHz, low-pass filtered at 1 kHz, and analyzed with CLAMPEX 10.4 software (Axon Instruments, Sunnyvale, CA). We performed field recordings from each fish for 20 minutes.

Calcium imaging with light sheet microscopy

Calcium imaging was performed on a custom-built light sheet microscope (Supplemental Figure 2.2). The system is a modified version of the OpenSPIM setup (Pitrone et al., 2013), as described in our previous work (Liu et al., 2019b). The microscope is controlled through a custom-written LabVIEW program using a Dell Precision 5810 Tower with 32GB RAM and a quad-core Intel(R) Xeon(R) E5-1603 v3 processor. We followed the protocol described by Huisken lab (Kaufmann et al., 2012; Weber et al., 2014). Transgenic zebrafish larvae (*elavl3*:GCaMP5g; gad1b:RFP; mitfaw2/w2) at 5 to 7 dpf of development were immobilized using 100μM of alpha-bungarotoxin. The fish were then immersed in a 0.2% agarose solution and inserted into a 1cm cut FEP tube. The tube was then sealed with 3% agarose gel and sealed with parafilm. Each fish was imaged at approximately the same horizontal plane referenced from the dorsal surface of the tectum (Supplemental Figure 2.2) continuously for 2 to 10 minutes under the same laser power (10mW, 99.21 w/at the sample). Imaging data was collected at 33-50 frames per second (fps) for each single channel. For experiments imaging PTZ-induced neural

activity, larvae were treated with 15 mM of PTZ for 40 min before mounting for light-sheet imaging.

Image Preprocessing

To address any potential artifacts resulting from the larvae's motion during the light-sheet imaging experiments, we first applied the "subpixel image registration" procedure (Guizar-Sicairos et al., 2008). In this process, the first frame of the video was considered the target image. The subsequent frames of the video were aligned with the first frame by optimizing the cross-correlation between the registered subsequent frames and the first frame.
Afterward, we proceeded to identify and correct potential change points resulting from fluctuations in the environmental light conditions. To accomplish this, we extracted the background signal by computing the average signal from the pixels situated at the four-square corners (7.8 μm × 7.8 μm) of the images. The detection of temporal change points was achieved using the "Pelt" function from the Python package "ruptures" version 1.0.2 (Truong et al., 2020) utilizing default arguments for model fitting and setting the argument "pen" to 10 for prediction. Subsequently, for each identified temporal change point, denoted as t, we individually computed the intensity change level for each pixel. This was accomplished by calculating the difference between the median fluorescence intensity of the pixel during the time interval from $t - 2$ seconds to t and the time interval from t to $t + 2$ seconds. Then, we corrected the artifacts caused by the environmental light conditions for each pixel by subtracting the estimated intensity change level attributed to each change point. Finally, we applied K-nearest neighbor (KNN) smoothing method to denoise the signals and remove the potential outliers of the signal. The

KNN smoothing also enhance the robustness of our frameworks against the estimation error caused during the change point detection procedure. The number of neighbors is set as 7. Next, we normalized the signal of each pixel by calculating fluorescence intensity changes (ΔF/F). This normalization procedure also helped eliminate the decaying effect of the fluorescence. Whole frame average intensities were computed for each image time series. The first 100 frames (4.4 seconds) were omitted from this computation because the LSM excitation light initially activates neural activity in the larvae. Then fluorescence intensity changes (ΔF/F) were calculated using the sliding window method described (Patel et al., 2015; Liu and Baraban, 2019). This method involves finding the median value in the window interval before each data point (F_{t0}), subtracting the mean (F_{μ}) of the data points below the median from the original data point($F_{t0-\Delta t}$), then normalizing by dividing this result by the same mean value. This process is described by the following equation:

$$\Delta F/F = \frac{F_{t0} - F_{\mu}}{F_{\mu}}$$

Image Analysis

We performed a Fourier Transform on the one-dimensional fluorescence traces to get the frequency spectra. Then we calculated the absolute value of the real part of the frequency spectrum and normalized it to the maximum value of the frequency spectrum. This analysis was performed for three fish each from three different groups. One group was the fish without any chemical treatment or genetic mutation, here referred to as control. The second group was the fish which were treated with PTZ, here referred to as PTZ-treated. The third group was the genetically mutated fish, here referred to as *gad1b*$^{-/-}$ mutant (O'Connor et al., 2019).

In order to compare across the changes in neural activity within the optic tectum of the zebrafish larva, we register our image times series to the zebrafish brain atlas (Kunst et al., 2019b) The masks of regions of interests are downloaded from the brain atlas website (https://fishatlas.neuro.mpg.de/).

To determine the position of the imaged plane in 3D, we conducted a search among the atlas images, with the objective of maximizing the cross-correlation with the average image obtained from our collected video.

The brain atlas used in this process was segmented into multiple regions of interest (ROIs). Treating the average brain image from our collected video as the target image, we applied a non-rigid image registration method to align the atlas image with our average brain image. This allowed us to accurately map the positions of the ROIs in our data. The non-rigid image registration is achieved with the "Symmetric Diffeomorphic Registration" method from the python package "dipy" version 1.3.0. (Garyfallidis et al., 2014). Once the ROIs in our dataset were segmented, we proceeded to extract the signal from each ROI. This was accomplished by calculating the average intensity of the image pixels within each ROI.

Subsequently, we proceeded to explore both static and dynamic functional connectivity among the identified ROIs using the extracted signals. For static functional connectivity, we computed the Pearson correlation directly between the extracted signals from each pair of ROIs. This analysis provided insights into the overall interregional connectivity during the experiments.

To uncover the dynamic nature of the functional interactions among the ROIs, we employed a sliding-window framework, inspired by the work of (Zalesky et al., 2014; Hindriks et al., 2016). This framework allowed us to investigate the dynamic functional connectivity, capturing the variations in interregional connectivity over time. Specifically, we use a tapered

window of length 20 s. We slide the window in time at a temporal resolution of 3s over the 5-min interval and get a continuous series of snapshots of the ROIs signals. For each snapshot, we calculated a correlation matrix for the ROIs using Pearson correlation. Finally, we got a series of correlation matrices (regions × regions × windows). We considered two regions to be connected at any snapshot if the corresponding correlation was larger than 0.6. The frequency of connections between the two sides of the brain and within each side of the brain were summarized.

Experimental Design and Statistical Analysis

For the HPLC-ECD experiments with 7 dpf larval samples, we assayed 5 replicates, in this case, 5 single larval heads. For the adult samples, we used 5 male and 5 female brains to account for potential gender differences across the genotypes tested. The selection of 5 biological replicates came from discussions with HPLC experts to capture enough data for proper statistics. The results of these experiments were analyzed and plotted using GraphPad Prism (La Jolla, CA). We plotted normalized values from all replicates for each genotype with the mean and standard deviation. We performed a one-way ANOVA to test statistical significance across the groups.

For the PTZ dose-response assay, we used 15-20 7 dpf zebrafish per treatment group for each genotype tested. When we assayed a *gad1b* heterozygous incross, we randomly sorted zebrafish into pools of 20 with the assumption that ~5 fish per genotype would be in each treatment group. When we assayed crosses of known genotypes, we used 20 zebrafish per treatment group when assaying the *gad1b* allele and 15 zebrafish per treatment group when assaying the gad1a allele. The *gad1b* heterozygous incross resulted in unequal numbers of each

genotype for that experiment, thus the resulting N value is not the same across each genotype. However, each of the 10 minute assays were performed 3 times for each genotype. Taking all experiments into account, we assayed at least 42 larvae for each genotype at each PTZ treatment which provides more than sufficient biological and technical replicates for statistics. Gender is not determined in 7 dpf larvae, so we did not consider sex differences in this experiment. The results of these experiments were plotted using GraphPad Prism (La Jolla, CA). Due to unequal numbers across the genotypes, we plotted the percentages of responding fish of each genotype at each dose with standard deviation across the three trials. We performed no additional statistical analyses on these data.

For the electrophysiology experiments, we used at least ten fish per genotype or treatment group. This is the standard number of replicates used in the field to capture any natural variation that occurs across a population. The raw trace data is reported, so there were no statistical analyses performed on these data.

For the analysis of brain connectivity, five wild-type fish, nine PTZ-treated wildtype fish, seven *gad1b* mutant fish, and five PTZ-treated *gad1b* mutant fish were analyzed. Using the sliding window framework, we calculated the frequency of the functional connectivity within and between the two half sides of brains for each single run of each fish. To test whether there is any difference of the connectivity frequency between different groups, we applied the Wilcoxon rank sum test (Mann and Whitney, 1947) for each two different groups and calculated the P-values based on the corresponding Mann-Whitney U statistics.

Code Accessibility

https://github.com/Knerlab/neural-activity-analysis

Results

Zebrafish homozygous null for *gad1a* or *gad1b* exhibit reduced levels of GABA in the brain and increased neural activity.

CRISPR-Cas9 mediated genome editing was used to generate sets of indels in the *gad1a* and *gad1b* genes in zebrafish. Two indels, allele ga2404 for *gad1a* and allele ga2303 for *gad1b*, were predicted null mutations and selected for this study (Figure 2.1A). Zebrafish heterozygous for mutations in gad1a or *gad1b* were crossed to generate homozygous mutant lines. Zebrafish homozygous for $gad1a^{ga2404}$ or $gad1b^{ga2303}$ have normal gross body morphology and are viable and fertile.

Larval zebrafish harboring mutations in *gad1a* or *gad1b* are sensitive to pharmacological perturbations in GABA signaling (Figure 2.1B). Larval zebrafish of different *gad* genotypes at 7 day post fertilization (7 dpf) were exposed for 10 min to different doses of the proconvulsive compound pentylenetetrazol (PTZ), which is a non-competitive GABA antagonist and scored for the first appearance of Stage II or Stage III motor behaviors during the 10-minute exposure interval. As first described by Baraban (2005), Stage II behavior is characterized by a rapid, tight circular swim trajectory, and Stage III behavior is characterized by a loss of posture and mobility for 1-3 s. During these experiments, all larvae exhibited normal swimming behavior in the absence of PTZ and in a visually and sonically neutral environment. Larvae mutant for gad1a or gad1b were more sensitive to PTZ than were wild-type larvae (Figure 2.1B). Notably, almost half of the $gad1b^{-/-}$ larvae and about 7% of the $gad1a^{-/-}$ larvae, but none of the wild-type larvae, exhibited Stage II/III motor behavior when exposed to 1 mM PTZ. These results suggest that GABA levels are reduced in the $gad1a^{ga2404}$ and $gad1b^{ga2303}$ mutant lines, with the greater reduction associated with $gad1b^{ga2303}$.

High-performance liquid chromatography with electrochemical detection (HPLC-ECD) was used to assess the levels of GABA, glutamine, glutamate, and monoamine neurotransmitters in the brains *gad1a*^{ga2404} and *gad1b*^{ga2303}mutant zebrafish compared to wild type fish (Supplemental Tables 2-4). Levels of GABA, glutamine and glutamate were assessed separately from serotonin (5-HT), 5-Hydroxyindoleacetic acid (5-HIAA), dopamine (DA), norepinephrine (NE), and 3-Methoxy-4-hydroxyphenylglycol (MHPG) because of different requirements in sample preparation. Amino acid and monoamine neurotransmitter data for adult brains was obtained using 20 individual brains for wild-type, *gad1a*$^{-/-}$ and *gad1b*$^{-/-}$, and 10 brains for *gad1*$^{+/-}$ with equal numbers of brains for each sex. Brain samples were age and sex matched between genotypes. Brain weights ranged from 1.2 mg to 7.2 mg (mean = 4.2 mg sd = 1.3) for wild-type fish, 0.7 to 4.0 mg (mean = 2.0 mg sd=0.8) for *gad1a*$^{-/-}$ 1.1 mg to 7.4 mg (mean = 3.9 mg sd = 2.0) for *gad1b*$^{+/-}$, and 1.0 to 7.0 mg (mean = 3.5 mg sd=1.5) for *gad1b*$^{-/-}$. Decreased levels of GABA were measured in the adult brains of fish mutants for *gad1a* or *gad1b*. The average normalized concentration of GABA in adult wild-type brain was determined to be 921 ng/mg of tissue (sd = 261) compared to 678 ng/mg of tissue (sd = 256) for fish homozygous mutant for *gad1a*^{ga2304}, 743 ng/mg of tissue (sd=221) for fish heterozygous mutant for *gad1b*^{ga2303}, and 652 ng/mg of tissue (sd = 135) for fish homozygous mutant for *gad1b*^{ga2303} (Figure 2.1C). Zebrafish heterozygous for *gad1a*^{ga2404} were not tested. Male and female fish exhibited comparable levels of GABA within genotypes (data not shown). Comparable levels of glutamate, glutamine, serotonin (including 5-Hydroxyindoleacetic acid), dopamine, and norepinephrine (including 3-Methoxy-4-hydroxyphenylglycol) were measured in the adult brains of all genotypes (Figure 2.1, Figure S2.4). These data support that *gad1a*^{ga2404} and *gad1b*^{ga2303} are functional null mutations for *gad1a* and *gad1b*, respectively.

Determining neurotransmitter levels in 7 dpf larvae was more challenging because of the small amounts of tissue obtained from each animal. It was not practical to dissect out the brains; therefore, for these experiments, heads were dissected just posterior to the otocyst and anterior to the pectoral fins as these were clearly identifiable morphological features that could be easily used to guide cuts. Cuts were made at an angle to avoid the swim bladder and yolk and to try to minimize the amounts of non-neural tissues included in the sample. The average amount of tissue collected from single 7 dpf larval zebrafish heads was 0.20 mg (sd = 0.14), with no significant differences between genotypes (data not shown). HPLC-ECD analyses were performed using pools of 10 larval heads for each genotype (N = 5 pooled samples/ dataset). The average amount of tissue in each pool was 2.52 mg (sd = 0.46). Decreased GABA levels were measured for *gad1b*$^{-/-}$larvae but not *gad1a*$^{-/-}$ larvae (Figure S2.5). The average normalized concentration of GABA in wild-type larvae was determined to be 20.9 nM/mg of tissue (sd = 2.3) compared to 8.2 nM/mg of tissue for *gad1b*$^{-/-}$larvae (sd = 1.7). The average normalized concentration of GABA in *gad1a*$^{-/-\ \text{larvae}}$ was determined to be 24.4 nM/mg of tissue (sd = 4.2). Comparable concentrations of glutamate and glutamine were measured across all genotypes (Table S4, Figure S2.5). Monoamine neurotransmitters were not assessed for 7 dpf larvae. These results indicate that Gad1b enzymatic activity produces a large percentage of the GABA found in the 7 dpf larval zebrafish brain.

Extracellular electrophysiology was used to measure local field potentials in the optic tecta of *gad1a*^{ga2404} or *gad1b*^{ga2303} homozygous mutant 7 dpf larval zebrafish to compare to those recorded from wild-type larvae, wild-type larvae exposed to 15 mM PTZ, and larval zebrafish homozygous mutant for *scn1ab* (Figure 2.1D). Ten larvae were used for each condition. Larvae homozygous mutant for *gad1a*^{ga2404} or *gad1b*^{ga2303} exhibited increased electrographic activity in

the optic tectum compared to wild-type larvae, with the larger increase associated with mutations in *gad1b*. The pattern of activity observed in *gad1b*$^{-/-}$ larvae was most like that observed for wild-type larvae treated with 15 mM PTZ than for 7 dpf larvae homozygous mutant for scn1a. The scn1a gene encodes for a subunit of the Nav1.1 voltage-gated sodium channel (Grone et al., 2017). Notably, both *gad1b* mutant larvae and wild-type larvae treated with 15 mM PTZ exhibited increased amplitude of high-frequency discharges punctuated with high-amplitude, low frequency discharges. These results show that *gad1b* gene function plays a more significant role than gad1a for normal neural signaling in the optic tectum. Additionally, these results indicate that GABAergic neurons in the optic tectum mediate activity in a relatively large set of neural circuits with similar properties, the existence of which is revealed in the similar electrographic features observed for both *gad1b* mutant larvae and wild-type larvae treated with 15 mM PTZ, but not in *scn1a* mutant larvae (Figure 2.1D).

gad1b and _gad2_ genes are expressed by most GABAergic neurons in the developing zebrafish optic tectum.

Expression of *gad1a*, *gad1b*, and *gad2* in the optic tectum was assessed by mRNA in situ hybridization at 3 dpf and 5 dpf both in whole-mount and in horizontal sections cut through the optic tectum. Connections between the retina and optic tectum become functional between 3-4 dpf (Stuermer, 1988; Burrill and Easter, 1994; Easter and Nicola, 1996, 1997; Niell and Smith, 2005). By 5 dpf, larvae track and capture prey indicating a functional visual system (Niell and Smith, 2005). Anatomically, the larval tectum has two distinct regions, one composed of neuronal cell bodies, known as the stratum periventricular (SPV), and the other a superficial neuropil that is organized into layers (Figure 2.2H-I). The neuropil contains the dendrites and

axons of tectal neurons, a sparse mixture of tectal interneurons and afferent axons arriving at the tectum, mostly from the retina (Nevin et al., 2010; Kunst et al., 2019a).

At 3 dpf, *gad1a*, *gad1b*, and *gad2* exhibit distinct patterns of expression in the developing brain (Figure 2.2A-C). *gad1a* is predominantly expressed by cells in a longitudinal domain adjacent to the ventral midline that extends from the hypothalamus through the tegmentum and in clusters of cells in the hindbrain. No appreciable expression is detected in neurons in the telencephalon or in the optic tectum. *gad1b* is predominantly expressed by clusters of cells in the telencephalon, diencephalon, optic tectum, and hindbrain. *gad2* expression overlaps with *gad1a* and *gad1b* in the brain, but *gad1a* and *gad1b* are mostly expressed by separate cells in the forebrain, midbrain, and hindbrain.

In the larval optic tectum at 5 dpf, *gad1b* and *gad2* are expressed by cells in the neuropil and SPV (Figure 2.2D-F). Notably, *gad1b* and *gad2* are expressed by neurons with cell bodies located superficially in the neuropil between the stratum opticum (SO) and the stratum fibroseum et griseum superficiale (SFGS) laminae, likely superficial interneurons (SINs), and in a subset of neurons with cell bodies located in the deep layers of the neuropil (Figure 2.2G, J-N). These latter neurons are likely GABAergic pyramidal neurons (PyrNs) (Nevin et al., 2010; Kunst et al., 2019a; DeMarco et al., 2020). *gad1b* and *gad2* expression in the SPV is detected in clusters of cells, some of which are likely periventricular interneurons (PVINs). The SPV is comprised of radial glia and at least 19 different types of neurons (Nevin et al., 2010; Robles et al., 2011; Kunst et al., 2019a; DeMarco et al., 2020). Of these, GABAergic PVINs make up approximately 20% of the neurons in the SPV (Scott et al., 2007; Scott and Baier, 2009). *gad1a* transcripts were detected mostly in cells in the SPV.

To further elucidate coexpression of the three *gad* genes, HCR in situ, which has a more sensitive detection method, was performed for the three genes on 5 dpf fish (Figure 2.2 J-N). *gad1b* and *gad2* still showed complete coexpression within the optic tectum. *gad1a,* however, was found to sometimes be coexpressed with *gad1b* and *gad2* and sometimes it was found to be expressed on its own. The levels of *gad1a* transcripts detected were lower than those of *gad1b* and *gad2*, especially within the neuropil. Interestingly, *gad1a* seemed to have its highest detection of transcripts in the superficial (dorsal) layer of the SPV. As *gad1a* transcripts are detected at a lower extent than *gad1b*, it makes sense that the *gad1b* mutants are the ones that have the more apparent phenotype as they would have more cells with decreased GABA than would the *gad1a* mutants.

As a second means of assessing *gad1b* expression in the tectum, reporter gene expression was assessed in larvae stably transgenic for the *gad1b*-reporter transgene TgBAC[gad1b:loxP-DsRed-loxP-GFP] (Satou et al., 2013). This reporter drives DsRed expression in putative SINs and PyrNs in the tectal neuropil and in neurons in the SPV (Figure S2.6). Together, these data indicate that null mutations in *gad1b* should result in a reduction in GABA in neurons involved in processing visual information in the optic tectum.

gad1b null larvae exhibit increased neural activity in the optic tectum.

To assess spatiotemporal patterns of neural activity in the optic tectum, calcium imaging was performed using 5 dpf larval zebrafish stably harboring Tg(elavl3:GCaMP5g), which drives expression in most if not all neurons in the optic tectum (Ahrens et al., 2013a; Ahrens et al., 2013b). Imaging was performed using a custom built light sheet microscope (LSM), the details of which have been published prior (Liu et al., 2019b). Larvae at 5 dpf were chosen because

larvae at this stage of development can track and capture prey and avoid predators (Niell and Smith, 2005), which are behavioral indicators of a functional visual system, and, in our hands, are more easily imaged than larvae at older stages of development even with pigment suppression. It should be noted that the size of the visual receptive field has been reported to increase between the stages of 4 dpf to 6 dpf and then reduce by 8-9 dpf (Zhang et al., 2011). Thus, imaging at 5 dpf captures the behavior of neuronal assemblies during the period in which the tectal circuitry is undergoing developmentally and functionally driven refinement. Five recordings were made from each larvae, with ten larvae used for each condition (*gad1b*$^{+/+}$, *gad1b*$^{+/+}$ exposed to 15 mM PTZ, *gad1b*$^{-/-}$, and *gad1b*$^{-/-}$ exposed to 15 mM PTZ).

Under the conditions used for these experiments, *gad1b*$^{+/+}$ larvae exhibited intermittent increases in GCaMP5g fluorescence predominantly in the neuropil of the anterior tectum and within the superficial neuropil layers (Figure 2.3A, 4B). A typical example is shown by plotting the relative standard deviation (RSD) of each pixel as measured over 2 min at 46 fps. Calcium activity typically increased in the anterior tectum and propagated anterior to posterior within the SO or SFGS (data not shown). Activity was largely independent for each hemi-tecta. An increase in GCaMP5g fluorescence was detected in cell bodies in the SPV, but the largest relative changes in GCaMP5g fluorescence occurred in the neuropil, which is consistent with previous observations that information processing in the teleost tectum appears to take place predominantly, if not exclusively, in the neuropil (Kinoshita et al., 2002; Nevin et al., 2010). Spectral analysis revealed that fluctuations in the GCaMP5g signal occurred predominantly at 3.84 Hz, 7.63 Hz and 8.20 (Figure 2.3D).

gad1b mutant larvae exhibited changes in both spatial and temporal aspects of the Ca2+ signals relative to *gad1b* normal larvae (Figure 2.3). Like *gad1b*$^{+/+}$ larvae, changes in GCaMP5g

fluorescence typically initiated in the anterior tectum and propagated posteriorly within neuropil layers, however, there was an expansion in the amount of superficial neuropil that exhibited increased GCaMP5g fluorescence, especially in the areas surrounding putative SINs. In these embryos, increased GCaMP5g fluorescence was often detected in cell bodies in the SPV, typically in concert with increased fluorescence in discrete areas of the neuropil. Spectral analysis revealed fluctuations in the GCaMP5g signal were occurring predominantly at 4.16, 8.35 and 9.65 Hz (Figure 2.3D).

To assess the impact of an acute reduction in GABAergic signaling, *gad1b*$^{+/+}$ larvae were exposed to 15 mM PTZ. These larvae exhibited widespread changes in GCaMP5g fluorescence that included all regions of the neuropil and often cell bodies in the SPV. In these larvae, activity often propagated posterior to anterior in the tectum (data not shown). Spectral analysis revealed fluctuations in the GCaMP5g signal were occurring predominantly at 5.91 and 8.15 Hz (Figure 2.3D). The PTZ data indicates that GABA is acting predominantly as an inhibitory neurotransmitter in the tecta of 5 dpf larvae and that GABAergic circuits are governing information flow through tectal circuits.

Regional activity within the optic tectum was assessed for individual larvae (Figures 2.4, 2.5) and then compared within experimental groups and across conditions (Figure 6). In wild-type larvae, in the absence of PTZ, activity was largely restricted to the neuropil (Figures 2.4A, 2.5A). Within the neuropil of a hemitecta, correlated spikes of calcium activity were observed in the regions of the SO and SFGS, but not all activity in SFGS correlated with that of the SO. The timing of activity in the neuropil adjacent to the SPV usually correlated with that of the SFGS. Activity of the left and right hemitecta appeared to be mostly independent of each other. Exposure of wild-type larvae to PTZ resulted in concomitant spikes of calcium activity across all

layers of the neuropil as well as within the SPV (Figure 2.4C,H; 2.5B,E,H). Interestingly, exposure of wild-type fish to PTZ resulted no correlation between the left and right hemitecta (Figure 2.4H). Like wild-type, larvae null for gad1b exhibited correlated activity between the SO and SFGS, but not all activity in the SFGS correlated with the SO, and changes in activity in the SFGS often correlated with changes in the neuropil adjacent to the SPV. Unlike wild-type larvae, concomitant spikes of calcium activity were observed in both the SFGS and in neuronal soma in the SPV (Figure 2.4C,G; 2.5C,F,I). Exposure of *gad1b*$^{-/-}$ larvae to PTZ resulted in increased, correlated activity in both the left and right hemitecta (Figure 2.4I).

Assessment of the connection frequency, Figure 2.6, revealed that *gad1b* mutant larvae exhibited greater variance than wild-type fish for connectivity within a hemitecta and between the left and right tecta. Interestingly, the connectivity in *gad1b* mutant larvae exposed to PTZ was significantly higher than that of wild-type larvae exposed to PTZ under the same conditions both within a hemitecta and between the left and right sides of the tectum.

Discussion

Our study investigated the impact of genetically reduced GABAergic signaling on the network dynamics of neuronal populations in the optic tectum of larval zebrafish. We combined genetics and high-speed light sheet imaging of calcium dynamics to investigate the neural response of zebrafish larvae null for the *gad1b* gene compared to wild-type larvae in the presence and absence of PTZ. We used a cross-correlation analysis between different brain regions to indicate potential connectivity. Comparing connectivity data within and between experimental groups revealed that *gad1b* mutant fish exhibited increased connectivity within and between hemitecta compared to wild-type larvae.

Zebrafish have three gad genes known as *gad1a*, *gad1b*, and *gad2*. The *gad1a* and *gad1b* genes are paralogs, which likely arose due to a gene duplication event. By mRNA *in situ* hybridization, we showed that cells in the forebrain, inner-nuclear layer of the retina, optic tectum, and hindbrain of larval zebrafish express *gad1b*. At the same developmental time points, strong *gad1a* expression was observed mainly in the hindbrain, with some expression detected in the midbrain and forebrain. These results suggest that specific GABAergic neurons in the zebrafish brain express *gad1a* and *gad1b* and that the two genes are subject to different regulatory inputs. We are still determining if some neurons in the brain co-express *gad1a* and *gad1b*. As predicted by differences in the expression patterns of the two genes, fish mutant for *gad1b* exhibited a more significant decrease in brain GABA levels, a higher sensitivity to PTZ, and a larger increase in baseline neural activity in the optic tectum than did fish mutant for *gad1a*. Cells null for either *gad1a* or *gad1b* likely produce GABA through the action of Gad2 but at lower levels than wild-type cells.

The premise of this study was that genetic reduction of GABA synthesis would result in altered functional connectivity in the developing optic tectum of the zebrafish. In vertebrates, neural circuits are constructed via activity-independent mechanisms and refined by activity-dependent mechanisms. GABAergic signaling has been shown to act as a trophic factor to regulate cell proliferation, neural migration, neurite growth, and synapse formation, as well as mediate neural activity (Ganguly et al., 2001; Kriegstein and Owens, 2001; Ben-Ari, 2002; Manent et al., 2005; Represa and Ben-Ari, 2005; Akerman and Cline, 2007; Ben-Ari et al., 2007). Therefore, perturbations in GABAergic signaling during development can generate different neurological phenotypes depending on when, where, and how signaling is altered. Reduced GABAergic signaling during development has been reported to alter neuron numbers in

the brain. In mice, focal pharmacological inhibition of GABAergic signaling in the somatosensory cortex resulted in decreased cell death and increased numbers of neurons in the somatosensory cortex (Duan et al., 2020). A similar study in zebrafish showed that an increase in activity in the brain leads to a decrease in total neuron numbers but an increase in the excitatory-to-inhibitory cell ratio (Brenet et al., 2019). Although the impact of reduced GABAergic signaling on cell survival differs between the two studies, the net effect for both was to shift the excitatory/inhibitory balance in the young brain. An increase in activity would lead to various forms of synaptic plasticity, including long-term potentiation of synaptic responses and subsequent stable alterations in neural networks (Holmes and Ben-Ari, 2001).

Our experiments showed that loss of function mutations in *gad1b* resulted in increased coordinated activity in the larval optic tectum that was different from that observed by acute perturbation of GABAergic signaling by exposure to PTZ. The activity observed in *gad1b* null larvae likely reflects changes in the architecture and information processing of tectal microcircuits. Architecturally, our data suggest that *gad1b* mutant larvae retained more synaptic connections than those present in wild-type larvae. The most substantial support for this idea comes from the different activity phenotypes associated with PTZ exposure. Whereas exposure to wild-type larvae resulted in synchronized activity within either the left or right hemitecta, exposure to *gad1b* null larvae resulted in synchronized activity in both the left and right tecta. Given that PTZ acts the same way in both wild-type and *gad1b* mutant genotypes, the differences in activity elicited by PTZ exposure likely reflect differences in the geometry of the neuronal networks in wild-type compared to *gad1b* mutant larvae. The spatiotemporal pattern of PTZ-induced activity observed in *gad1b* null larvae is consistent with increased connections in the *gad1b* null tectum relative to the wild-type tectum. An increase in connectivity, measured by

magnetic resonance imaging (MRI), has been reported for some children with seizure disorders (Radmanesh et al., 2020; Banerjee et al., 2021).

Information processing is also likely altered in *gad1b* null larvae. The tectum processes spatial information in the visual field, including object location and movement (Gahtan et al., 2005; Del Bene et al., 2010; Nevin et al., 2010). RGC axons enter the tectal neuropil from the anterior side and arborize at one of six retinorecipient laminae (Xiao et al., 2005; Xiao and Baier, 2007; Robles et al., 2013; Robles et al., 2014; Kunst et al., 2019a). In fish that have developed normally, information processing mainly occurs in the tectal neuropil (Kinoshita et al., 2002; Kinoshita and Ito, 2006), with spatial filtering achieved by feedforward inhibition (Del Bene et al., 2010). A reduction in GABAergic signaling, especially in SIN neurons, is expected to result in increased activity in the neuropil in response to a visual stimulus, with deeper layers of the neuropil exhibiting greater activity (Del Bene et al., 2010). Consistent with this expectation, *gab1b* mutant larvae exhibited more widespread activity than in wild-type larvae but less than in wild-type larvae exposed to PTZ.

Our results indicate that a reduction in GABAergic signaling during early brain development results in increased connectivity concomitant with reduced precision of information flow within the brain. In the case of larval zebrafish, our results predict that *gad1b* mutant larvae will exhibit reduced visual acuity.

Acknowledgments

The authors wish to thank Dr. Scott Baraban for generously providing us with the line of *scn1b* mutant zebrafish. The authors thank Brian Condie, Andrew Sornborger, Lindsey Beebe, Madison Grant, Karl Kudyba, and Ashley Rasys for helpful discussion on this project. The authors also wish to acknowledge the UGA Honors Program and the Center for Undergraduate

Research Opportunities which supported Mr. J. Branson Beyers and Ms. Hannah Schriver in the form of CURO Summer Fellowships and CURO Research Assistantships. This work was supported by the National Institutes of Health (Grant No. R01NS090645 to JDL, PAK, and F31NS115496 to YL) and the National Science Foundation (Grant No. 1350654 to PAK). The authors also acknowledge the assistance of the Biomedical Microscopy Core at the University of Georgia with imaging using Zeiss LSM 710 confocal microscope.

Figures

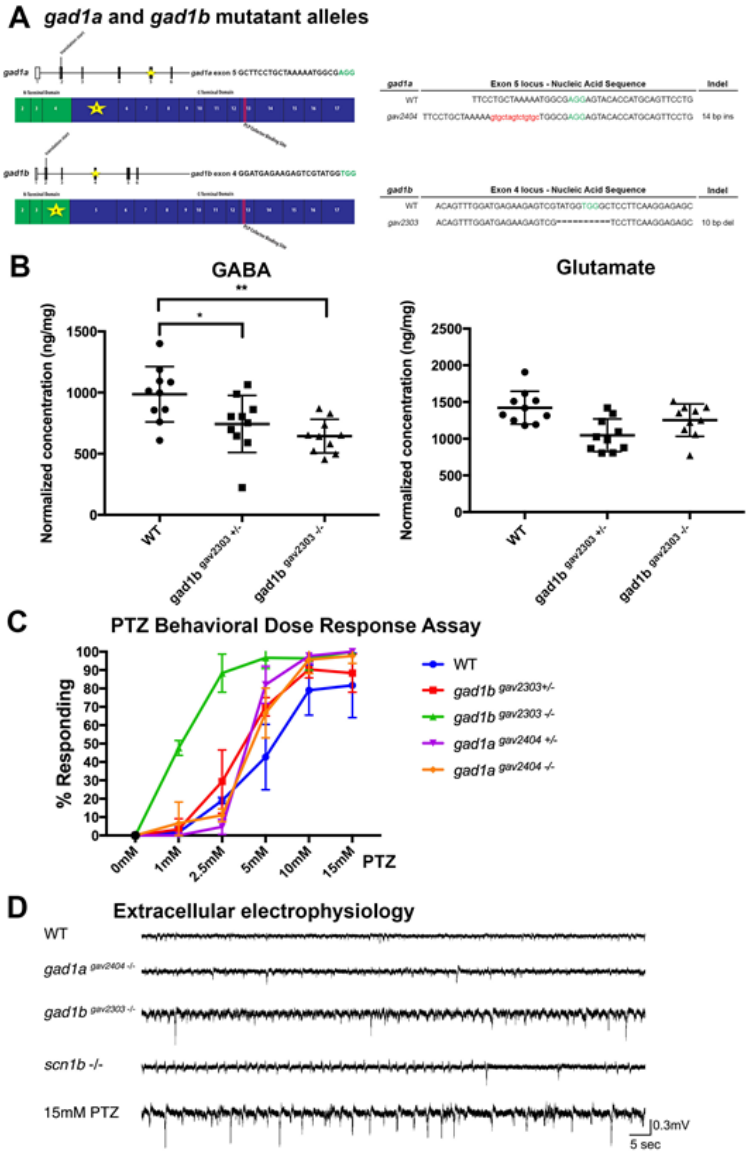

Figure 2.1: *gad1b* mutant larvae exhibit increased neural activity.

(A) Location of 10 bp deletion. (B) GABA and glutamate levels in the brains of *gad1b*$^{+/+}$, *gad1b*$^{+/-}$, and *gad1b*$^{-/-}$ fish as measured by HPLC with electrochemical detection. Samples were normalized and run as described previously (Ross and Filipov 2006, Coban and Filipov 2007); N=10 animals/genotype. (C) PTZ dose-response assay on 7 dpf *gad1a* and *gad1b* mutant larvae. Fish were sorted into groups of 10-20 per genotype for each treatment group and assayed for stage II and stage III behavioral phenotypes for 10 minutes. Assays were performed three times each. N>42 for each genotype at each dose. (D) Representative traces of extracellular recordings made from 7 dpf *gad1b*$^{-/-}$ mutant larvae compared to wild-type (WT), *gad1a*$^{-/-}$, *scn1b*$^{-/-}$, and WT larvae exposed to 15 mM PTZ. N>10 for each genotype/treatment.

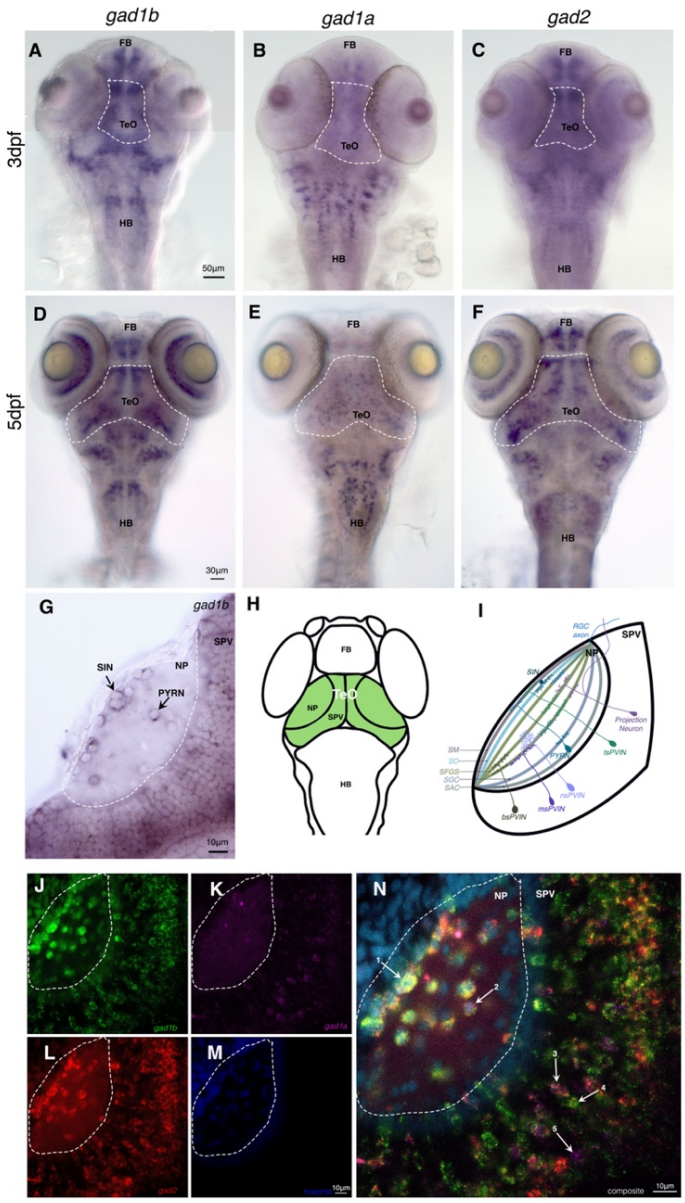

Figure 2.2: *gad1a* and *gad1b* expression in the larval zebrafish brain.

(a-c). 3dpf RNA whole mount *in situ* hybridization of *gad1b*, *gad1a*, and *gad2* and (d-f) 5dpf whole mount in situ hybridization with a dashed line outlining the optic tectum. (g). 10-micron section of *gad1b* expression in the optic tectum. Dashed line outlining the neuropil. (h). Schematic of larval zebrafish highlighting optic tectum in green. (i) schematic of a hemitectum showing examples of cell bodies and their neurite patterns in the neuropil. (j-n) 5dpf HCR RNA in situ of *gad1a, gad1, gad2*, and Hoechst nucleic acid labeling. Dashed outline highlighting the neuropil. Arrows indicate 1) SIN expressing gad1b and gad2. 2)PYRN expressing all 3 *gad* genes. 3-5) SPV neurons expressing 3) all 3 *gad* genes, 4) *gad1b* and *gad2* only, 5) *gad1a* only. FB: forebrain, TeO: optic tectum, HB: hindbrain, NP: Neuropil, SPV: stratum periventricular, SINS: superficial interneurons, PYRN: pyramidal neurons

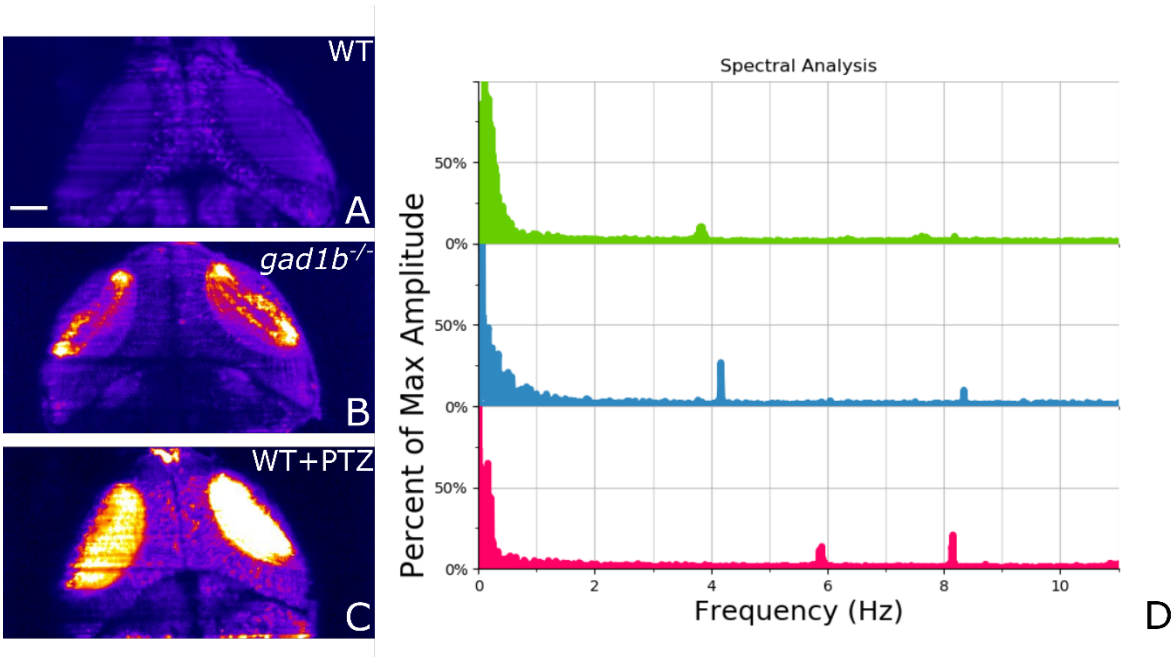

Figure 2.3: Spectral Analysis

(A)-(C) Plot of the standard deviation over the mean of the GCaMP signal for wild-type, *gad1b*$^{-/-}$ mutant, and wild-type treated with PTZ. Analysis is done using the first 100 frames with imaging speed of 25fps (~4 seconds) of each recording. (D) Frequency analysis of 10-minute recordings with photobleaching corrected in deltaF calculations. Wild-type, *gad1b*$^{-/-}$ and, PTZ treated fish each show distinct frequencies in the temporal response. The relevant peaks are 3.84Hz, 7.63Hz, and 8.20Hz for wildtype. The scale bar in (A) is 50 microns.

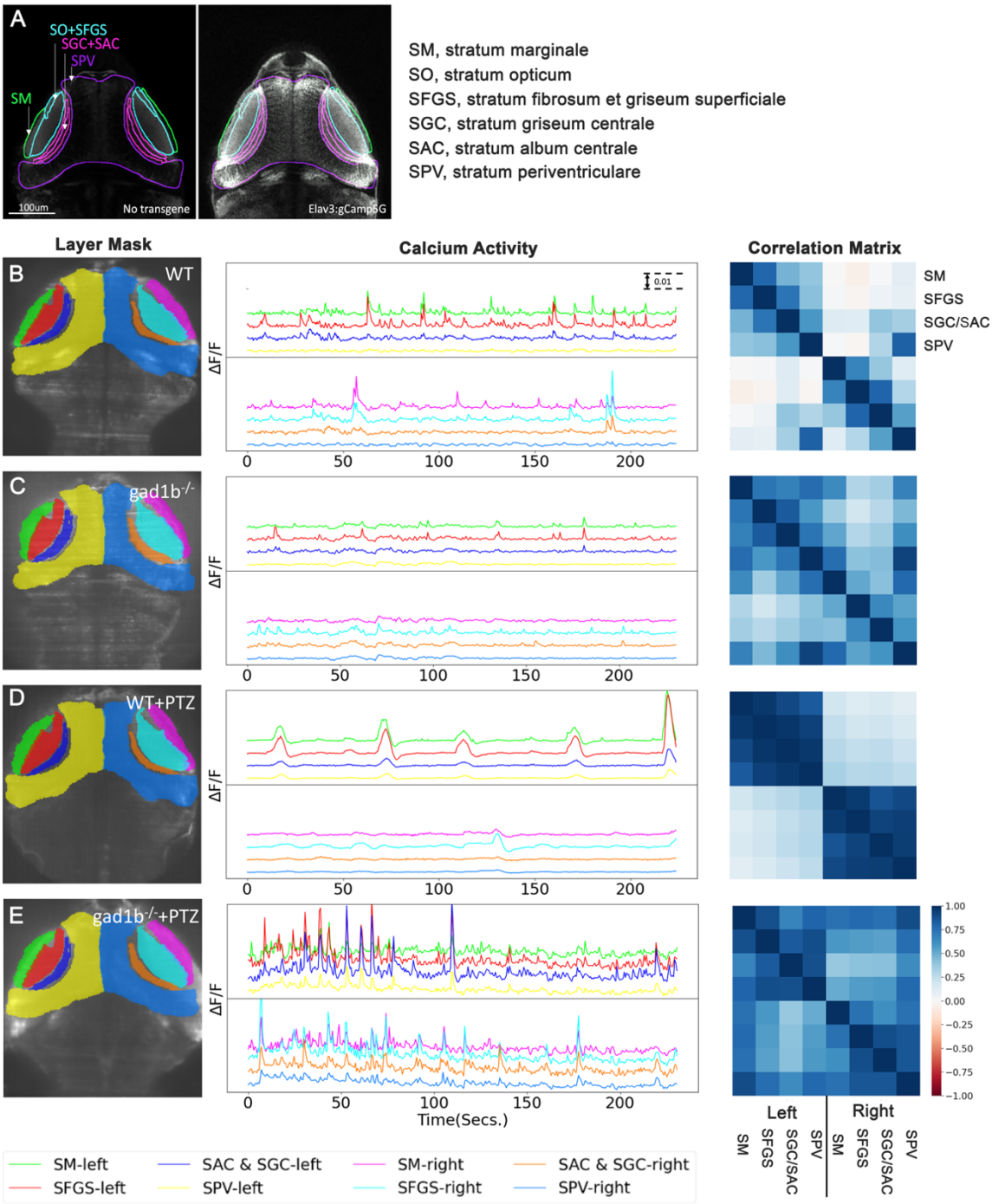

Figure 2.4: Calcium activity by tectal region.

(A) Regions of the optic tectum. (B) Neural activity in the wild-type optic tectum. (C) Neural activity in the *gad1b*$^{-/-}$ tectum. (D) Neural activity in wild-type larva treated with PTZ. (E) Neural activity in a *gad1b*$^{-/-}$ larva treated with PTZ. SM, stratum marginale; SO, stratum opticum; SFGS, stratum fibrosum et griseum superficiale; SGC, stratum griseum centrale, SAC, stratum album centrale

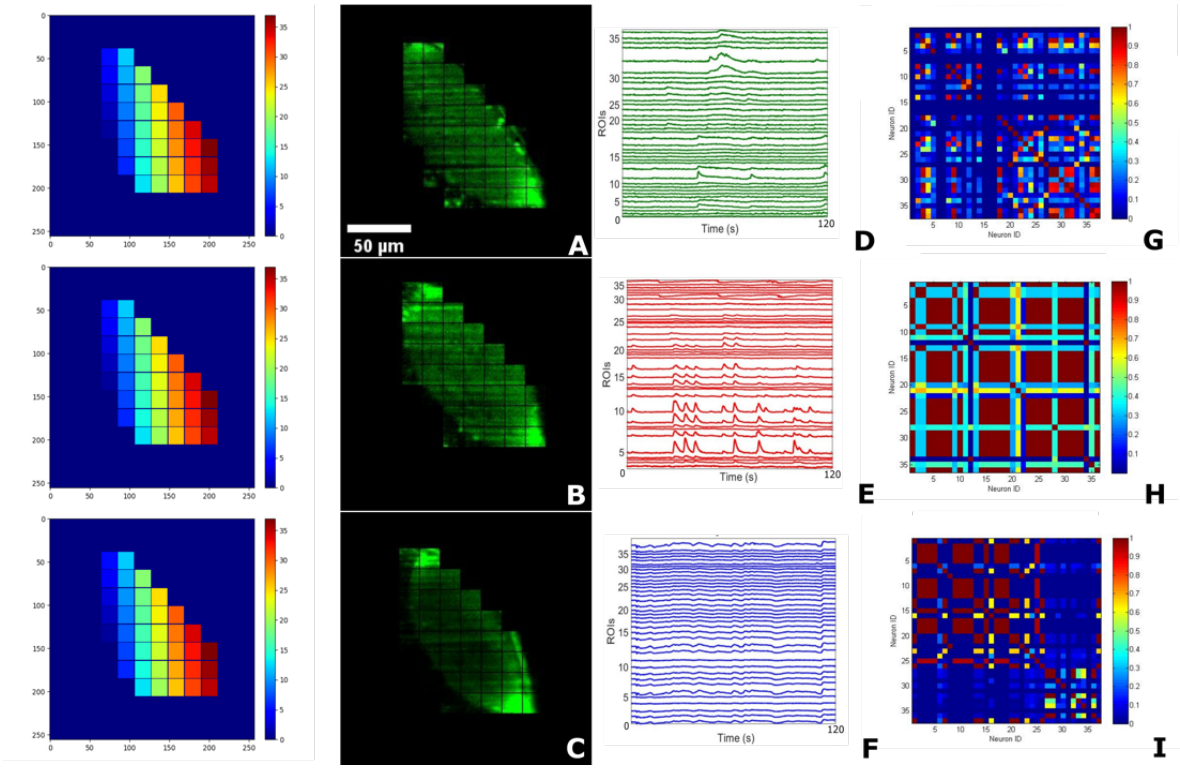

Figure 2.5: Optic Tectum Analysis.

The analysis is like Figure 4 but measures activity in different regions of the optic tectum. (A)-(C) Images of the right tectum in WT, PTZ treated and *gad1b*$^{-/-}$ zebrafish larva. (D)-(F) activity in the different regions. (G)-(I) Corresponding correlation matrices.

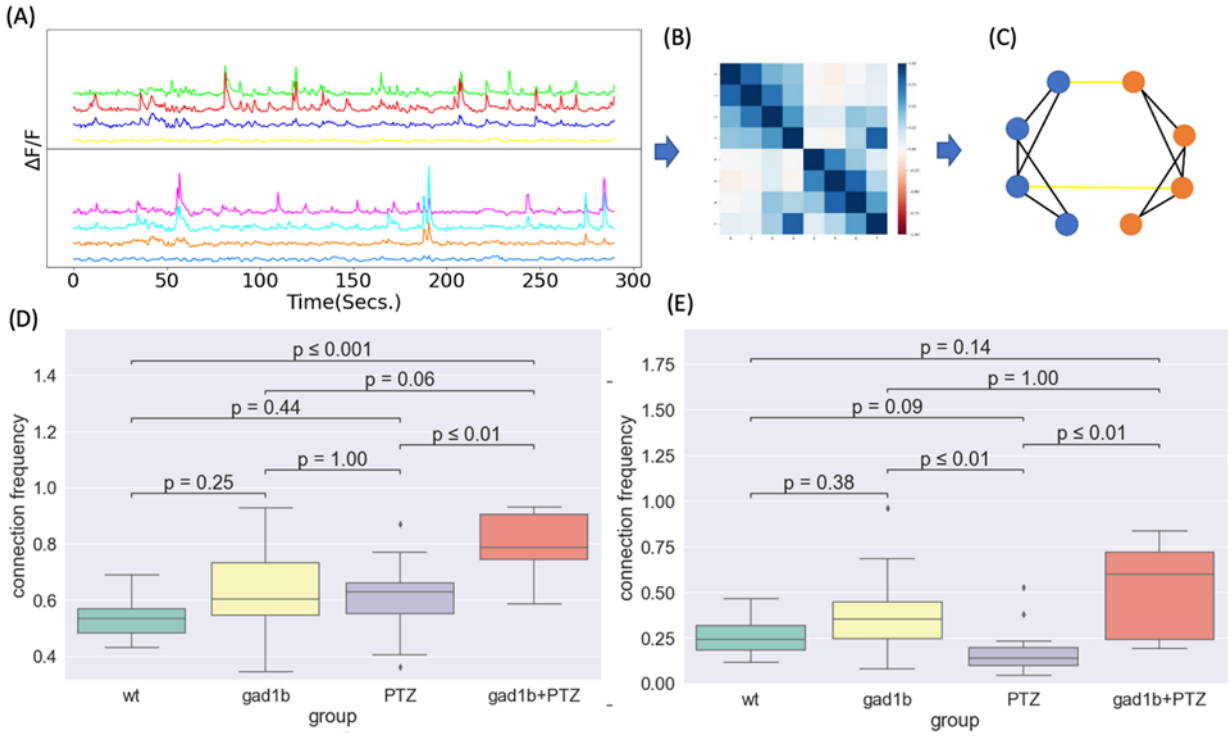

Figure 2.6: Connectivity analysis

(a) The correlation of activity is calculated using a 20s sliding window with a 3s step size. (b) The correlation matrix between the different regions. (c) A connectivity map is created between the different regions by counting regions as connected for a correlation greater than 0.5. (d) The connectivity between regions on the same side of the brain is compared between the different types. (e) The connectivity between regions on different sides of the brain. N = 5 fish per group with 2-3 recordings per fish.

References

Abrahams BS, Geschwind DH (2008) Advances in autism genetics: on the threshold of a new neurobiology. Nature reviews genetics 9:341-355.

Ahrens MB, Huang KH, Narayan S, Mensh BD, Engert F (2013a) Two-photon calcium imaging during fictive navigation in virtual environments. Front Neural Circuits 7:104.

Ahrens MB, Orger MB, Robson DN, Li JM, Keller PJ (2013b) Whole-brain functional imaging at cellular resolution using light-sheet microscopy. Nat Methods 10:413-420.

Akerman CJ, Cline HT (2007) Refining the roles of GABAergic signaling during neural circuit formation. Trends Neurosci 30:382-389.

Antinucci P, Hindges R (2016) A crystal-clear zebrafish for in vivo imaging. Scientific Reports 6:29490.

Arevian AC, Kapoor V, Urban NN (2008) Activity-dependent gating of lateral inhibition in the mouse olfactory bulb. Nat Neurosci 11:80-87.

Asada H, Kawamura Y, Maruyama K, Kume H, Ding RG, Kanbara N, Kuzume H, Sanbo M, Yagi T, Obata K (1997) Cleft palate and decreased brain gamma-aminobutyric acid in mice lacking the 67-kDa isoform of glutamic acid decarboxylase. Proc Natl Acad Sci U S A 94:6496-6499.

Asada H, Kawamura Y, Maruyama K, Kume H, Ding R, Ji FY, Kanbara N, Kuzume H, Sanbo M, Yagi T, Obata K (1996) Mice lacking the 65 kDa isoform of glutamic acid decarboxylase (GAD65) maintain normal levels of GAD67 and GABA in their brains but are susceptible to seizures. Biochem Biophys Res Commun 229:891-895.

Avitan L, Pujic Z, Molter J, Van De Poll M, Sun B, Teng H, Amor R, Scott EK, Goodhill GJ (2017) Spontaneous Activity in the Zebrafish Tectum Reorganizes over Development and Is Influenced by Visual Experience. Curr Biol 27:2407-2419 e2404.

Banerjee S, Dong M, Lee MH, O'Hara N, Juhasz C, Asano E, Jeong JW (2021) Deep Relational Reasoning for the Prediction of Language Impairment and Postoperative Seizure Outcome Using Preoperative DWI Connectome Data of Children With Focal Epilepsy. IEEE Trans Med Imaging 40:793-804.

Baraban SC (2005) Modeling Epilepsy and Seizures in Developing Zebrafish Larvae. In: Models of Seizures and Epilepsy, 1 Edition (Pitkänen A, Schwartzkroin PA, Moshé SL, eds), pp 189-198. 30 Corporate Drive, Suite 400, Burlington, MA 01803: Elsevier Academic Press.

Baraban SC, Dinday MT, Hortopan GA (2013) Drug screening in Scn1a zebrafish mutant identifies clemizole as a potential Dravet syndrome treatment. Nature communications 4:2410.

Baraban SC, Taylor MR, Castro PA, Baier H (2005) Pentylenetetrazole induced changes in zebrafish behavior, neural activity and c-fos expression. Neuroscience 131:759-768.

Barker AJ, Baier H (2015) Sensorimotor decision making in the zebrafish tectum. Curr Biol 25:2804-2814.

Beck S, Hallett M (2011) Surround inhibition in the motor system. Exp Brain Res 210:165-172.

Ben-Ari Y (2002) Excitatory actions of gaba during development: the nature of the nurture. Nat Rev Neurosci 3:728-739.

Ben-Ari Y (2006) Seizures Beget Seizures: The Quest for GABA as a Key Player. 18:135-144.

Ben-Ari Y, Gaiarsa JL, Tyzio R, Khazipov R (2007) GABA: a pioneer transmitter that excites immature neurons and generates primitive oscillations. Physiol Rev 87:1215-1284.

Brenet A, Hassan-Abdi R, Somkhit J, Yanicostas C, Soussi-Yanicostas N (2019) Defective Excitatory/Inhibitory Synaptic Balance and Increased Neuron Apoptosis in a Zebrafish Model of Dravet Syndrome. Cells 8.

Bruford EA, Braschi B, Denny P, Jones TEM, Seal RL, Tweedie S (2020) Guidelines for human gene nomenclature. Nat Genet 52:754-758.

Bult CJ, Blake JA, Smith CL, Kadin JA, Richardson JE, Mouse Genome Database G (2019) Mouse Genome Database (MGD) 2019. Nucleic Acids Res 47:D801-D806.

Burgstaller J, Hindinger E, Gesierich B, Baier H (2019) Light-sheet imaging and graph-theoretical analysis of antidepressant action in the larval zebrafish brain network. bioRxiv.

Burrill JD, Easter SS, Jr (1994) Development of the retinofugal projections in the embryonic and larval zebrafish (*Brachydanio rerio*). J Comp Neurol 346:583-600.

Chatron N et al. (2020) Bi-allelic GAD1 variants cause a neonatal onset syndromic developmental and epileptic encephalopathy. Brain 143:1447-1461.

Coban A, Filipov NM (2007) Dopaminergic toxicity associated with oral exposure to the herbicide atrazine in juvenile male C57BL/6 mice. J Neurochem 100:1177-1187.

Condie BG, Bain G, Gottlieb DI, Capecchi MR (1997) Cleft palate in mice with a targeted mutation in the gamma-aminobutyric acid-producing enzyme glutamic acid decarboxylase 67. Proc Natl Acad Sci U S A 94:11451-11455.

de Curtis M, Avoli M (2016) GABAergic networks jump-start focal seizures. Epilepsia 57:679-687.

Del Bene F, Wyart C, Robles E, Tran A, Looger L, Scott EK, Isacoff EY, Baier H (2010) Filtering of visual information in the tectum by an identified neural circuit. Science 330:669-673.

DeMarco E, Xu N, Baier H, Robles E (2020) Neuron types in the zebrafish optic tectum labeled by an id2b transgene. J Comp Neurol 528:1173-1188.

Duan ZRS, Che A, Chu P, Modol L, Bollmann Y, Babij R, Fetcho RN, Otsuka T, Fuccillo MV, Liston C, Pisapia DJ, Cossart R, De Marco Garcia NV (2020) GABAergic Restriction of Network Dynamics Regulates Interneuron Survival in the Developing Cortex. Neuron 105:75-92 e75.

Easter SS, Jr., Nicola GN (1996) The development of vision in the zebrafish (Danio rerio). Dev Biol 180:646-663.

Easter SS, Jr., Nicola GN (1997) The development of eye movements in the zebrafish (Danio rerio). Dev Psychobiol 31:267-276.

Erlander MG, Tobin AJ (1991) The structural and functional heterogeneity of glutamic acid decarboxylase: a review. Neurochem Res 16:215-226.

Erlander MG, Tillakaratne NJK, Feldblum S, Patel N, Tobin AJ (1991) Two genes encode distinct glutamate decarboxylases. Neuron 7:91-100.

Flores-Herr N, Protti DA, Wassle H (2001) Synaptic currents generating the inhibitory surround of ganglion cells in the mammalian retina. J Neurosci 21:4852-4863.

Forster D, Helmbrecht TO, Mearns DS, Jordan L, Mokayes N, Baier H (2020) Retinotectal circuitry of larval zebrafish is adapted to detection and pursuit of prey. eLife 9.

Forster D, Arnold-Ammer I, Laurell E, Barker AJ, Fernandes AM, Finger-Baier K, Filosa A, Helmbrecht TO, Kolsch Y, Kuhn E, Robles E, Slanchev K, Thiele TR, Baier H, Kubo F

(2017) Genetic targeting and anatomical registration of neuronal populations in the zebrafish brain with a new set of BAC transgenic tools. Sci Rep 7:5230.

Gabriel JP, Trivedi CA, Maurer CM, Ryu S, Bollmann JH (2012) Layer-specific targeting of direction-selective neurons in the zebrafish optic tectum. Neuron 76:1147-1160.

Gaetz W, Bloy L, Wang DJ, Port RG, Blaskey L, Levy SE, Roberts TP (2014) GABA estimation in the brains of children on the autism spectrum: measurement precision and regional cortical variation. Neuroimage 86:1-9.

Gahtan E, Tanger P, Baier H (2005) Visual prey capture in larval zebrafish is controlled by identified reticulospinal neurons downstream of the tectum. J Neurosci 25:9294-9303.

Galanopoulou AS (2010) Mutations affecting GABAergic signaling in seizures and epilepsy. Pflugers Arch 460:505-523.

Ganguly K, Schinder AF, Wong ST, Poo M (2001) GABA itself promotes the developmental switch of neuronal GABAergic responses from excitation to inhibition. Cell 105:521-532.

Garyfallidis E, Brett M, Amirbekian B, Rokem A, Van Der Walt S, Descoteaux M, Nimmo-Smith I (2014) Dipy, a library for the analysis of diffusion MRI data. Frontiers in Neuroinformatics 8.

Geschwind DH (2009) Advances in autism. Annual review of medicine 60:367-380.

Glykys J, Dzhala VI, Kuchibhotla KV, Feng G, Kuner T, Augustine G, Bacskai BJ, Staley KJ (2009) Differences in cortical versus subcortical GABAergic signaling: a candidate mechanism of electroclinical uncoupling of neonatal seizures. Neuron 63:657-672.

Grama A, Engert F (2012) Direction selectivity in the larval zebrafish tectum is mediated by asymmetric inhibition. Front Neural Circuits 6:59.

Grone BP, Maruska KP (2016) Three Distinct Glutamate Decarboxylase Genes in Vertebrates. Sci Rep 6:30507.

Grone BP, Qu T, Baraban SC (2017) Behavioral Comorbidities and Drug Treatments in a Zebrafish scn1lab Model of Dravet Syndrome. eNeuro 4.

Guizar-Sicairos M, Thurman ST, Fienup JR (2008) Efficient subpixel image registration algorithms. Optics Letters 33:156-158.

Helmbrecht TO, Dal Maschio M, Donovan JC, Koutsouli S, Baier H (2018) Topography of a Visuomotor Transformation. Neuron 100:1429-1445 e1424.

Higashijima S-i, Mandel G, Fetcho JR (2004) Distribution of prospective glutamatergic, glycinergic, and GABAergic neurons in embryonic and larval zebrafish. Journal of Comparative Neurology 480:1-18.

Hildebrand DGC et al. (2017) Whole-brain serial-section electron microscopy in larval zebrafish. Nature 545:345-349.

Hindriks R, Adhikari MH, Murayama Y, Ganzetti M, Mantini D, Logothetis NK, Deco G (2016) Can sliding-window correlations reveal dynamic functional connectivity in resting-state fMRI? Neuroimage 127:242-256.

Holmes GL, Ben-Ari Y (2001) The neurobiology and consequences of epilepsy in the developing brain. Pediatr Res 49:320-325.

Hunter PR, Lowe AS, Thompson ID, Meyer MP (2013) Emergent properties of the optic tectum revealed by population analysis of direction and orientation selectivity. J Neurosci 33:13940-13945.

Isaacson JS, Strowbridge BW (1998) Olfactory reciprocal synapses: dendritic signaling in the CNS. Neuron 20:749-761.

James N, Liu X, Bell A (2016) A fluorescence in situ hybridization (FISH) protocol for stickleback tissue. Evol Ecol Res 17:603-617.

Kaufmann A, Mickoleit M, Weber M, Huisken J (2012) Multilayer mounting enables long-term imaging of zebrafish development in a light sheet microscope. Development 139:3242.

Kim J, Namchuk M, Bugawan T, Fu Q, Jaffe M, Shi Y, Aanstoot HJ, Turck CW, Erlich H, Lennon V, Baekkeskov S (1994) Higher autoantibody levels and recognition of a linear NH2-terminal epitope in the autoantigen GAD65, distinguish stiff-man syndrome from insulin-dependent diabetes mellitus. J Exp Med 180:595-606.

Kimmel CB, Ballard WW, Kimmel SR, Ullmann B, Schilling TF (1995) Stages of embryonic development of the zebrafish. Dev Dyn 203:253-310.

Kinoshita M, Ito E (2006) Roles of periventricular neurons in retinotectal transmission in the optic tectum. Prog Neurobiol 79:112-121.

Kinoshita M, Ueda R, Kojima S, Sato K, Watanabe M, Urano A, Ito E (2002) Multiple-site optical recording for characterization of functional synaptic organization of the optic tectum of rainbow trout. Eur J Neurosci 16:868-876.

Koyama M, Pujala A (2018) Mutual inhibition of lateral inhibition: a network motif for an elementary computation in the brain. Curr Opin Neurobiol 49:69-74.

Kramer A, Wu Y, Baier H, Kubo F (2019) Neuronal Architecture of a Visual Center that Processes Optic Flow. Neuron 103:118-132 e117.

Kriegstein AR, Owens DF (2001) GABA may act as a self-limiting trophic factor at developing synapses. Sci STKE 2001:pe1.

Kunst M, Laurell E, Mokayes N, Kramer A, Kubo F, Fernandes AM, Forster D, Dal Maschio M, Baier H (2019a) A Cellular-Resolution Atlas of the Larval Zebrafish Brain. Neuron 103:21-38 e25.

Kunst M, Laurell E, Mokayes N, Kramer A, Kubo F, Fernandes AM, Förster D, Dal Maschio M, Baier H (2019b) A Cellular-Resolution Atlas of the Larval Zebrafish Brain. Neuron 103:21-38.e25.

Lai F, Fagernes Cathrine E, Nilsson Goran E, Jutfelt F (2016) Expression of genes involved in brain GABAergic neurotransmission in three-spined stickleback exposed to near-future CO_2. Conserv Physiol 4:cow068.

Lai F, Fagernes Cathrine E, Jutfelt F, Nilsson Goran E (2017) Erratum: Expression of genes involved in brain GABAergic neurotransmission in three-spined stickleback exposed to near-future CO_2. Conserv Physiol 5:cox004.

Lee S, Zhou ZJ (2006) The synaptic mechanism of direction selectivity in distal processes of starburst amacrine cells. Neuron 51:787-799.

Legay F, Pelhate S, Tappaz ML (1986) Phylogenesis of brain glutamic acid decarboxylase from vertebrates: immunochemical studies. J Neurochem 46:1478-1486.

Levy LM, Dalakas MC, Floeter MK (1999) The stiff-person syndrome: an autoimmune disorder affecting neurotransmission of gamma-aminobutyric acid. Ann Intern Med 131:522-530.

Liu J, Baraban SC (2019) Network Properties Revealed during Multi-Scale Calcium Imaging of Seizure Activity in Zebrafish. eNeuro 6.

Liu Y, Dale S, Ball R, VanLeuven AJ, Sornborger A, Lauderdale JD, Kner P (2019a) Imaging neural events in zebrafish larvae with linear structured illumination light sheet fluorescence microscopy. Neurophotonics: SPIE.

Liu Y, Dale S, Ball R, VanLeuven AJ, Sornborger A, Lauderdale JD, Kner P (2019b) Imaging neural events in zebrafish larvae with linear structured illumination light sheet fluorescence microscopy. Neurophotonics 6:015009.

Lynex CN, Carr IM, Leek JP, Achuthan R, Mitchell S, Maher ER, Woods CG, Bonthon DT, Markham AF (2004) Homozygosity for a missense mutation in the 67 kDa isoform of glutamate decarboxylase in a family with autosomal recessive spastic cerebral palsy: parallels with Stiff-Person Syndrome and other movement disorders. BMC Neurol 4:20.

Manent JB, Demarque M, Jorquera I, Pellegrino C, Ben-Ari Y, Aniksztejn L, Represa A (2005) A noncanonical release of GABA and glutamate modulates neuronal migration. J Neurosci 25:4755-4765.

Mann HB, Whitney DR (1947) On a Test of Whether one of Two Random Variables is Stochastically Larger than the Other. The Annals of Mathematical Statistics 18:50-60, 11.

Marachlian E, Avitan L, Goodhill GJ, Sumbre G (2018) Principles of Functional Circuit Connectivity: Insights From Spontaneous Activity in the Zebrafish Optic Tectum. Front Neural Circuits 12:46.

Marquart GD, Tabor KM, Horstick EJ, Brown M, Geoca AK, Polys NF, Nogare DD, Burgess HA (2017) High-precision registration between zebrafish brain atlases using symmetric diffeomorphic normalization. Gigascience 6:1-15.

Miyata S, Kakizaki T, Fujihara K, Obinata H, Hirano T, Nakai J, Tanaka M, Itohara S, Watanabe M, Tanaka KF, Abe M, Sakimura K, Yanagawa Y (2021) Global knockdown of glutamate decarboxylase 67 elicits emotional abnormality in mice. Mol Brain 14:5.

Mullins M (1995) Genetic nomenclature guide. Zebrafish. Trends Genet:31-32.

Muto A, Ohkura M, Abe G, Nakai J, Kawakami K (2013) Real-time visualization of neuronal activity during perception. Curr Biol 23:307-311.

Naumann EA, Fitzgerald JE, Dunn TW, Rihel J, Sompolinsky H, Engert F (2016) From Whole-Brain Data to Functional Circuit Models: The Zebrafish Optomotor Response. Cell 167:947-960 e920.

Nevin LM, Robles E, Baier H, Scott EK (2010) Focusing on optic tectum circuitry through the lens of genetics. BMC Biol 8:126.

Niell CM, Smith SJ (2005) Functional imaging reveals rapid development of visual response properties in the zebrafish tectum. Neuron 45:941-951.

Nikolaou N, Lowe AS, Walker AS, Abbas F, Hunter PR, Thompson ID, Meyer MP (2012) Parametric functional maps of visual inputs to the tectum. Neuron 76:317-324.

O'Connor MJ, Beebe LL, Deodato D, Ball RE, Page AT, VanLeuven AJ, Harris KT, Park S, Hariharan V, Lauderdale JD, Dore TM (2019) Bypassing Glutamic Acid Decarboxylase 1 (Gad1) Induced Craniofacial Defects with a Photoactivatable Translation Blocker Morpholino. ACS Chem Neurosci 10:266-278.

Oh WJ, Westmoreland JJ, Summers R, Condie BG (2010) Cleft palate is caused by CNS dysfunction in Gad1 and Viaat knockout mice. PLoS One 5:e9758.

Patel TP, Man K, Firestein BL, Meaney DF (2015) Automated quantification of neuronal networks and single-cell calcium dynamics using calcium imaging. J Neurosci Methods 243:26-38.

Pietri T, Romano SA, Perez-Schuster V, Boulanger-Weill J, Candat V, Sumbre G (2017) The Emergence of the Spatial Structure of Tectal Spontaneous Activity Is Independent of Visual Inputs. Cell Rep 19:939-948.

Pitrone PG, Schindelin J, Stuyvenberg L, Preibisch S, Weber M, Eliceiri KW, Huisken J, Tomancak P (2013) OpenSPIM: an open-access light-sheet microscopy platform. Nat Meth 10:598-599.

Popova E (2015) GABAergic neurotransmission and retinal ganglion cell function. Journal of comparative physiology A, Neuroethology, sensory, neural, and behavioral physiology 201:261-283.

Puts NA, Harris AD, Crocetti D, Nettles C, Singer HS, Tommerdahl M, Edden RA, Mostofsky SH (2015) Reduced GABAergic inhibition and abnormal sensory symptoms in children with Tourette syndrome. J Neurophysiol 114:808-817.

Radmanesh M, Jalili M, Kozlowska K (2020) Activation of Functional Brain Networks in Children With Psychogenic Non-epileptic Seizures. Frontiers in human neuroscience 14:339.

Ramdya P, Engert F (2008) Emergence of binocular functional properties in a monocular neural circuit. Nat Neurosci 11:1083-1090.

Randlett O, Wee CL, Naumann EA, Nnaemeka O, Schoppik D, Fitzgerald JE, Portugues R, Lacoste AM, Riegler C, Engert F, Schier AF (2015) Whole-brain activity mapping onto a zebrafish brain atlas. Nat Methods 12:1039-1046.

Represa A, Ben-Ari Y (2005) Trophic actions of GABA on neuronal development. Trends Neurosci 28:278-283.

Robertson CE, Ratai EM, Kanwisher N (2016) Reduced GABAergic Action in the Autistic Brain. Curr Biol 26:80-85.

Robles E, Smith SJ, Baier H (2011) Characterization of genetically targeted neuron types in the zebrafish optic tectum. Front Neural Circuits 5:1.

Robles E, Filosa A, Baier H (2013) Precise lamination of retinal axons generates multiple parallel input pathways in the tectum. J Neurosci 33:5027-5039.

Robles E, Laurell E, Baier H (2014) The retinal projectome reveals brain-area-specific visual representations generated by ganglion cell diversity. Curr Biol 24:2085-2096.

Ronneberger O, Liu K, Rath M, Ruebeta D, Mueller T, Skibbe H, Drayer B, Schmidt T, Filippi A, Nitschke R, Brox T, Burkhardt H, Driever W (2012) ViBE-Z: a framework for 3D virtual colocalization analysis in zebrafish larval brains. Nat Methods 9:735-742.

Ross MK, Filipov NM (2006) Determination of atrazine and its metabolites in mouse urine and plasma by LC-MS analysis. Anal Biochem 351:161-173.

Satou C, Kimura Y, Hirata H, Suster ML, Kawakami K, Higashijima S (2013) Transgenic tools to characterize neuronal properties of discrete populations of zebrafish neurons. Development 140:3927-3931.

Schoppa NE, Urban NN (2003) Dendritic processing within olfactory bulb circuits. Trends Neurosci 26:501-506.

Scott EK, Baier H (2009) The cellular architecture of the larval zebrafish tectum, as revealed by gal4 enhancer trap lines. Front Neural Circuits 3:13.

Scott EK, Mason L, Arrenberg AB, Ziv L, Gosse NJ, Xiao T, Chi NC, Asakawa K, Kawakami K, Baier H (2007) Targeting neural circuitry in zebrafish using GAL4 enhancer trapping. Nat Methods 4:323-326.

Solimena M, Folli F, Aparisi R, Pozza G, De Camilli P (1990) Autoantibodies to GABA-ergic neurons and pancreatic beta cells in stiff-man syndrome. N Engl J Med 322:1555-1560.

Stuermer CA (1988) Retinotopic organization of the developing retinotectal projection in the zebrafish embryo. J Neurosci 8:4513-4530.

Swanson OK, Maffei A (2019) From Hiring to Firing: Activation of Inhibitory Neurons and Their Recruitment in Behavior. Frontiers in molecular neuroscience 12.

Tao L, Lauderdale JD, Sornborger AT (2011) Mapping Functional Connectivity between Neuronal Ensembles with Larval Zebrafish Transgenic for a Ratiometric Calcium Indicator. Front Neural Circuits 5:2.

Tepper JM, Wilson CJ, Koos T (2008) Feedforward and feedback inhibition in neostriatal GABAergic spiny neurons. Brain Res Rev 58:272-281.

Thisse C, Thisse B (2008) High-resolution in situ hybridization to whole-mount zebrafish embryos. Nat Protoc 3:59-69.

Thompson AW, Vanwalleghem GC, Heap LA, Scott EK (2016) Functional Profiles of Visual-, Auditory-, and Water Flow-Responsive Neurons in the Zebrafish Tectum. Curr Biol 26:743-754.

Tremblay R, Lee S, Rudy B (2016) GABAergic Interneurons in the Neocortex: From Cellular Properties to Circuits. Neuron 91:260-292.

VanLeuven AJ, Park S, Menke DB, Lauderdale JD (2018) A PAGE screening approach for identifying CRISPR-Cas9-induced mutations in zebrafish. Biotechniques 64:275-278.

Vanwalleghem GC, Ahrens MB, Scott EK (2018) Integrative whole-brain neuroscience in larval zebrafish. Curr Opin Neurobiol 50:136-145.

Vucinic D, Cohen LB, Kosmidis EK (2006) Interglomerular center-surround inhibition shapes odorant-evoked input to the mouse olfactory bulb in vivo. J Neurophysiol 95:1881-1887.

Wang Y, Xu C, Xu Z, Ji C, Liang J, Wang Y, Chen B, Wu X, Gao F, Wang S, Guo Y, Li X, Luo J, Duan S, Chen Z (2017) Depolarized GABAergic Signaling in Subicular Microcircuits Mediates Generalized Seizure in Temporal Lobe Epilepsy. Neuron 95:92-105 e105.

Weber M, Mickoleit M, Huisken J (2014) Multilayer Mounting for Long-term Light Sheet Microscopy of Zebrafish. Journal of Visualized Experiments : JoVE:51119.

Westerfield M (1993) The zebrafish book : a guide for the laboratory use of zebrafish (Brachydanio rerio). Eugene, OR: M. Westerfield.

Westerfield M, ed (2007) The zebrafish book: A guide for the laboratory use of zebrafish (Danio rerio), 5 Edition. Eugene, OR: University of Oregon Press.

Wu C, Sun D (2015) GABA receptors in brain development, function, and injury. Metab Brain Dis 30:367-379.

Wu Y, Dal Maschio M, Kubo F, Baier H (2020) An Optical Illusion Pinpoints an Essential Circuit Node for Global Motion Processing. Neuron.

Xiao T, Baier H (2007) Lamina-specific axonal projections in the zebrafish tectum require the type IV collagen Dragnet. Nat Neurosci 10:1529-1537.

Xiao T, Roeser T, Staub W, Baier H (2005) A GFP-based genetic screen reveals mutations that disrupt the architecture of the zebrafish retinotectal projection. Development 132:2955-2967.

Yokoi M, Mori K, Nakanishi S (1995) Refinement of odor molecule tuning by dendrodendritic synaptic inhibition in the olfactory bulb. Proc Natl Acad Sci U S A 92:3371-3375.

Yoon JW, Yoon CS, Lim HW, Huang QQ, Kang Y, Pyun KH, Hirasawa K, Sherwin RS, Jun HS (1999) Control of autoimmune diabetes in NOD mice by GAD expression or suppression in beta cells. Science 284:1183-1187.

Yu M, Xi Y, Pollack J, Debiais-Thibaud M, Macdonald RB, Ekker M (2011) Activity of dlx5a/dlx6a regulatory elements during zebrafish GABAergic neuron development. Int J Dev Neurosci 29:681-691.

Zalesky A, Fornito A, Cocchi L, Gollo LL, Breakspear M (2014) Time-resolved resting-state brain networks. Proceedings of the National Academy of Sciences 111:10341-10346.

Zhang M, Liu Y, Wang SZ, Zhong W, Liu BH, Tao HW (2011) Functional elimination of excitatory feedforward inputs underlies developmental refinement of visual receptive fields in zebrafish. J Neurosci 31:5460-5469.

Supplemental Tables and Figures

Supplemental Table 2.1: Sequences used to make gBLOCK gene fragments for *in situ* hybridization experiment

gene	**gBLOCK fragment/sequence, for *in vitro* transcription**
gad1a	TGTCTGGAGCTGTCGGAGTATCTCTACCACAAGATCAAGAACAGAGAAGGATATGA GATGGTGTTTCAAGGGGAGCCACAGCACACAAATGTATGTTTCTGGTACATTCCTCC AAGCCTGCGGCTTCTGCCAGATGGAGAGGAGAAACGACATCGGCTTCATAAGGTC GCCCCAAAGATCAAGGCACTGATGATGGAGTGCGGGACAACAATGGTGGGCTACC AGCCTCAGGGTGAGAAGGTTAACTTCTTCAGGATGGTGGTCTCCAATCCGGCGGTT ACCAGGTCTGACATTGACTTCCTGATCGATGAGATAGAAAGACTGGGACAGGATTT ATAGAGAACGCAGAACAAGTTCAGTAGATGTAAATCATCTGGAAATGGAGGAGGCA ATCAGACGTGTTGTATCAGCTCGATGTTCCAGAGAATTAGGCCCTGTCCACAGAAA CACAGCTA
gad2	TCTACAACAAGATTAAGGACAGGGAAGGATATCAGATGGTGTTTGATGGAAAGCCG CAGCATACCAATGTGTGTTTCTGGTACCTTCCACCGGGCGTGCGCTACCTGGAGGA CAAAGTGGAGAGGATGAAGCGTCTGCACAAGGTTGCCCCTGTAATCAAAGCCAGAA TGATGGAGTACGGCACGACCATGGTGAGCTACCAGCCACAGGGAGACAAGGTCAA CTTCTTCCGCATGGTCATCTCCAATCCAGCCGCTACCTTTGAAGACATTGACTTCCT CATTGAAGAGATCGAGCGACTGGGGCAGGATCTTTAAAACTTACCGCACCAAAACC TGTTACTCCCGTGTCCCTGGATGGATTGCATATTTGTTGTGAATGTAACGGTAAATC TCTGATTCCTCTTCTCCAAAGTCACATTTAAAC

Supplemental Table 2.2: *gad1b* genotyping primer set

Orientation	***gad1b* probe oligo sequence**	
Fwd	*5'-ATTTAGGTGACACTATAGTTCTTCCGAATGGTGGTCTC-3'*	**SP6**
Rev	*5'-TAATACGACTCACTATAGGGTTCACCTCACAAAGGTGCTG-3'.*	**T7**

Supplemental Table 2.3: Screening and sequencing primers.

	Forward (5'-3')	**Reverse (5'-3')**
***gad1a* screening**	CATTAGCATTGACTTGACCGAG	AGCAGGAACTGCATGGTGTA
***gad1a* sequencing**	ACTCAGCGATGCAATGTCAG	TGTGCATGGTCTTCATCACC
***gad1b* screening**	CCCGTGTTGTAATGATGCAG	GTGAAGCGCTCATTGTTGTC
***gad1b* sequencing**	TCCCAGTAAAACTCCAACCG	GCGAACAGGTTGGAGAAATC

Supplemental Table 2.4: Mean normalized concentration of GABA in adult brains by genotype and comparisons of the mean by one-way ANOVA.

	WT	*gad1b*$^{ga2303\ +/-}$	*gad1b*$^{ga2303\ -/-}$	WT and Het ($p < 0.05$)	WT and -/- ($p < 0.05$)	Het and -/- ($p < 0.05$)
GABA	987 ng/mg	743.3 ng/mg	644.6 ng/mg	Yes: $p = 0.0324$	Yes: $p = 0.0023$	No

Supplemental Table 2.5: Mean normalized concentration of neurotransmitters in adult brains by genotype and comparisons of the mean by one-way ANOVA.

	WT	*gad1b*$^{ga2303\ +/-}$	*gad1b*$^{ga2303\ -/-}$	WT:Het ($p < 0.05$)	WT:-/- ($p < 0.05$)	Het:-/- ($p < 0.05$)
Serotonin (5-HT)	0.3025 ng/mg	0.261 ng/mg	0.3166 ng/mg	No	No	No
Serotonin Metabolite (5-HIAA)	0.2186 ng/mg	0.2254 ng/mg	0.1912 ng/mg	No	No	No
Dopamine (DA)	0.1536 ng/mg	0.205 ng/mg	0.1575 ng/mg	No	No	No
Glutamate	1,423 ng/mg	1,046 ng/mg	1,252 ng/mg	Yes $p = 0.0022$	No	No
Glutamine	1,342 ng/mg	1,138 ng/mg	1,155 ng/mg	No	No	No
Norepinephrine (NE)	1.051 ng/mg	1.007 ng/mg	1.113 ng/mg	No	No	No
Norepinephrine Metabolite (MHPG)	26.81 ng/mg	31.34 ng/mg	24.56 ng/mg	No	No	No

Supplemental Table 2.6: Mean normalized concentration of neurotransmitters in 7 dpf larvae by genotype and comparisons of the mean by one-way ANOVA.

	WT	*gad1b*$^{ga2303\ +/-}$	*gad1b*$^{ga2303\ -/-}$	*gad1a*$^{ga2404\ -/-}$	WT:Het ($p < 0.05$)	WT:-/- ($p < 0.05$)	Het:-/- ($p < 0.05$)
Serotonin (5-HT)	0.073 ng/mg	0.035 ng/mg	0.015 ng/mg	n/a	No	No	No
Serotonin Metabolite (5-HIAA)	1.485 ng/mg	1.625 ng/mg	0.8693 ng/mg	n/a	No	No	No
GABA	60.59 ng/mg	25.17 ng/mg	56.61 ng/mg	0.6367 ng/mg	No	No	No
Glutamate	324.1 ng/mg	477.1 ng/mg	357.8 ng/mg	294.8 ng/mg	No	No	No
Glutamine	716.8 ng/mg	724.8 ng/mg	3,259 ng/mg	724.8 ng/mg	No	No	No
Norepinephrine (NE)	0.5743 ng/mg	0.1233 ng/mg	0.414 ng/mg	n/a	No	No	No
Norepinephrine Metabolite (MHPG)	1,081 ng/mg	1,107 ng/mg	614.5 ng/mg	n/a	No	No	No
Dopamine (DA)	n/a	n/a	n/a	n/a	n/a	n/a	n/a

Supplemental Table 2.7: HCR Probe and Amplifier Set.

HCR Probe-initiator	Amplifier
gad1a-B3	594
gad1b-B1	488
gad2-B4	546

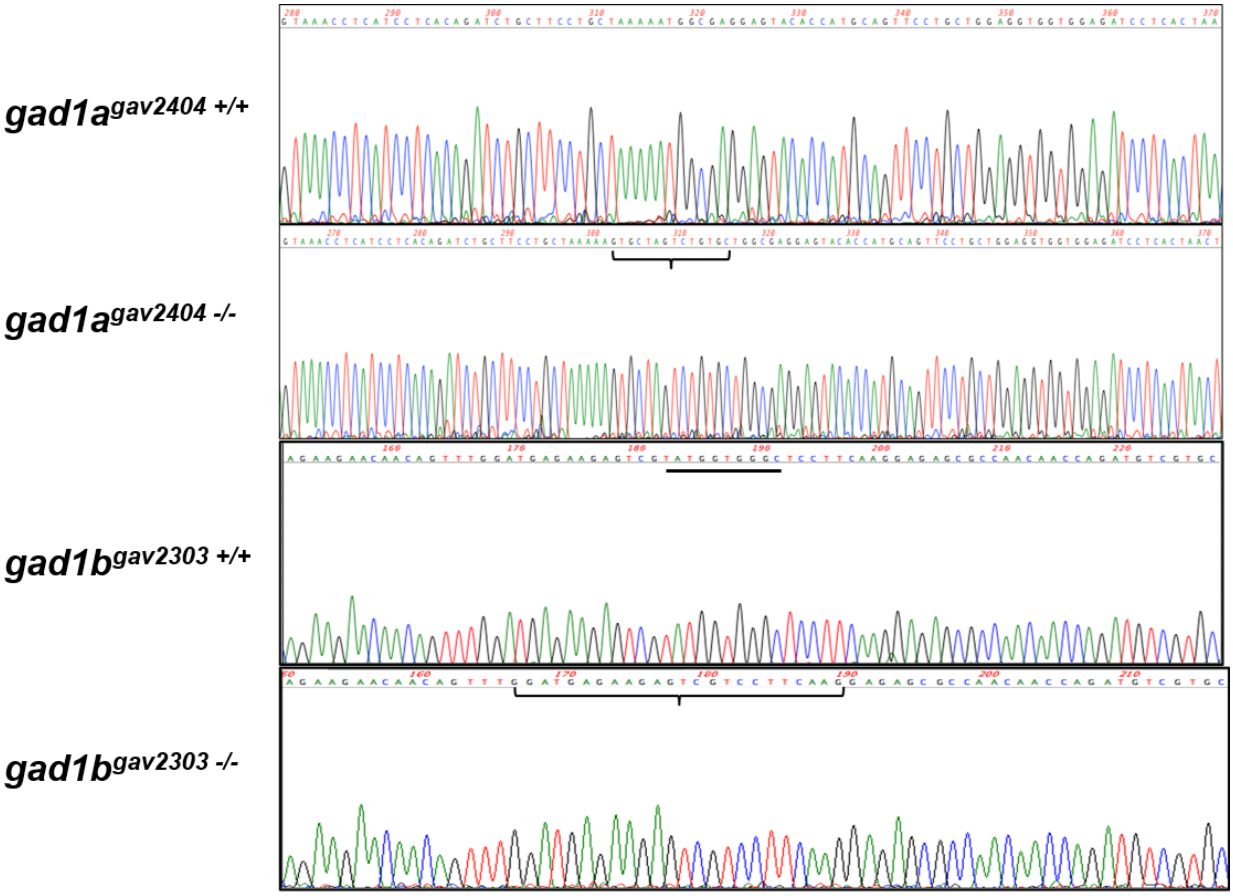

Supplemental Figure 2.1: Sequence for *gad1a*^{ga2404} and *gad1b*^{ga2303} alleles.

Sequence verification of homozygous mutations in *gad1a* and *gad1b* that we generated. The bracket in *gad1a* $^{-/-}$ represents the 14 bp insertion that is not present in wild-type. The black line in *gad1b* $^{+/+}$ indicates the 10 bp that are deleted. The bracket in *gad1b* $^{-/-}$ shows the sequence with the 10 bp deletion(Guizar-Sicairos et al., 2008)

.

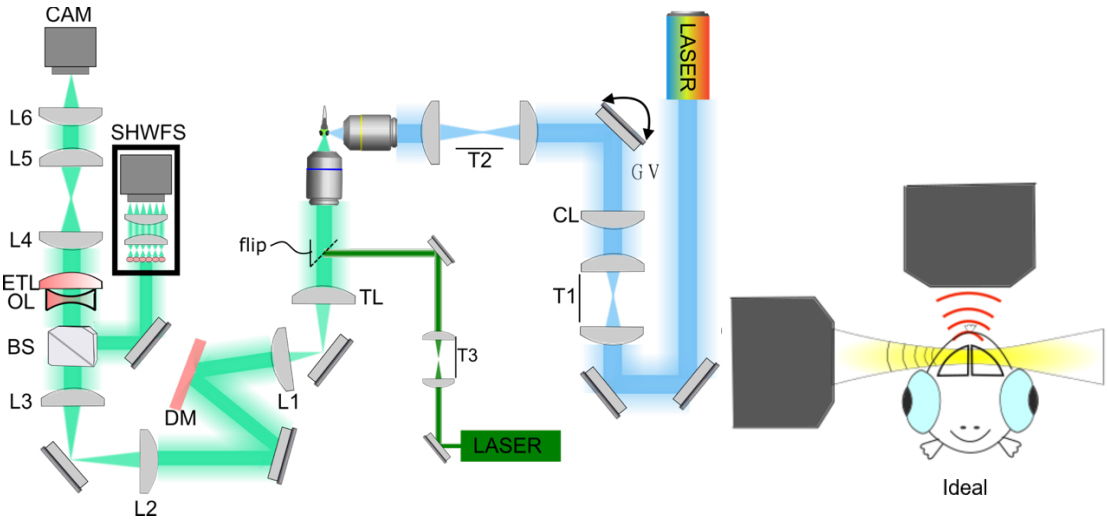

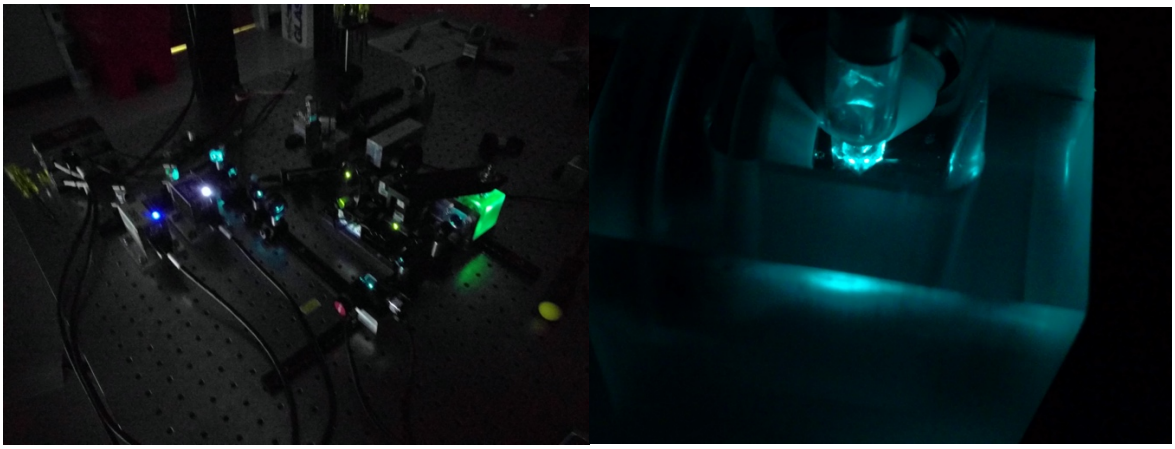

Supplemental Figure 2.2: Schematic of the optical setup.

A 10x 0.3NA water dipping objective was used as the illumination objective and a 40x 0.8NA water dipping objective was used as the detection objective lens. DM stands for deformable mirror; T1: 2x magnification lens pair (25mm and 50mm efl); T2: 5/3 demagnification lens pair (50mm and 30mm); TL:Tube lens (180mm efl); A green He-Ne laser and T3: magnification lens pair (25mm and 200mm efl) is used to calibrate the home-built Shack-Hartmann Wave front Sensor L1-2: Relay lenses (f1=100mm; f2=200mm). L3-4: Relay lenses (f4=300mm and f3=200mm); L5-6 is a magnifying lens pair(300mm and 150mm efl) to give an overall magnification of 26.67 for the final image. CL, cylinder lens (50mm efl).

We use a 10x 0.3NA and a 20X 0.5NA Olympus watering dipping objective lens for illumination and detection, respectively (UMPLFLN10XW, Olympus UMPLFLN20XW). A cylindrical lens

(f=50mm) in the illumination path forms an elliptical beam at the back-pupil plane of the 10X objective lens. This creates a thin static Gaussian light sheet with thickness (full width half maximum) of 6.6 µm. The system is capable of two-color imaging with a 488nm laser and a 561nm laser (Coherent OBIS LX 50 mW, Coherent OBIS LS 50 mW). The overall magnification of the imaging system is 33X, which results in a 399 µm field of view (FOV) with a 0.195µm pixel size. When the camera (Hamamatsu ORCA flash 4.0 V2) is operated at 33-50 frames per second for single channel.

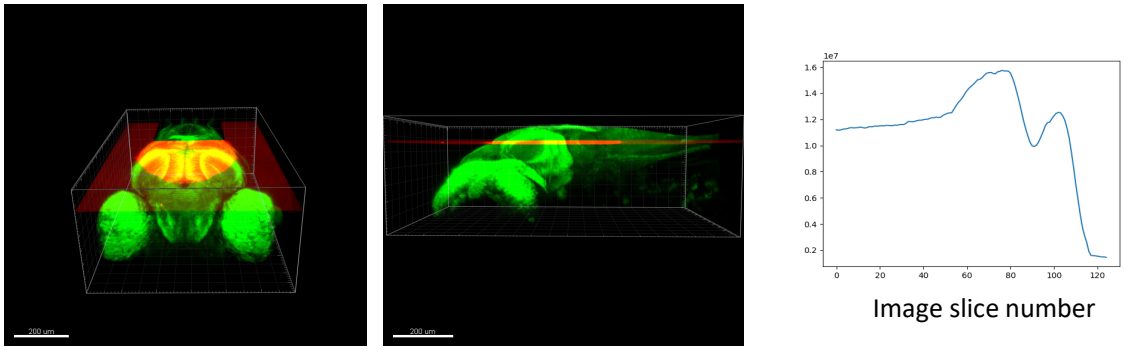

Supplemental Figure 2.3: Target imaging plane.

The imaging plane was determined located at 75 to 81 µm from the dorsal surface. and mapped to a standardized brain

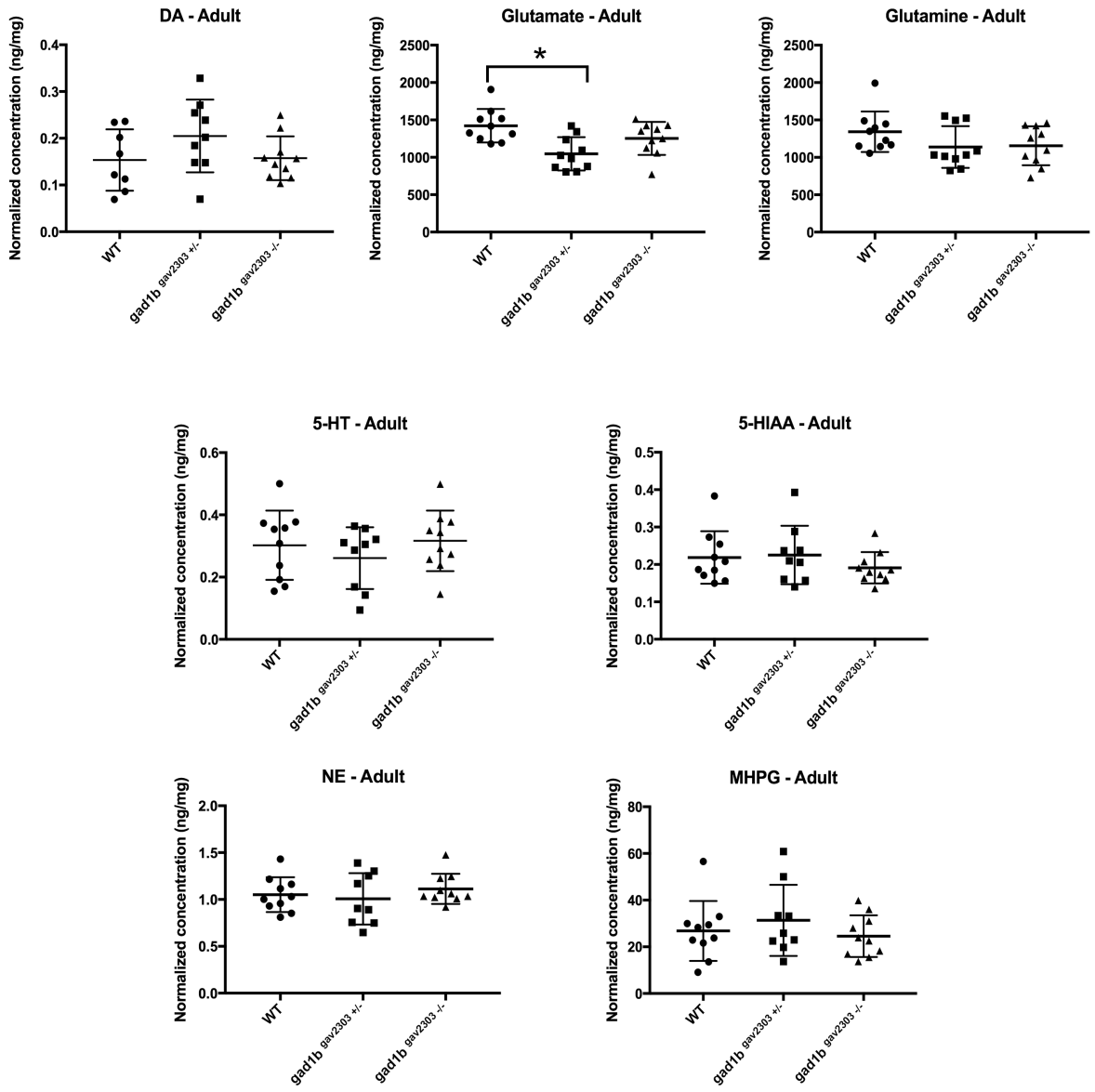

Supplemental Figure 2.4: HPLC-ECD showing the levels other neurotransmitters tested in WT, *gad1b*$^{ga2303\ +/-}$ and *gad1b*$^{ga2303\ -/-}$ adult zebrafish brains.

Normalized concentrations of 7 other neurotransmitters tested in the three genotypes. Abbreviations: 5-HT = serotonin; 5-HIAA = a serotonin metabolite; DA = dopamine; NE = norepinephrine; MHPG = a norepinephrine metabolite. There is no statistically significant change in any of these levels of neurotransmitter across these genotypes except for a decrease in glutamate between WT and *gad1b* $^{+/-}$ (noted with an asterisk).

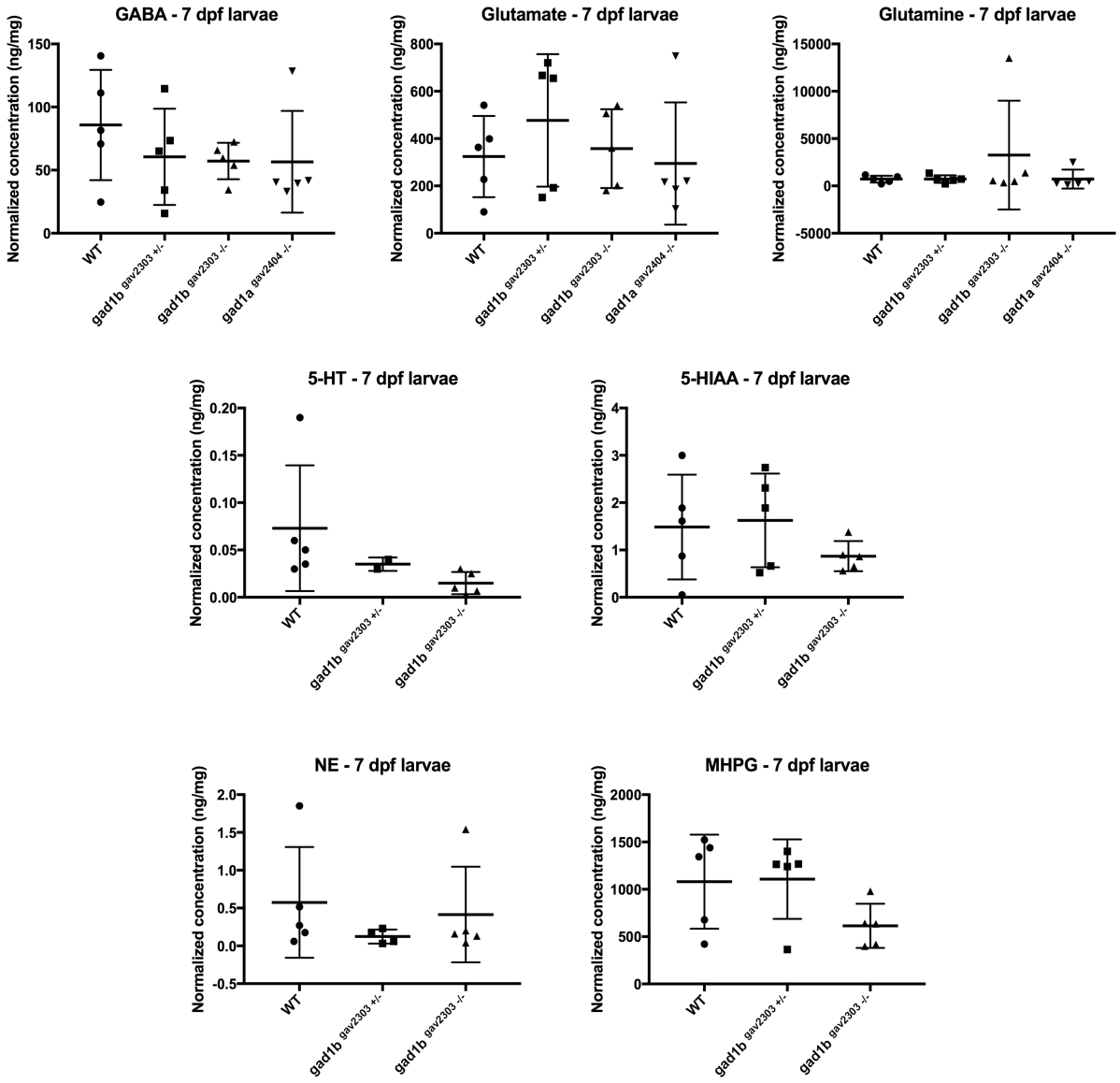

Supplemental Figure 2.5: HPLC-ECD showing the levels other neurotransmitters tested in 7 dpf WT, *gad1b*$^{ga2303\ +/-}$, *gad1b*$^{ga2303\ -/-}$ and *gad1a*$^{ga2404\ -/-}$ larvae.

Normalized concentrations of all neurotransmitters tested in the three genotypes. Abbreviations: 5-HT = serotonin; 5-HIAA = a serotonin metabolite; NE = norepinephrine; MHPG = a norepinephrine metabolite. There is no statistically significant change in any of these levels of neurotransmitter across these genotypes. There is frequently a large amount of variation among these samples.

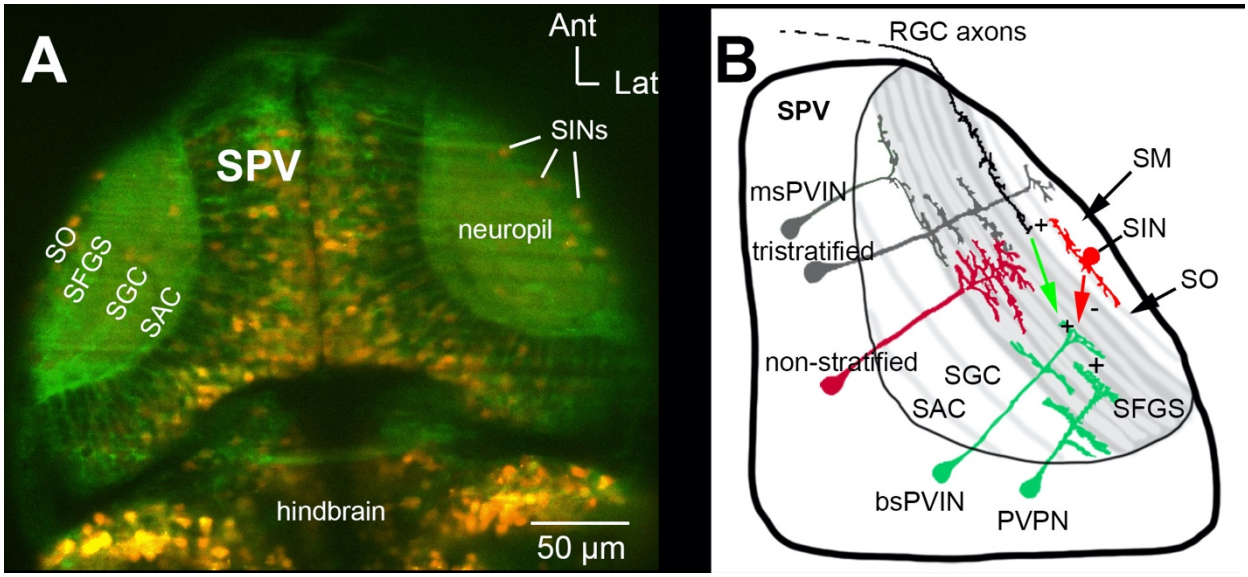

Supplemental Figure 2.6: Optic Tectum Layers

(A) Dorsal view of the optic tectum of a 6 dpf larval zebrafish Tg[*elavl3:GCaMP5g*]; TgBAC[*gad1b:loxP-DsRed-loxP-GFP*]. All neurons express GCaMP5g (green). Neurons expressing TgBAC[*gad1b:loxP-DsRed-loxP-GFP*] (Satou et al., 2013) are in red. (B) Cartoon of the tectum showing cell types and neuropil layers. SINs, bsPVINs, and PVPNs form a hypothetical microcircuit (Nevin et al., 2010). stratum opticum (SO); stratum fibrosum et griseum superficiale (SFGS); stratum griseum centrale (SGC); stratum album centrale (SAC); stratum periventricular (SPV)

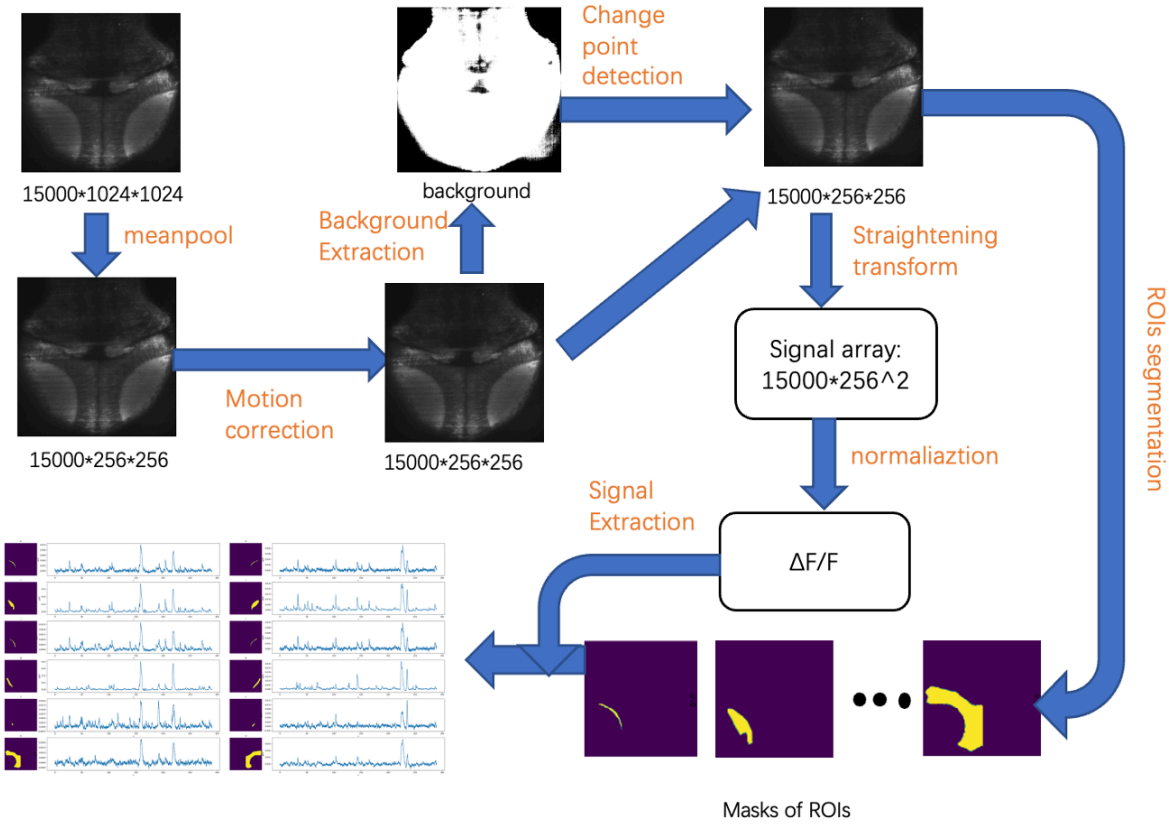

Supplemental Figure 2.7: Change point detection workflow.

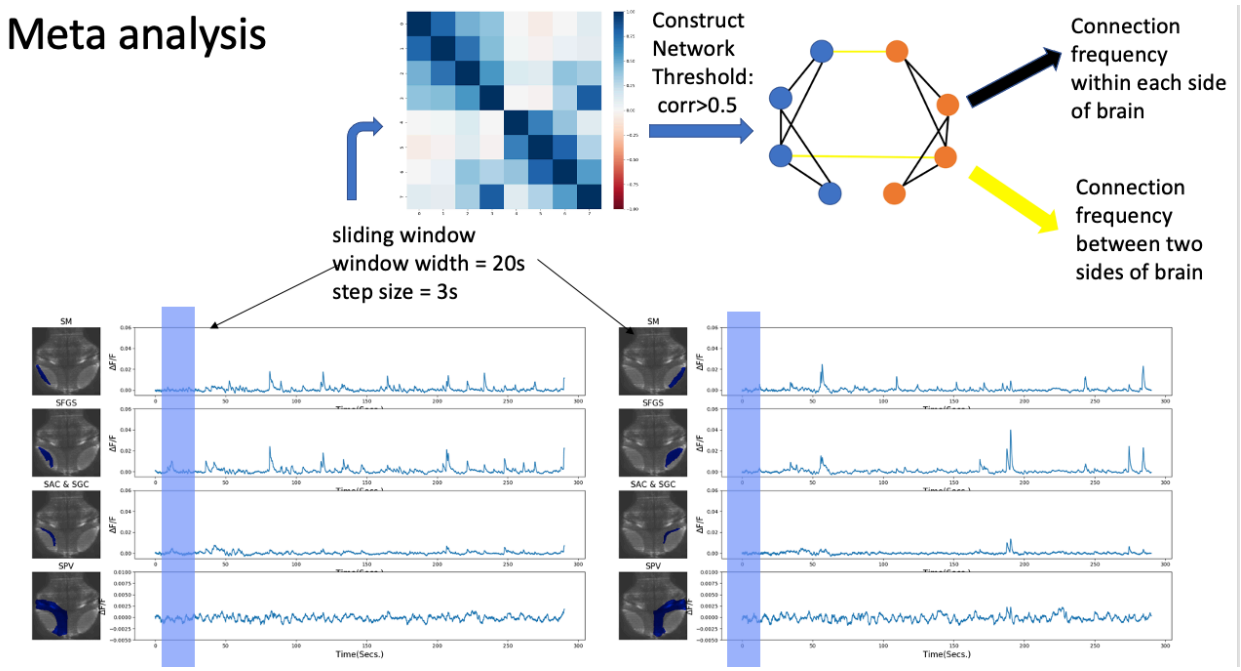

Supplemental Figure 2.8: Meta Analysis Workflow

CHAPTER 3

DECREASED GABA DURING DEVELOPMENT LEADS TO INCREASED CELL NUMBERS AND ALTERS THE EXCITATORY TO INHIBITORY CELL RATIO

Carly R Duffy, Bingxi Liu, Yang Liu, Peter Kner, James D Lauderdale, To be submitted to Developmental Biology

Abstract

The excitatory-to-inhibitory (E/I) balance is an important part of maintaining the appropriate development of neural circuitry in the brain. Disrupting this balance can dysregulate synaptic pruning and lead to a decrease in neural circuitry refinement. GABA, one of the main inhibitory neurotransmitters, plays a crucial role in maintaining the E/I balance. GABA is produced by the conversion of glutamate into GABA by glutamic acid decarboxylase (GAD). In zebrafish, there are three *gad* genes, *gad1a*, *gad1b*, and *gad2*. This makes zebrafish a unique model as *gad1b* mutants and *gad1a* mutants are viable. In the *gad1b*$^{-/-}$ null mutants, there is an increase in neural activity that displays an increase in synchronicity between both sides of the brain, suggesting there could be increased connections or synapses within these mutant's brains. We investigate this by performing volumetric cell counts in WT and mutant fish expressing Tg(*dlx5a.dlx6a:GFP*). The transgene reports expression of the *dlx5a* and *dlx6a* genes. Their expression is functionally significant as the dlx gene family of transcription factors plays an important role in GABAergic neuron development. We found that *gad1b* mutants had a greater number of these neurons compared to WT fish at 8dpf. We also found that the ratio of inhibitory to excitatory neurons was raised in the mutant optic tectum neuropil as there were significantly more Tg(*gad1b:DSRed*) neurons and significantly fewer Tg(*vglut2a:GFP*) neurons. These changes in cellular numbers would be consistent with seeing an increase in neural activity in these fish and could lead to sensory processing issues, as the neural circuitry may not be as defined as in WT fish.

Introduction

During early development, the brain retains a large level of neuroplasticity. There is a rapid formation of synapses that leaves an overabundance of connections, and as development progresses, the unused connections get eliminated through synaptic pruning, which is assumed to be regulated by the excitatory-inhibitory (E/I) balance (Ganguly & Poo, 2013; Nevin et al., 2008). Any disruption in this balance can cause dysregulation of synaptic pruning leading to unrefined neural circuitry, and this is the assumed cause of numerous neurological disorders such as schizophrenia, anxiety, and autism spectrum disorder (ASD). Well known as one of the main inhibitory neurotransmitters, γ- amino butyric acid (GABA) plays an important role during development, along with the excitatory neurotransmitter glutamate. Together, GABA and glutamate are fundamental in maintaining the fine balance of excitation to inhibition (Akerman & Cline, 2007). Therefore, decreased levels of GABA signaling are also associated with numerous neurological disorders as the E/I balance would be disrupted.

GABA is formed by the conversion of glutamate into GABA by glutamic acid decarboxylase (GAD) (Martin & Rimvall, 1993). Humans and most vertebrates have 2 GAD genes, GAD1 (Glutamic Acid Decarboxylase 1) and GAD2 (Glutamic Acid Decarboxylase 2) (Erlander et al., 1991). In humans, mutations in the GAD1 gene are associated with seizures presumably due to reduced synaptic GABA (Chatron et al., 2020; Lynex et al., 2004). Also, work in post-mortem brain tissue of humans with autism reports seeing a downregulation in GABA-$_A$ receptors, which would also block GABA signaling (Zhao et al., 2022). In mice, a null mutation in the GAD1 gene leads to neonatal fatality, making it difficult to study the effects of the mutation on neural activity and brain development in mammals (Asada et al., 1996, 1997; Condie et al., 1997; Kakizaki et al., 2015)

Characterization of the *gad1a* and *gad1b* null mutants revealed that the *gad1b* mutants display "ictal" like events as seen through electrophysiology data, and light sheet imaging of these mutants shows that neural activity is less confined to clear pathways (Liu et al., n.d.). Also, calcium imaging on the light sheet revealed that the *gad1b* mutants display an increase in synchronicity between the right and left sides of the optic tectum, which is suggestive of increased connections (Liu et al., n.d.). This is indicative of having a more complex neural circuitry.

The transcription factor DLX (Distal-less Homeobox) also plays a role in maintaining the E/I balance as it regulates the production of GABAergic neurons by promoting differentiation in their precursor cells (Ghanem et al., 2003; Le et al., 2017; MacDonald et al., 2010; Yu et al., 2011). The transgene used in this paper, Tg(*1.4dlx5a-dlx6a:GFP*), (Zerucha et al., 2000), reports the expression of the *dlx5a* and *dlx6a* genes in the zebrafish. Expression of *dlx5a* begins in early development at the 1-4 somite range (Thisse & Thisse, 2005). By 1 day post-fertilization (dpf), *dlx5a* is expressed strongly in the forebrain (Thisse & Thisse, 2005) and continues to be expressed in the forebrain at 5 dpf. *dlx5a* expression is also reported in the 6 months post-fertilization adult zebrafish forebrain.(Mendes et al., 2020) However, within the optic tectum, the expression of *dlx5a* appears sparse and begins to shut down by 2dpf (Thisse & Thisse, 2005), and it is not detected within the optic tectum in adults (Mendes et al., 2020)

In our studies, we look at developmental stages past 4dpf, when *dlx5a* is no longer detected through mRNA in situ. The Tg(*1.4dlx5a-dlx6a:GFP*) transgene, however, does express in the optic tectum during later stages of development (Zerucha et al., 2000). Since this transgene faithfully captures *dlx* expression in the 1dpf zebrafish and in the forebrain at later developmental ages, we believe this reporter to be a good tool for labeling GABAergic

precursors in optic tectum. The sparse labeling of the Tg(*1.4dlx5a-dlx6a:GFP*) in the optic tectum allows for accurate volumetric cell counts, and it is functionally significant since DLX proteins are transcription factors that regulate GAD genes. Therefore, to investigate potential changes in neural connectivity, we focused on GFP positive cell numbers in WIK (henceforth referred to as WT) larvae expressing the Tg(*1.4dlx5a-dlx6a:GFP*) and the *gad1b*$^{-/-}$ mutants expressing the Tg(*1.4dlx5a-dlx6a:GFP*) transgene.

Prior research looking at Tg(*1.4dlx5a-dlx6a:GFP*) neuron numbers at 5 dpf in an *scn1lab,* which codes for a voltage-gated sodium channel, mutant saw no significant difference than WT numbers at the same age (Grone et al., 2017). However, additional work in zebrafish has shown that in a morphant of *scn1lab*, there was an overall increase in the ratio of excitatory to inhibitory expressing cells at 4 dpf and 5dpf (Brenet et al., 2019). However, within zebrafish, there is a structural reorganization between 5 and 6 dpf that begins subsiding at 7-8 dpf (Avitan et al., 2017). It is believed this time of high spontaneous activity at 5 and 6 dpf is when the brain is learning which neurons to retain for fine-tuned circuitry (Avitan et al., 2017). Interestingly, there has been work in mice showing a vesicular GABA transporter (VGAT) conditional knockout and a $GABA_A$ receptor conditional knockout both have increased levels of neural synchronicity and participation in network activity which leads to interneuron survival as they are protected from apoptosis (Duan et al., 2020).

Typically, in studies of brain development in the zebrafish, prior research has ceased investigations at 5 dpf despite evidence that the brain is undergoing abundant neural refinement at that age (Avitan et al., 2017; S.C. Baraban et al., 2005; Scott C. Baraban et al., 2013; Grone et al., 2017; Hortopan et al., 2010). Since GABA signaling plays an important role in these critical points of establishing neural circuits, there is good cause for belief that the *gad1b*$^{-/-}$ larvae brain

may have less refined neural circuitry. Therefore, we investigated total cell numbers continuing past the period of spontaneous neural activity as well as the excitatory-to-inhibitory cellular ratio after the said period. We found that at 8dpf, there are more Tg(*1.4dlx5a-dlx6a:GFP*) neurons in the optic tectum, and that there is a decrease in the ratio of Tg(*vglut2a:GFP*) to Tg(*gad1b:DSRed*) expressing cells in the superficial layer of the neuropil.

Materials and Methods

Fish rearing and genotyping

Adult and larval zebrafish (*Danio rerio*) were obtained from lines maintained in the University of Georgia Zebrafish Facility following standard procedures (Westerfield, 2007). Embryos and larvae were staged using standard staging criteria (Kimmel et al., 1995; Westerfield, 2007). Wild-type fish of the WIK strain were originally obtained from the Zebrafish International Research Center (ZIRC). Fish Transgenic for TgBAC(*1.4dlx5a-dlx6a:GFP*) were obtained from Marc Ekker (Zerucha et al., 2000). Fish transgenic for TgBAC[*gad1b*: loxP-DsRed-loxP-GFP] (Satou et al., 2013)were obtained from Dr.Shin-ichi Higashijima. Fish transgenic for TgBAC(*vglut2a:GFP*) were obtained from Dr. Harold Burgess with permission from Dr.Shin-ichi Higashijima. All adult fish were maintained in an Aquatic Habitats (Apopka, FL) multi-rack system. Habitat water consisted of reverse osmosis filtered/sterilized water to which sodium bicarbonate and other salts (Instant Ocean, Aquarium Systems, Inc., Mentor, OH, USA) were added to maintain pH from 7.0-7.4 and conductivity between 400 and 430 µS. All experimental procedures were conducted in accordance with National Institutes of Health guidelines for the use of zebrafish in research under protocols approved and overseen by the University of Georgia Institutional Animal Care and Use Committee.

Transgenics were crossed to *gad1b* $^{-/-}$ or *gad1b*$^{+/-}$ fish and genotyped for *gad1b* $^{+/-}$. Lines exhibiting fluorescence were then in-crossed and genotyped until transgenic *gad1b* $^{-/-}$ mutants expressing the transgenes were identified. Fish were genotyped through fin clip and PAGE analysis described in Chapter 2. Offspring positive for RFP from a *gad1b*$^{-/-}$ fish crossed to WIK, Tg(*gad1b*:DSRed) are genotyped using PAGE analysis similar to before. However, due to the presence of the *gad1b* genome sequence in the BAC, all fish expressing RFP show a strong WT band on the gel whether WT, heterozygous, or homozygous. To work around this, Tg(*gad1b:DSRed*) fish showing a mutant band on the PAGE were crossed to non-transgenic *gad1b*$^{-/-}$ fish. RFP-positive offspring were removed from the larval population, and non-RFP-expressing fish were pooled together for genotyping to determine if the RFP-expressing parent was homozygous mutant or heterozygous. Any presence of a WT band means the parent is *gad1b*$^{+/-}$

Fish are sorted for fluorescence on a Zeiss Stemi SV 11 dissecting scope using an Xcite-series 120Q fluorescent illumination system. For live imaging of Tg(*dlx5a-dlx6a:GFP*), larvae are dark-reared to 4, 6, 8, and 10dpf. 10dpf larvae were provided with a small amount of GEMMA micro 75 starting at 8dpf to avoid nutritional deficiencies leading to death. For live confocal imaging, Tg(*gad1b:DSRed), Tg(vglut2a:*GFP*),* larvae are dark-reared until 6dpf and 8dpf. Larvae were treated with 0.003% PTU starting at 20 hpf and the solution was changed out each day until imaging.

For HCR in situs, WT Tg(*1.4dlx5a-dlx6a:GFP*)$^{tg/0}$ fish are dark-reared until 6dpf. Fish are euthanized in 6.4mg/mL tricaine MS-2222 (Syndel, Lot 15521) and fixed in 1ml 4% PFA at room temperature for 2 hours. Fish are rinsed 3X in 1X PBS-Tween and then transitioned

through 3 steps into methanol. 3 washes are done in methanol, and fish are stored until ready for usage.

Light sheet imaging

WT, Tg*(1.4dlx5a-dlx6a: GFP)* and *gad1b*$^{-/-}$, Tg*(1.4dlx5a-dlx6a: GFP)* larvae at ages 4, 6, 8, and 10 dpf were anesthetized with 1.6mg/100ml Tricaine (MS-2222)(SYNDEL) (diluted from a 4mg/ml stock) and mounted in 0.5% SeaPlaque low melt agarose (BioProdcuts, Cat # 50100) and pipetted up into a small mounting tube. Once solidified, the agarose/fish can be slowly pushed out from the mounting tube and placed for light sheet imaging. Approximately 210 images are taken through the brain every 1.5 µm. The Z stack is saved as a tiff that can be opened in ImageJ. The aspect ratio is set within ImageJ where 1 pixel equals 0.2444789 µm x0.2444789 µm and Z=1.5 µm. Background levels are subtracted from all slices and the file is saved as a new tiff (Figure 3.1A-B). The layout of the LSFM(Figure 1B, Figure S1) is a modification of the design used in our collaborator's previous work and incorporates the ETL as in Fahrbach et al (Fahrbach et al., 2013; Liu et al., 2020, 2023).

Cell counts with IMARIS Spots analysis.

Processed tiff files from light sheet imaging, are converted into .ims files using the IMARIS file converter. Within IMARIS, cells are counted using the “spots” function (Figure 3.1C-D). Cell size is set at 6.5 µM and Z stretching is taken into consideration. Thresholding is handled manually, as automatic thresholding leads to vastly different results between samples. Once spots are counted, XYZ filters are used to mask out the optic tectum (Figure 3.1C-D). Spots that remain that are not part of the optic tectum are deleted manually. Due to not being able to distinguish the tegmentum from the optic tectum, the tegmentum is included in counts. Counts are plotted in GraphPad PRISM where a Mann-Whitney multiple t-test is performed.

Volume measurements on ImageJ

To normalize the data to tecta volume, measurements were taken on ImageJ using the tiff files (Figure 3.1E-F) An equation for the volume of an oval was used to gather an estimated volume for the right and left sides of the optic tectum, and those two values were added together to obtain an estimated total tectal volume (Figure 3.1F). For Z measurements, the first stack containing tecta slices was subtracted from the last stack of the tecta and multiplied by 1.5µm to get the dorsal-to-ventral measurement of the tectum (Figure 3.1F). For the radii of the oval, measurements were taken in the middle stack of the tectum from anterior to posterior diagonal and from left to right diagonal for both sides of the tectum, (Figure 3.1E) Raw and normalized values were plotted and analyzed in the PRISM software.

TUNEL and Keyence microscopy

TUNEL was performed using the DeadEnd fluorometric TUNEL system from Promega(Lot# 0000505372), following the manufacturer's protocol with optimizations. *gad1b* and WT fish treated with 0.003% PTU are fixed at 6 and 7 dpf and dehydrated into methanol. Samples are washed in 6%H2O2 in methanol and then rehydrated into PBST. Samples are permeabilized in 20µg/ml Proteinase K in PBST for 30 minutes rocking at room temperature. The Proteinase K solution is diluted with 2 quick PBST washes. The samples are then post-fixed in 4% PFA for 20 minutes at room temperature. Samples are washed 5 times in PBST before proceeding with equilibration and the TUNEL reaction takes place as described in the manufacturer’s protocol. To prepare for imaging, samples are stained with 1X DAPI to label nuclei and then washed in a 10 mM CUSO4, 50 mM ammonium acetate solution to decrease background fluorescence due to lipofuscin from blood cells. TUNEL samples are mounted in 70% anti-fade glycerol on glass slides with a petroleum jelly wall to prevent flattening of the

samples. Imaging was done on a Keyence BZ-X710 using the 20x objective. The quick full-focus feature was used to create a max-intensity projection of the optic tectum. TUNEL labeling was counted manually within the optic tectum. Tectal boundaries were based on the DAPI labeling. Results were plotted in Prism and a Mann-Whitney multiple t-test was performed using GraphPad Prism.

Confocal Microscopy and live imaging for *gad1b*: *vglut2a* ratio

For ratios of Tg(*gad1b*: *DSRed*) to Tg(*vglut2a*: *GFP*) expressing cells, images were obtained of live zebrafish at 6dpf and 8dpf on a Zeiss LSM880 using the 20X objective for both WT and *gad1b*$^{-/-}$ mutant fish. Fish were anesthetized in tricaine (MS-222-SYNDEL) and mounted in 3% methylcellulose containing tricaine. A wall made from petroleum jelly was used to prevent the fish from being flattened. Images were taken from a dorsal down view, however, due to fish turning because of the yolk, images were taken with a slight tilt as shown in Figure 3.5 focusing on the dorsal layers of the neuropil containing superficial interneurons.

Cell counts were obtained using the ImageJ manual cell counter plugin. A dorsal image capturing a superficial layer of the tectal neuropil was used to count Tg(*gad1b: DSred*)-positive and Tg(*vglut2a: GFP*)-positive cells. Raw data of total *gad1b* and total *vglut2a* expressing cells were plotted and analyzed in Prism, and the ratio was plotted of vglut2a/gad1b was calculated in Excel and analyzed in Prism. A Mann-Whitney multiple t-test was performed within PRISM GraphPad.

Confocal microscopy live imaging tg(*dlx5a.dx6a:GFP*) and tg(*gad1b:DSRed*)

WT, Tg(*1.4dlx5a-dx6a:GFP*), Tg(*gad1b:DSRed*) and *gad1b*$^{-/-}$, Tg(1.4*dlx5a-dx6a:GFP*), Tg(*gad1b:DSRed*) fish are anesthetized for imaging in tricaine in egg water as described earlier and mounted in 3% methylcellulose in egg water containing tricaine to keep fish anesthetized

through imaging. Visualization is done on the LSM880 focusing on the neuropil of the optic tectum. Photos were analyzed to assess Tg(*gad1b:DSRed*) and Tg(1.4*dlx5a-dlx6a:GFP*) co-expression.

HCR in situ hybridizations and immunofluorescence.

To determine the co-expression of *gad1b* and *gad1a* with Tg(*1.4dlx5a-dlx6a:GFP*), HCR in situ with anti-GFP immunofluorescence was performed according to the manufacturer's protocol at Molecular Probes and as described in chapter 2, with a modification at the amplification step. For anti-GFP immunolabeling, 2 µl of anti-GFP-Alexa 647(Invitrogen, Cat#A-31852) was added to the hairpin reaction mixture. For probe and hairpin sets see Table 3.1. A Zeiss LSM880 was used to image at 20x, 40x, and 63x objectives.

Results

***gad1b*$^{-/-}$ larvae have a greater number of Tg(*dlx5a.dlx6a:GFP*) expressing cells compared to WT at 8 dpf**

In one of our recent studies, we found that *gad1b*$^{-/-}$ larvae displayed an overall increase in neural activity within the optic tectum. This increase in neural activity was found to have a higher level of synchronicity between the left and right sides of the optic tectum (Liu et al., n.d.). We believe this higher level of synchronicity could be due to an increase in synaptic connectivity. It is possible that developing with an interrupted E/I balance has dysregulated synaptic pruning, leading to less fine-tuned circuitry. To test this idea, we imaged GFP-expressing cell bodies that label GABAergic interneuron precursor cells throughout development in the optic tectum of WT, Tg*(1.4dlx5a-dlx6a:GFP*), and in *gad1b*$^{-/-}$, Tg(*1.4dlx5a-dlx6a:GFP*) larvae (Figure 3.1 A) using light sheet microscopy (Figure 3.1 B). We then performed

volumetric cell counts with the "spots" analysis function on IMARIS (Figure 3.1 C-D). To visualize changes in a developing embryo, we imaged the GFP-expressing cell bodies in the optic tectum of the larvae at 4, 6, 8, and 10dpf. These time points span a functionally significant developmental period where a high level of circuitry refinement is thought to take place (Avitan et al., 2017) This transgene was chosen due to the role of the *dlx5a/dlx6a* genes in regulating GABAergic neuron development and the transgene's sparse expression within the optic tectum.

Throughout development, the WT larvae were found to have a decrease in the total number of Tg(*dlx5a.dlx6a:GFP)* expressing neurons in the optic tectum (, Figure 3.2A Table 3.1). They have an average of 564.1 ± 94.7(SD) GFP-expressing cells at 4dpf which decreased to 527.3 ± 103.5(SD) GFP-expressing cells at 6dpf, further decreasing to 483.8 ± 94.5 (SD) GFP-expressing cells at 8dpf, and then showing a slight increase to an average of 511.2 ± 102.6 (SD) GFP-expressing cells at 10dpf (Figure 2A, Table S3.1). Despite decreasing GFP cell numbers, they exhibited an increase in the volume of their optic tectum with an average of 3.7± 0.41 $*10^5$ (SD) μm^3 at 4dpf, $4.5*10^5$ ± 0.79(SD) μm^3 at 6dpf, 4.8 ± 0.95(SD) $*10^5$ μm^3 at 8dpf, and 4.4 ± 0.58 $*10^5$(SD) μm^3 at 10dpf (Figure 3.1E-F, Figure 3.2D). When normalizing the cell number to the volume of the optic tectum, the WT larvae showed a decrease in the density of GFP-expressing cells with an average of 151.5 ± 24.8 (SD) cells/100μm^3 at 4dpf which decreased to an average of 119.2 ± 26.1 (SD) cells/100μm^3 at 6dpf and further decreased to an average of 104.2 ± 30.7 (SD) cells/100μm^3 at 8dpf, and a slight increase to 119.1 ± 23.7 (SD) cells/100μm^3 at 10dpf (Figure 3.2G).

Meanwhile, Tg(1.4*dlx5-dlx6a:GFP*) expressing cells did not vary as appreciably between developmental time points in *gad1b*$^{-/-}$ larvae (Figure 3.2B, Table S3.2). They had an average of 513.8 ± 95.3 (SD) GFP-expressing cells at 4 dpf which then increased to an average of 545.6±

85.6 (SD) GFP-expressing cells at 6 dpf. The cell number did not change significantly at 8 dpf with an average of 544.2±107.3 (SD) GFP-expressing cells followed by another increase to an average of 565.2 (SD) GFP-expressing cells at 10 dpf (Figure 3.2B, Table S3.2). Like WT, *gad1b*$^{-/-}$ larvae's optic tectum volume also increased throughout development with an average of 2.7±0.45*10^5 (SD) μm^3 at 4dpf, 3.2±0.55*10^5 (SD) μm^3 at 6dpf, 3.7±0.60X10^5 (SD) μm^3 at 8 dpf, and 3.5±0.90*10^5 (SD) μm^3 at 10dpf (Figure 3.2E). When normalizing the cell number to the volume of the optic tectum, *gad1b*$^{-/-}$ larvae displayed a decrease in the average cell density in the optic tectum over the course of development with an average of 192.6±40.7 (SD) cells/100μm^3 at 4dpf which decreased to an average of 176.5±41.0 (SD) cells/100μm^3 at 6dpf and further decreasing to an average of 150.6±35.7 (SD) cells/100μm^3 at 8dpf. There was a slight increase to an average of 169.2±49.6 (SD) cells/100μm^3 at 10dpf (Figure 3.2H)

When comparing the WT to *gad1b*$^{-/-}$ larvae, it is found that the mutants have significantly more GFP-expressing neurons at 8dpf than WT (Figure 3.2C). Additionally, the volume of the optic tectum of *gad1b*$^{-/-}$ larvae is significantly less than that of WT at all developmental time points imaged (Figure 3.2F). Subsequently, when normalizing the cell numbers to tectum volume for each larva, we found that this density of cells was significantly higher in *gad1b*$^{-/-}$ fish at all time points (Figure 3.2I)

gad1b$^{-/-}$ larvae have less TUNEL at 6 dpf and 7 dpf.

Since a decrease in cell numbers was observed in only the WT larvae, fluorescent terminal deoxynucleotidyl transferase dUTP nick end labeling (TUNEL) was performed to detect any apoptosis that may be taking place in WT but not *gad1b* mutants. Images were captured using the quick full-focus function on a Keyence BZ-X710 to create a max-intensity projection

of the larvae's optic tectum. These images were used to count cells labeled with TUNEL in the optic tectum, of which boundaries were determined based on DAPI staining (Figure 3.3A).

We were not able to detect any apoptosis taking place between 3-5 dpf in WT fish and *gad1b*$^{-/-}$ larvae (data not shown). Since we observed a significant difference in GFP cell numbers between WT and *gad1b*$^{-/-}$ at 8 dpf, we chose to check for apoptosis at 6 and 7 dpf. At 6 dpf, we began to detect TUNEL signal in the optic tectum of WT larvae and *gad1b*$^{-/-}$ larvae, indicating apoptosis may be taking place. There was an average of 30.0±7.5 (SD) TUNEL cells in WT larvae and 15.1±5.8 (SD) TUNEL cells in *gad1b*$^{-/-}$ larvae. (Figure 3.3B-C, Table S3.3). We also detected TUNEL in both genotypes at 7 dpf with an average of 47.7±16.9 (SD) TUNEL cells in WT larvae and 13.0±7.5 (SD) puncta in *gad1b*$^{-/-}$ larvae. We found that at both 6 dpf and 7 dpf, *gad1b*$^{-/-}$ larvae had significantly less TUNEL labeling than WT larvae (Figure 3.3 B-C).

gad1b and _gad1a_ expression in GABAergic precursors in the optic tectum

A transcription factor from the family of *dlx* genes is required to make GABAergic neurons as they regulate GAD expression, particularly *dlx5a* (Ghanem et al., 2003; Le et al., 2017). However, *dlx5a* is not expressed in the optic tectum past 2dpf. Therefore, we used a *dlx* expression transgene that does not shut down in later developmental ages. This transgene faithfully replicates *dlx* expression in the early forebrain and tectum and matches *dlx* expression in the forebrain at 5df. To test if there were any *dlx5a* expressing cells in the tecum at 5dpf that have been previously missed, we probed using HCR, a more sensitive detection method. We were unable to detect any *dlx5a* transcripts in the optic tectum at this age (Figure S3.6).

Consequently, to validate whether *gad1b* was co-expressed as expected in the cell population labeled by Tg(*dlx5a.dlx6a:GFP*) in our lineage of WIK, Tg(*1.4-dlx5a-dlx6a:GFP*) larvae at later developmental stages, we performed live imaging of Tg(*dlx5a.dlx6a:GFP*),

Tg(*gad1b:DSRed*) in double transgenic WT larvae at 6dpf and 8 dpf, as well as in situ hybridizations of *gad1b* and *gad1a* with antibody labeling of GFP in 6dpf WT Tg(*1.4-dlx5a-dlx6a:GFP*) larvae.

Live imaging of 6dpf and 8dpf WT, Tg(*dlx5a.dlx6a:GFP*), Tg(*gad1b:DSRed*) on a Zeiss LSM 880 confocal microscope showed the majority of Tg(*dlx5a.dlx6a:GFP*) larvae express the Tg(*gad1b:DSRed*) transgene at both 6dpf and 8dpf throughout the tectum (6dpf Figure 3.5A, 8dpf data not shown, Figure S3.5) Some expressed Tg(*gad1b:DSRed*) at a low level and some expressed the *gad1b* transgene at a high level. This is observed in superficial layers of the optic tectum neuropil (Figure 3.5A) and in deeper SPV layers. (Figure 3.5B) Particularly, superficial interneurons (SINs) had a higher level of expression than deeper neurons in the SPV and the neuropil. (Sigure 3.5A, Figure S3.5). A small number of Tg(*dlx5a.dlx6a:GFP*) positive cells did not co-express with Tg(*gad1b:DSRed*) (Figure 3.5A).

In the larval zebrafish optic tectum, *gad1b* transcripts are detected in many neurons in the SPV and neuropil. Approximately 50% (not quantitated) of *gad1b*-expressing neurons are expressed with *gad1a* (Figure 3.6A-B, Figure S3.4) (Liu et al., n.d.). As far as cells with *gad1a*-detected transcripts, these cells mostly co-expressed with *gad1b*, though *gad1a* transcripts are also detected in a small number of cells without *gad1b* expression (not quantitated) (Figure 3.6B) (Liu et al., n.d.)Therefore, *gad1a* transcripts are detected in fewer neurons than *gad1b,* with sparse expression in the neuropil. Particularly, there is little expression of *gad1a* in SINs. (Figure 3.6A)

To investigate which population of *gad1b* positive cells are co-expressed in Tg(*dlx5a.dlx6a:GFP*) expressing cells, we performed mRNA in situ labeling of *gad1a* and *gad1b* transcripts and immunofluorescence labeling of GFP in 6dpf Tg(*1.4dlx5a-dlx6a:GFP)* larvae.

We found the Tg(*dlx5a.dlx6a:GFP*) positive cells represent both *gad1a* positive and *gad1b* positive cells and *gad1b* positive only cells(Figure 3.6A-B). We never detected *gad1a* expressed without *gad1b* in Tg(*dlx5a.dlx6a:GFP*) cells (Figure 3.6A-B). We also saw that some GFP-positive cells did not express either *gad1a* or *gad1b* (Figure 3.6B).

***The vglut2a:gad1b* ratio decreases in *gad1b*$^{-/-}$ larvae tecal neuropil.**

To investigate if the altered numbers of GABAergic precursors in *gad1b* mutants affected the excitatory-to-inhibitory ratio in the optic tectum, we performed cell counts of RFP-positive inhibitory neurons and GFP-positive excitatory neurons. In these experiments, we imaged only one layer of the optic tectum in the neuropil. This avoided complications of ambiguously determining and assigning individual cells in the SPV due to the nature of the dense expression of tg(*gad1b:DSRed*) and tg(*vglut2a:GFP*) making it more difficult to recognize the boundaries of cells (Figure 3.6A). We chose to focus on cells expressed in the superficial layers of the optic tectum neuropil, likely the stratum opticum and stratum marginale where SINs are located (Figure 3.6A). SINs are significant to this study as they receive sensory information from multiple areas of the brain and are both excitatory and inhibitory.

We found that at 6 dpf WT larvae had an average of 74.45±21.54 (SD) Tg(*gad1b:DSRed*) expressing cells and 14.13±5.74 (SD) Tg(*vglut2a*:GFP) expressing cells, and at 8 dpf had an average of 58.18±25.81 (SD) Tg(*gad1b:DSRed*) expressing cells and 16.42±5.05 (SD) Tg(*vglut2a*:GFP) expressing cells. The *gad1b*$^{-/-}$ larvae at 6dpf had an average of 77.31(SD) 23.43 (SD) Tg(*gad1b:DSRed*) expressing cells, and15.27±5.64 (SD) Tg(*vglut2a*:GFP) expressing cells and at 8dpf had 69.51±22.91 (SD), Tg(*gad1b:DSRed*) expressing cells and 13.54±4.70 (SD) Tg(*vglut2a*:GFP) expressing cells (Figure 3.6B-C, Table S3.4).

At 6 dpf, there was no difference between WT and *gad1b* larvae for either Tg(*gad1b:DSRed*) expressing cell numbers or for Tg(*vglut2a*:GFP) expressing cell numbers (Figure 3.6B-C, Table S3.4). Therefore, the excitatory-inhibitory ratio was unaffected at 6dpf. (Figure 3.6D-E, Table S3.4) However, at 8 dpf there was a significant difference between WT and *gad1b*$^{-/-}$ larvae as the mutants had slightly more Tg(*gad1b:DSRed*) expressing SINs and slightly less Tg(*vglut2a*:GFP) expressing SINs than WT larvae (Figure 3.6B-C, Table S3.4). This led to a significant decrease at 8 dpf in the ratio of Tg(*vglut2a*:GFP)/Tg(*gad1b:DSRed*) expressing SINs (Figure 3.6D-E, Table S3.) as the WT average ratio was, 0.28±0.07 at 8dpf, and the mutants' average ratio was 0.20±0.06 (SD). This is consistent with seeing a change in the raw number of total Tg(*dlx5a.dlx6a:GFP*) expressing cells at 8 dpf but not 6 dpf (Figure 3.2C).

Discussion

Previously, we found that the *gad1b* mutants have an increase in neural activity that is less confined to clear pathways, and through a metanalysis, found there is an apparent increase in the synchronicity of their neural activity between the left and right sides of the optic tectum at 5dpf (Liu et al., n.d.). As these mutant larvae have developed with decreased levels of GABA, therefore interrupting their E/I balance, it is likely there is a dysregulation in their neural circuitry refinement, and with evidence of increased synchronicity, we can presume these mutants are experiencing dysregulated synaptic pruning where soma and their synapses that would have been targeted for elimination are kept due to their increased activity (Chapman et al., 2022; Chechik et al., 1998; Isaacson & Scanziani, 2011; Jill, 2020; Nevin et al., 2008; Paolicelli et al., 2011; Turko et al., 2019).

To investigate if this is the case in the *gad1b*$^{-/-}$ larvae, we measured the numbers of Tg(*dlx5a.dlx6a:GFP*) expressing neurons which represent a subset of GABAergic neurons. We found that at 8 dpf, the total number of Tg(*dlx5a.dlx6a:GFP*) expressing neurons in the optic tectum of the mutants was significantly larger than that of the WT larvae. This is consistent with the idea that the restructuring and pruning of unused neurons within the brain to fine-tune neural circuitry is taking place in zebrafish between days 5-6 dpf and has settled down by 8 dpf (Avitan et al., 2017; Marachlian et al., 2018). Interestingly, when measuring tectal volume, it became apparent that the *gad1b*$^{-/-}$ larvae had a consistently smaller size than WT despite having more neurons. When normalizing the cell counts to tecta volume, the density of cells per area in *gad1b*$^{-/-}$ larvae was significantly greater than the WT larvae at every stage measured.

Our results showing that *dlx5a* transcripts are not expressed in the optic tectum at 5 dpf is consistent with others' findings (Mendes et al., 2020). Publicly available HCR in situ data (Mapzebrain), does not detect *dlx5a* expression in the optic tectum of zebrafish at 5dpf (Shainer et al., 2023). Additionally, the Tg(*1.1dlx5a-dlx6a:GFP*) data on Mapzebrain, shows GFP expression similar to our transgenic data (Shainer et al., 2023). The HCR expression of *dlx5a* transcripts is far lesser than the transgenic GFP expression (Figure S3.6). This transgene is often used in studies of brain development and in labeling GABAergic precursors (Scott C. Baraban et al., 2013).

Since these experiments looked at later developmental stages than typically studied, we chose to validate the expression profile of the *gad1b* and *gad1a* paralogs. First, focusing on *gad1b*, using the transgene Tg(*gad1b:DsRed*), we found that the majority of the Tg(*1.4dlx5-dlx6a:GFP*) expressing cells, did coexpress with DSRed, meaning GABAergic precursors were still being labeled by the GFP cells. Secondly, since there is evidence of *gad1a* coexpression with

only some *gad1b* expressed cells, we wanted to probe for *gad1a*, as its co-expression with the *dlx* transgene has not been widely elucidated. We found that both *gad1b* positive cells and *gad1a* and *gad1b* positive cells are found coexpressed in GFP positive cells. Meaning the sparse labeling by the reporter transgene does not represent only one of those populations of cells. This also means there is potentially an increase in both *gad1b*-only cells and *gad1b* and *gad1a*-positive cells. It would be interesting to see if *gad1b* positive cells also positive for gad1a transcripts increase in the mutants or if only *gad1b* positive cells increase. As mentioned earlier, no GFP-labeled cells that express only *gad1a* transcripts were detected, meaning it is likely that the increase in cell numbers observed does not represent *gad1a*-only neurons. We also found that the transgene sometimes does not express either transcript. More investigation is needed to determine if the lack of co-expression in this small number of GFP-positive cells is a technical issue or a significant finding. If this finding is significant, then there could be an increase in cell numbers that are not expressing *gad1a* or *gad1b* transcripts.

The decreasing neuron numbers in the WT observed across development is consistent with the idea of synaptic pruning (Chechik et al., 1998; Jill, 2020). Since the *gad1b* mutants' neuron numbers were not decreasing, we tested if less apoptosis was occurring using TUNEL. We looked at 6 and 7 dpf since the largest difference was seen at 8 dpf. In the WT, we found that there is apoptosis taking place by 6 dpf in the optic tectum, and that amount of apoptosis increases at 7 dpf. However, the *gad1b*$^{-/-}$ mutants had significantly less apoptosis occurring at 6 dpf with no increase in apoptosis at 7 dpf, which is consistent with our results showing no decrease in the *gad1b*$^{-/-}$ larvae's cellular numbers at 8 dpf.

We then wanted to illuminate how this dysregulated synaptic pruning affects the ratio of excitatory cells to inhibitory cells. We focused on SINs in the optic tectum, which represents

both excitatory and inhibitory neurons, as SINs processing remains local within the brain, as they have short dendrites that communicate locally with other neurons of the optic tectum. We see that there is a decrease in the ratio of excitatory to inhibitory labeled SINS. Interestingly, we saw an increase in the *gad1b* cell population and a decrease in the *vglut2a* population leading to a decrease in the E/I cell ratio. It is possible that to make up for a lack of GABA due to the *gad1b* mutation, the brain is trying to increase the number of *gad1b*-expressing cells to increase the levels of GABA present and decrease the number of *vglut2a* expressing cells to lower the levels of excitation occurring since the current GABA levels cannot properly maintain the needed level of inhibition.

Our results are consistent with the reports from Duan et al 2020, where they found that increased activity synchronicity, in mice with a vesicular GABA transporter (VGAT) conditional knockout and a $GABA_A$ receptor conditional knockout led to interneuron survival not increased apoptosis. The *gad1b* mutants also display increased synchronicity in neural activity, and labeling of the 6 and 7 dpf *gad1b* mutants did detect less apoptosis occurring in their optic tectum than in WT. However, these results are the differing from what was observed in Brenet, et al 2019. They performed their studies on a *scn1lab* morphant in zebrafish, which serves as a model of a severe form of epilepsy, and their work also looked at the whole tecta ratio. It is possible their larvae were undergoing excitation toxicity, as they did see increased apoptosis and a total decrease in cellular numbers. The apoptosis we observe is consistent with what we see in the neuron numbers at 8dpf. This does not continue to 10dpf, however, that could be due to the larvae, particularly the mutants, not surviving out to 10 dpf well.

Acknowledgments

The authors wish to thank Dr. Heike Kroger, Sneha Mohan, Rida Osman, and Christina Sabine for their helpful discussions on this project. This work was supported by the National Institutes of Health (Grant No. R01NS090645 to JDL, PAK, and F31NS115496 to YL) and the National Science Foundation (Grant No. 1350654 to PAK). The authors also acknowledge the assistance of the Biomedical Microscopy Core at the University of Georgia with imaging using the Zeiss LSM 710 confocal microscope, Zeiss LSM 880, and the IMARIS software workstation.

Tables

Table 3.1 HCR probe and Amplifier set.

HCR Probe-initiator	Amplifier
gad1a-B3	594
gad1b-B1	488
dlx5a-B5	546

Table 3.2:. Genotyping primers.

	***gad1b* Genotyping Primer Sequence**
Forward Primer	CCCGTGTTGTAATGATGCAG
Reverse Primer	GTGAAGCGCTCATTGTTGTC

Figures

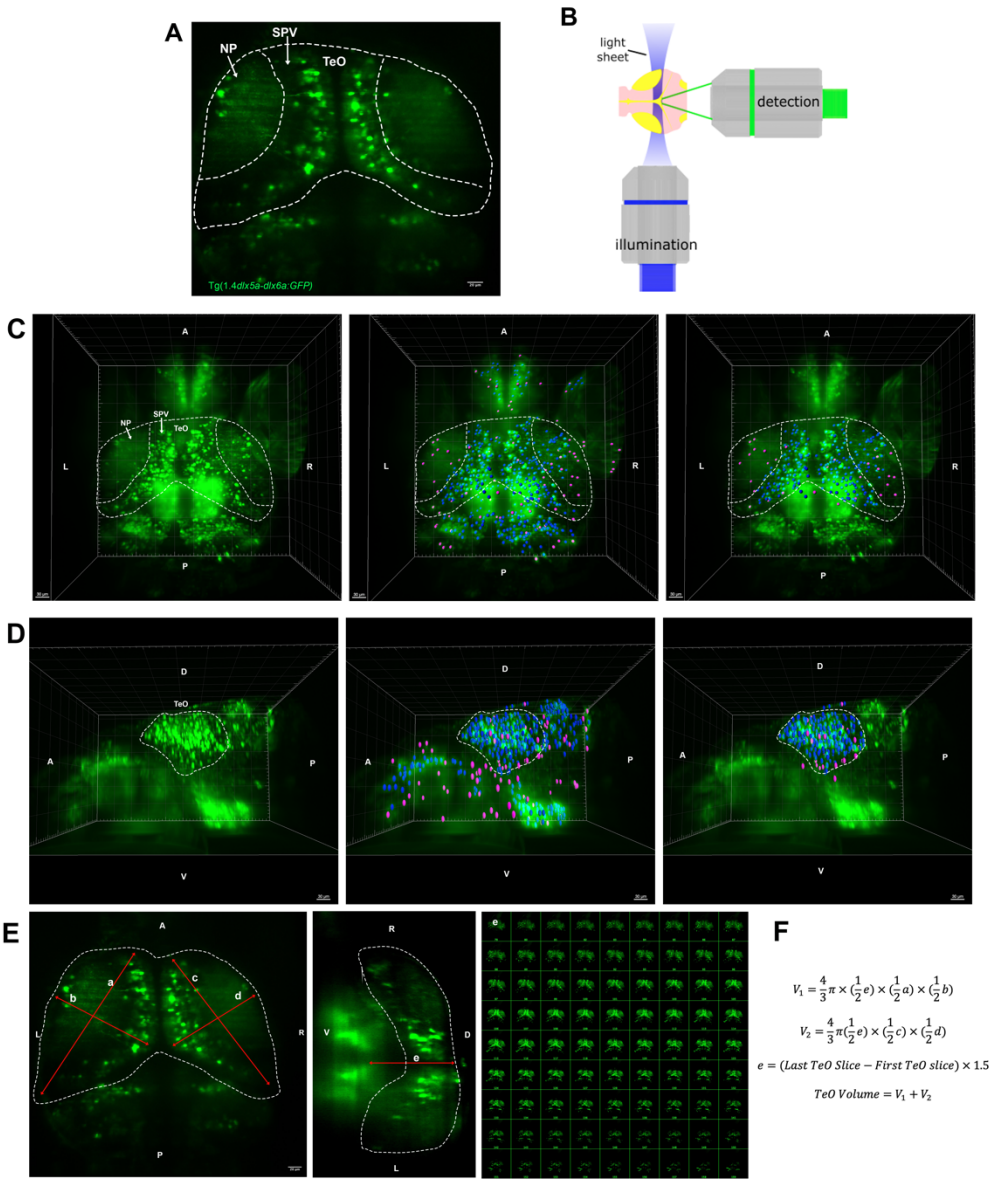

Figure 3.1: Volumetric cell counts in the optic tectum in *tg(dlx5a.dlx6a:GFP)* larvae.

A). A single plane of 1.5µm thick slice from light sheet imaging of tg(*dlx5a.dlx6a:GFP*). The optic tectum (TeO) and the neuropil (NP) are outlined with dashed white lines B). Schematic of the lightsheet microscope. C). Volumetric rendering of lightsheet data in IMARIS. Panels show a dorsal without spots (left), with all cells labeled as spots (middle), and with spots masked to the TeO (right). TeO is outlined in a dashed white line D). Panels show a side view of a 3D rendering of light sheet stacks in IMARIS (left), rendering with all cells labeled as spots(middle), and rendering with spots masked to the TeO (right). TeO is outlined in a dashed white line. E). Panels show diagrams of how measurements were taken to calculate tectum volume. F). The formulas used to calculate the volume of the tectum referencing a-e in (E).

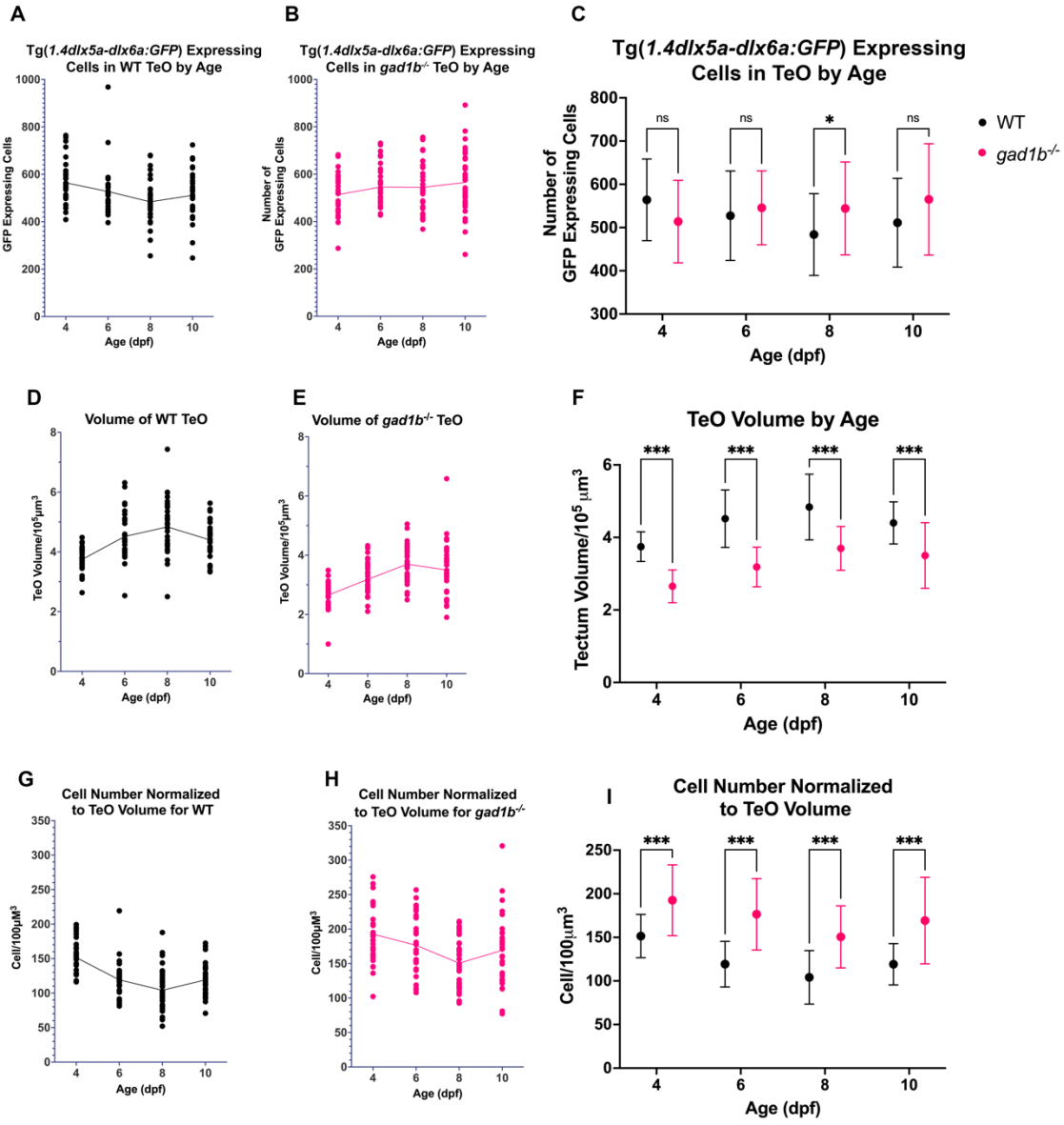

Figure 3.2: *gad1b*$^{-/-}$ mutants have increased cell-to-volume ratio compared to WT.

A-B). Results of volumetric tectum cell counts showing individual count values of WT (A) and *gad1b*$^{-/-}$ (B) C). Results of volumetric tectum cell counts showing the mean with SD. D-E). Total volumes of optic tectum individual values. F). Total volumes of optic tectum showing the mean with SD. G-H). Cell counts normalized to tectal volume individual values and I). Cell counts normalized to tectal volume showing the mean with SD. *=<0.033, **=<0.002, ***=<0.001

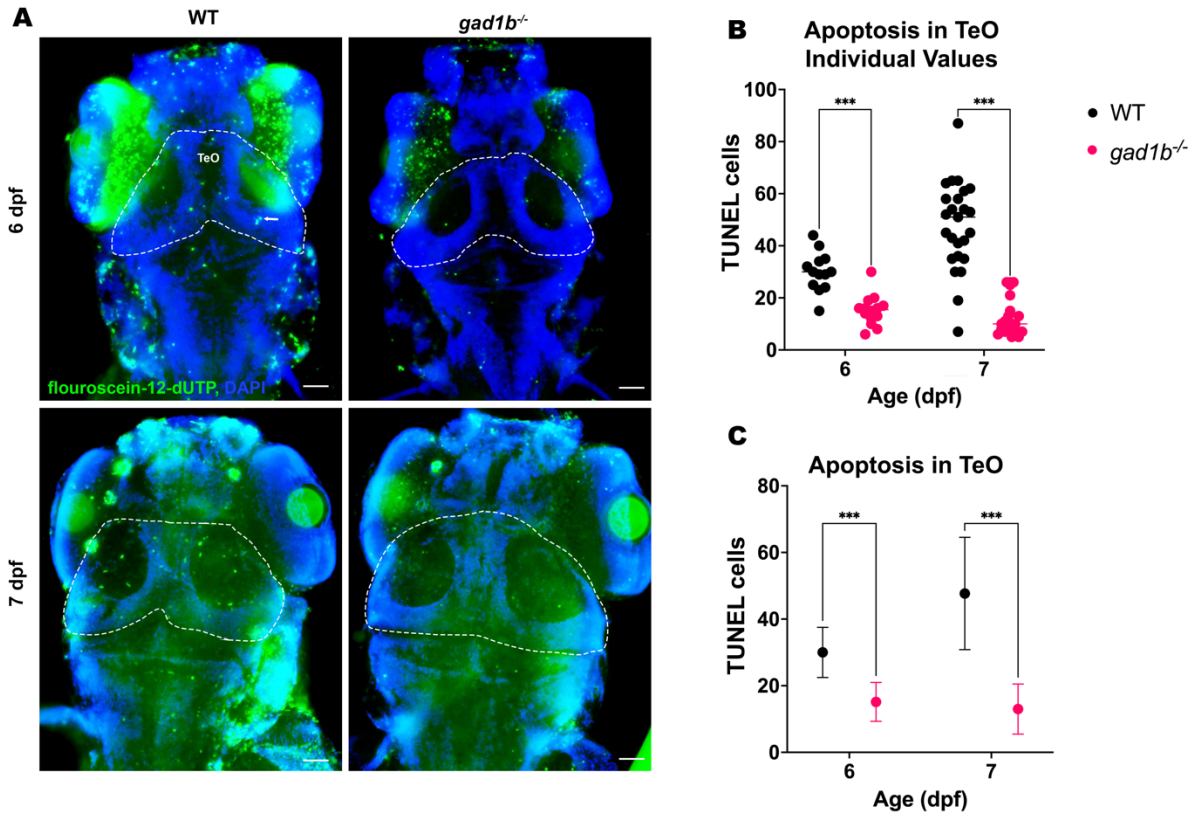

Figure 3.3: *gad1b*$^{-/-}$ fish have less apoptosis occurring than WT at 6 and 7 dpf

A) 6dpf and 7dpf WT and *gad1b*$^{-/-}$ larvae stained for apoptosis with TUNEL. Dashed outline highlights the optic tectum(TeO) B) Individual values of TUNEL counts within the optic tectum. C). Mean with SD of TUNEL counts within the optic tectum. ***=<0.001

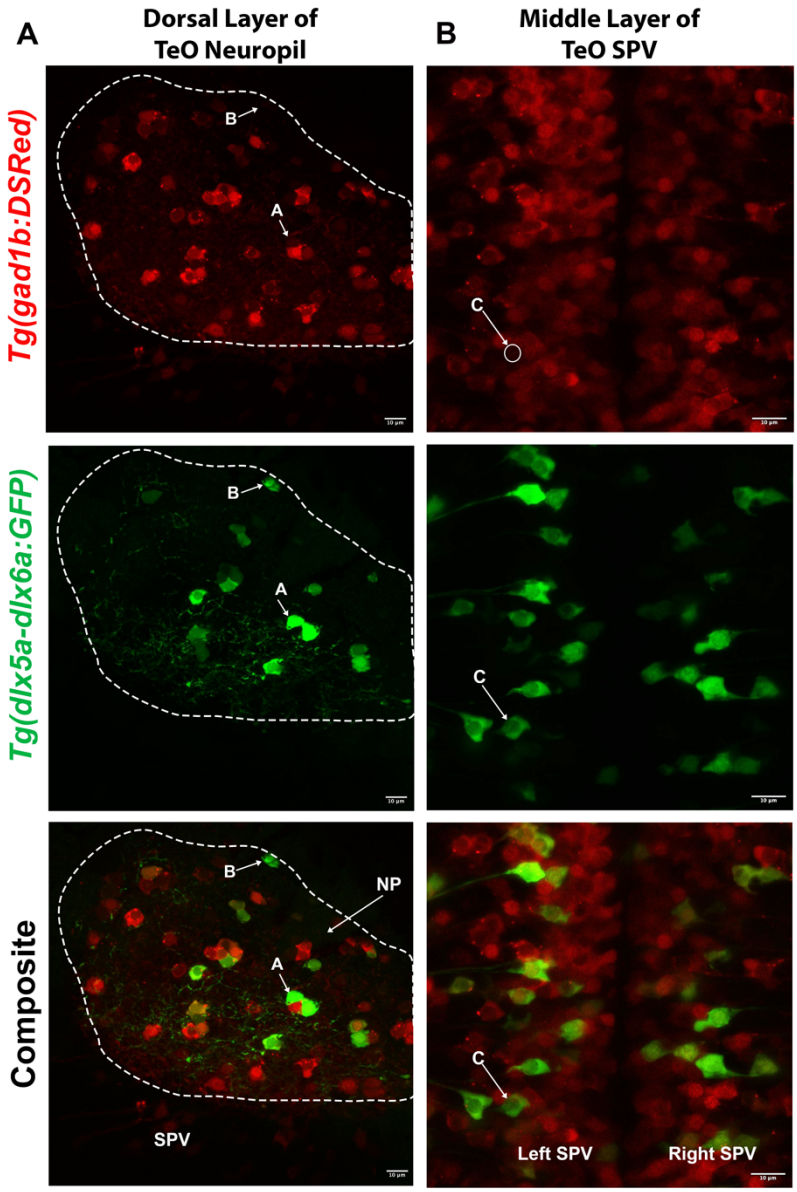

Figure 3.4: The majority of Tg(1.4*dlx5a-dlx6a:GFP*) expressing cells co-express with Tg(*gad1b*:*DSRed*)

A). A dorsal layer of the optic tectum showing superficial interneurons (SINS). "A" and "B" show Tg(1.4*dlx5a-dlx6a:GFP*) expressing cells either not expressing or having low expression of Tg(*gad1b*:*DSRed*) B). A middle layer of the SPV layer of the optic tectum. "C" pointing out one Tg(1.4*dlx5a-dlx6a:GFP*) cell not expressing Tg(*gad1b*:*DSRed)*.

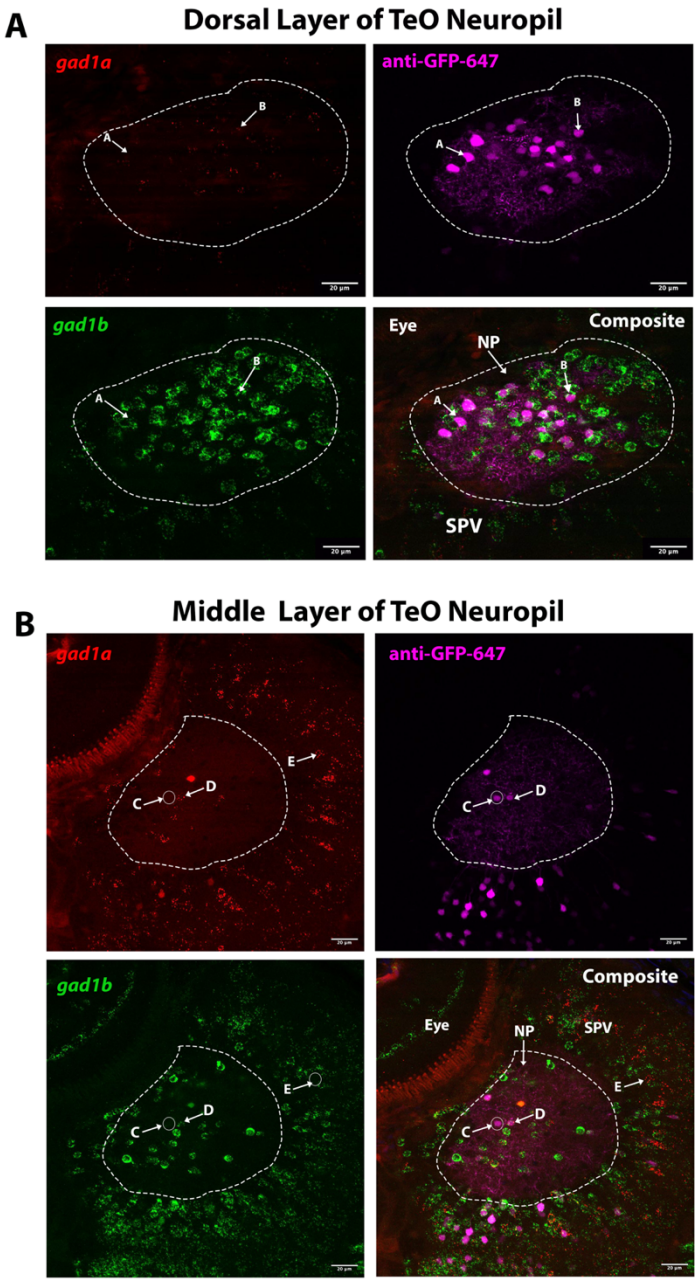

Figure 3.5: Dorsally located dlx GFP expressing cells in the neuropil of the optic tectum do not always co-express *gad1a* but do always co-express *gad1b*

HCR *in situ* labeling of *gad1a* (red), *gad1b* (green), and antibody labeling of GFP (magenta) in A). A dorsal layer of the optic tectum with the neuropil is outlined with a dashed white line. "A" points out a *gad1b*, GFP positive cell not expressing *gad1a.* "B" points out a *gad1b*, GFP positive cell expressing *gad1a* B). A middle layer of the optic tectum with the neuropil is outlined with a dashed white line. "C" is pointing out a GFP expressing cell that is not expressing *gad1b* or *gad1a*. "D" is pointing out a cell expressing *gad1a*, *gad1b* and GFP. "E" is pointing out a cell expressing *gad1a* only.

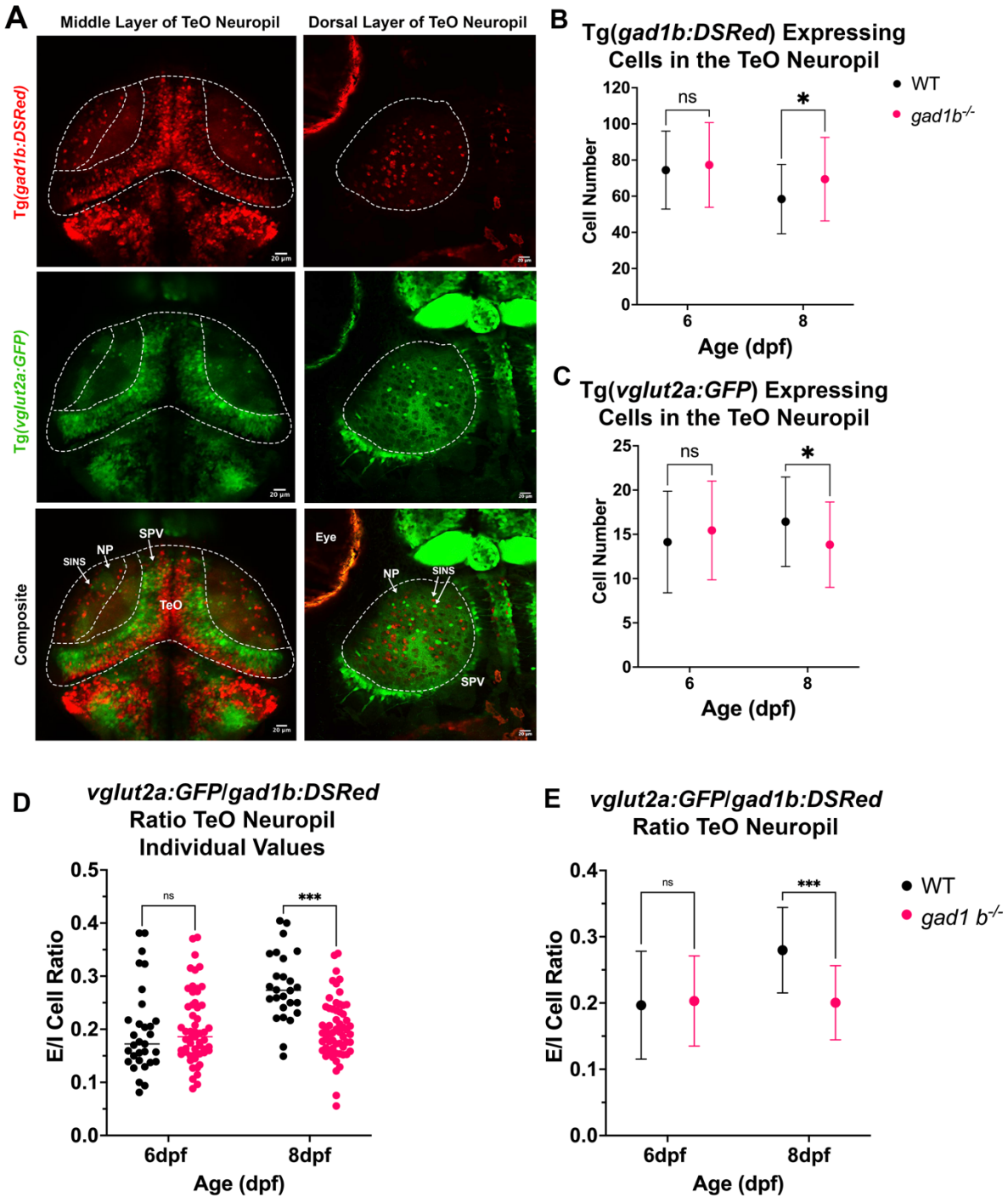

Figure3.6: *gad1b*$^{-/-}$ fish have an increased ratio of *gad1b* to *vglut2a* expressing cells.

A). Representative image showing a dorsal view of a middle tectum layer highlighting the neuropil and superficial interneurons (SINS) (left), and a dorsal view of a superficial layer of the optic tectum with a slight tilt in the mounting of the larva that exposes a large area of the superficial neuropil and likely SINS (right). B). Mean with SD of Tg(*gad1b*:*DSRed*) expressing

cells in the superficial neuropil. C). Mean with SD of Tg(*vglut2a:GFP*) expressing cells in the superficial neuropil. D). Individual values of the ratios of Tg(*vglut2a:GFP*) to Tg(*gad1b*:*DSRed*) expressing cells in the TeO. E). Mean with SD of the ratios of Tg(*vglut2a:GFP*) to Tg(*gad1b*:*DSRed*). Ns=nonsignificant, *=<0.033, ***=<0.001

References

Akerman, C. J. & Cline, H. T. (2007). Refining the roles of GABAergic signaling during neural circuit formation. *Trends in Neurosciences*, *30*(8), 382–389. https://doi.org/10.1016/j.tins.2007.06.002

Asada, H., Kawamura, Y., Maruyama, K., Kume, H., Ding, R., Ji, F. Y., Kanbara, N., Kuzume, H., Sanbo, M., Yagi, T. & Obata, K. (1996). Mice Lacking the 65 kDa Isoform of Glutamic Acid Decarboxylase (GAD65) Maintain Normal Levels of GAD67 and GABA in Their Brains but Are Susceptible to Seizures. *Biochemical and Biophysical Research Communications*, *229*(3), 891–895. https://doi.org/10.1006/bbrc.1996.1898

Asada, H., Kawamura, Y., Maruyama, K., Kume, H., Ding, R.-G., Kanbara, N., Kuzume, H., Sanbo, M., Yagi, T. & Obata, K. (1997). Cleft palate and decreased brain γ-aminobutyric acid in mice lacking the 67-kDa isoform of glutamic acid decarboxylase. *Proceedings of the National Academy of Sciences*, *94*(12), 6496–6499. https://doi.org/10.1073/pnas.94.12.6496

Avitan, L., Pujic, Z., Mölter, J., Poll, M. V. D., Sun, B., Teng, H., Amor, R., Scott, E. K. & Goodhill, G. J. (2017). Spontaneous Activity in the Zebrafish Tectum Reorganizes over Development and Is Influenced by Visual Experience. *Current Biology*, *27*(16), 2407-2419.e4. https://doi.org/10.1016/j.cub.2017.06.056

Baraban, S.C., Taylor, M. R., Castro, P. A. & Baier, H. (2005). Pentylenetetrazole induced changes in zebrafish behavior, neural activity and c-fos expression. *Neuroscience*, *131*(3), 759–768. https://doi.org/10.1016/j.neuroscience.2004.11.031

Baraban, Scott C., Dinday, M. T. & Hortopan, G. A. (2013). Drug screening in Scn1a zebrafish mutant identifies clemizole as a potential Dravet syndrome treatment. *Nature Communications*, *4*(1), 2410. https://doi.org/10.1038/ncomms3410

Brenet, A., Hassan-Abdi, R., Somkhit, J., Yanicostas, C. & Soussi-Yanicostas, N. (2019). Defective excitatory/inhibitory synaptic balance and increased neuron apoptosis in a zebrafish model of Dravet syndrome. *BioRxiv*, 781393. https://doi.org/10.1101/781393

Chapman, C. A., Nuwer, J. L. & Jacob, T. C. (2022). The Yin and Yang of GABAergic and Glutamatergic Synaptic Plasticity: Opposites in Balance by Crosstalking Mechanisms. *Frontiers in Synaptic Neuroscience*, *14*, 911020. https://doi.org/10.3389/fnsyn.2022.911020

Chatron, N., Becker, F., Morsy, H., Schmidts, M., Hardies, K., Tuysuz, B., Roselli, S., Najafi, M., Alkaya, D. U., Ashrafzadeh, F., Nabil, A., Omar, T., Maroofian, R., Karimiani, E. G., Hussien, H., Kok, F., Ramos, L., Gunes, N., Bilguvar, K., … Tajsharghi, H. (2020). Bi-allelic GAD1 variants cause a neonatal onset syndromic developmental and epileptic encephalopathy. *Brain*, *143*(5), 1447–1461. https://doi.org/10.1093/brain/awaa085

Chechik, G., Meilijson, I. & Ruppin, E. (1998). Synaptic Pruning in Development: A Computational Account. *Neural Computation*, *10*(7), 1759–1777. https://doi.org/10.1162/089976698300017124

Condie, B. G., Bain, G., Gottlieb, D. I. & Capecchi, M. R. (1997). Cleft palate in mice with a targeted mutation in the γ-aminobutyric acid-producing enzyme glutamic acid decarboxylase 67. *Proceedings of the National Academy of Sciences*, *94*(21), 11451–11455. https://doi.org/10.1073/pnas.94.21.11451

Duan, Z. R. S., Che, A., Chu, P., Modol, L., Bollmann, Y., Babij, R., Fetcho, R. N., Otsuka, T., Fuccillo, M. V., Liston, C., Pisapia, D. J., Cossart, R. & García, N. V. D. M. (2020). GABAergic Restriction of Network Dynamics Regulates Interneuron Survival in the Developing Cortex. *Neuron*, *105*(1), 75-92.e5. https://doi.org/10.1016/j.neuron.2019.10.008

Erlander, M. G., Tillakaratne, N. J. K., Feldblum, S., Patel, N. & Tobin, A. J. (1991). Two genes encode distinct glutamate decarboxylases. *Neuron*, *7*(1), 91–100. https://doi.org/10.1016/0896-6273(91)90077-d

Fahrbach, F. O., Gurchenkov, V., Alessandri, K., Nassoy, P. & Rohrbach, A. (2013). Light-sheet microscopy in thick media using scanned Bessel beams and two-photon fluorescence excitation. *Optics Express*, *21*(11), 13824. https://doi.org/10.1364/oe.21.013824

Ganguly, K. & Poo, M. (2013). Activity-Dependent Neural Plasticity from Bench to Bedside. *Neuron*, *80*(3), 729–741. https://doi.org/10.1016/j.neuron.2013.10.028

Ghanem, N., Jarinova, O., Amores, A., Long, Q., Hatch, G., Park, B. K., Rubenstein, J. L. R. & Ekker, M. (2003). Regulatory Roles of Conserved Intergenic Domains in Vertebrate Dlx Bigene Clusters. *Genome Research*, *13*(4), 533–543. https://doi.org/10.1101/gr.716103

Grone, B. P., Qu, T. & Baraban, S. C. (2017). Behavioral Comorbidities and Drug Treatments in a Zebrafish scn1lab Model of Dravet Syndrome. *ENeuro*, *4*(4), ENEURO.0066-17.2017. https://doi.org/10.1523/eneuro.0066-17.2017

Hortopan, G. A., Dinday, M. T. & Baraban, S. C. (2010). Spontaneous Seizures and Altered Gene Expression in GABA Signaling Pathways in a mind bomb Mutant Zebrafish. *The Journal of Neuroscience*, *30*(41), 13718–13728. https://doi.org/10.1523/jneurosci.1887-10.2010

Isaacson, J. S. & Scanziani, M. (2011). How Inhibition Shapes Cortical Activity. *Neuron*, *72*(2), 231–243. https://doi.org/10.1016/j.neuron.2011.09.027

Jill, S. (2020). Core Concept: How synaptic pruning shapes neural wiring during development and, possibly, in disease. *Proceedings of the National Academy of Sciences*, *117*(28), 16096. https://doi.org/10.1073/pnas.2010281117

Kakizaki, T., Oriuchi, N. & Yanagawa, Y. (2015). GAD65/GAD67 double knockout mice exhibit intermediate severity in both cleft palate and omphalocele compared with GAD67 knockout and VGAT knockout mice. *Neuroscience*, *288*, 86–93. https://doi.org/10.1016/j.neuroscience.2014.12.030

Le, T. N., Zhou, Q.-P., Cobos, I., Zhang, S., Zagozewski, J., Japoni, S., Vriend, J., Parkinson, T., Du, G., Rubenstein, J. L. & Eisenstat, D. D. (2017). GABAergic Interneuron Differentiation in the Basal Forebrain Is Mediated through Direct Regulation of Glutamic Acid Decarboxylase Isoforms by Dlx Homeobox Transcription Factors. *Journal of Neuroscience*, *37*(36), 8816–8829. https://doi.org/10.1523/jneurosci.2125-16.2017

Liu, Y., Chen, Y., Duffy, C. R., VanLeuven, A. J., Byers, J. B., Schriever, H. C., Ball, R. E., Carpenter, J. M., Gunderson, C. E., Filipov, N. M., Ma, P., Kner, P. A. & Lauderdale3, and J. D. (n.d.). *Decreased GABA levels during development results in increased connectivity in the larval zebrafish tectum*.

Liu, Y., Lawrence, K., Lauderdale, J. & Kner, P. (2020). Sensorless and sensor based adaptive optics for light sheet microscopy. *Adaptive Optics: Analysis, Methods & Systems*.

Liu, Y., Liu, B., Green, J., Duffy, C., Song, M., Lauderdale, J. D. & Kner, P. (2023). Volumetric light sheet imaging with adaptive optics correction. *Biomedical Optics Express*, *14*(4), 1757. https://doi.org/10.1364/boe.473237

Lynex, C. N., Carr, I. M., Leek, J. P., Achuthan, R., Mitchell, S., Maher, E. R., Woods, C. G., Bonthon, D. T. & Markham, A. F. (2004). Homozygosity for a missense mutation in the 67 kDa isoform of glutamate decarboxylase in a family with autosomal recessive spastic cerebral palsy: parallels with Stiff-Person Syndrome and other movement disorders. *BMC Neurology*, *4*(1), 20. https://doi.org/10.1186/1471-2377-4-20

MacDonald, R. B., Debiais-Thibaud, M., Talbot, J. C. & Ekker, M. (2010). The relationship between dlx and gad1 expression indicates highly conserved genetic pathways in the zebrafish forebrain. *Developmental Dynamics*, *239*(8), 2298–2306. https://doi.org/10.1002/dvdy.22365

Marachlian, E., Avitan, L., Goodhill, G. J. & Sumbre, G. (2018). Principles of Functional Circuit Connectivity: Insights From Spontaneous Activity in the Zebrafish Optic Tectum. *Frontiers in Neural Circuits*, *12*, 46. https://doi.org/10.3389/fncir.2018.00046

Martin, D. L. & Rimvall, K. (1993). Regulation of γ-Aminobutyric Acid Synthesis in the Brain. *Journal of Neurochemistry*, *60*(2), 395–407. https://doi.org/10.1111/j.1471-4159.1993.tb03165.x

Mendes, H. W., Taktek, M., Duret, T. & Ekker, M. (2020). Expression of dlx genes in the normal and regenerating brain of adult zebrafish. *PLoS ONE*, *15*(6), e0229549. https://doi.org/10.1371/journal.pone.0229549

Nevin, L. M., Taylor, M. R. & Baier, H. (2008). Hardwiring of fine synaptic layers in the zebrafish visual pathway. *Neural Development*, *3*(1), 36. https://doi.org/10.1186/1749-8104-3-36

Paolicelli, R. C., Bolasco, G., Pagani, F., Maggi, L., Scianni, M., Panzanelli, P., Giustetto, M., Ferreira, T. A., Guiducci, E., Dumas, L., Ragozzino, D. & Gross, C. T. (2011). *Synaptic Pruning by Microglia Is Necessary for Normal Brain Development*.

Satou, C., Kimura, Y., Hirata, H., Suster, M. L., Kawakami, K. & Higashijima, S. (2013). Transgenic tools to characterize neuronal properties of discrete populations of zebrafish neurons. *Development*, *140*(18), 3927–3931. https://doi.org/10.1242/dev.099531

Shainer, I., Kuehn, E., Laurell, E., Kassar, M. A., Mokayes, N., Sherman, S., Larsch, J., Kunst, M. & Baier, H. (2023). A single-cell resolution gene expression atlas of the larval zebrafish brain. *Science Advances*, *9*(8), eade9909. https://doi.org/10.1126/sciadv.ade9909

Thisse, C. & Thisse, B. (2005). *High Throughput Expression Analysis of ZF-Models Consortium Clones. ZFIN Direct Data Submission*. http://zfin.org

Turko, P., Groberman, K., Browa, F., Cobb, S. & Vida, I. (2019). Differential Dependence of GABAergic and Glutamatergic Neurons on Glia for the Establishment of Synaptic Transmission. *Cerebral Cortex*, *29*(3), 1230–1243. https://doi.org/10.1093/cercor/bhy029

Yu, M., Xi, Y., Pollack, J., Debiais-Thibaud, M., MacDonald, R. B. & Ekker, M. (2011). Activity of dlx5a/dlx6a regulatory elements during zebrafish GABAergic neuron development. *International Journal of Developmental Neuroscience*, *29*(7), 681–691. https://doi.org/10.1016/j.ijdevneu.2011.06.005

Zerucha, T., Stühmer, T., Hatch, G., Park, B. K., Long, Q., Yu, G., Gambarotta, A., Schultz, J. R., Rubenstein, J. L. R. & Ekker, M. (2000). A Highly Conserved Enhancer in the Dlx5/Dlx6Intergenic Region is the Site of Cross-Regulatory Interactions betweenDlx Genes in the Embryonic Forebrain. *The Journal of Neuroscience*, *20*(2), 709–721. https://doi.org/10.1523/jneurosci.20-02-00709.2000

Zhao, H., Mao, X., Zhu, C., Zou, X., Peng, F., Yang, W., Li, B., Li, G., Ge, T. & Cui, R. (2022). GABAergic System Dysfunction in Autism Spectrum Disorders. *Frontiers in Cell and Developmental Biology*, *9*, 781327. https://doi.org/10.3389/fcell.2021.781327

Supplementary Table and Figures

Supplemental Table 3.1: Cell Counts per larva in WT Tg(*1.4dlx5a-dlx6a:GFP*) cells through development

Total cell counts within the optic tectum. Each count is an individual larva as imaging is terminal.

	4 dpf	6 dpf	8 dpf	10dpf
1	472	482	580	631
2	535	465	507	546
3	503	478	395	598
4	409	429	496	586
5	439	968	256	387
6	615	513	475	498
7	498	734	495	664
8	457	439	360	503
9	543	511	420	501
10	514	445	458	459
11	613	454	598	724
12	673	587	400	458
13	555	550	322	528
14	764	525	520	669
15	502	558	360	466
16	755	478	472	561
17	585	396	637	421
18	547	511	680	451
19	602	486	470	536
20	641	517	469	627
21	740	518	457	504
22	458	516	535	448
23	715	492	450	572
24	582	544	434	247
25	596	484	620	513
26	505	556	678	545
27	560	529	433	311
28	470	556	538	511
29	512	581	463	414
30	563	518	481	458
31	-	-	513	-
32	-	-	487	-

33	-	-	508	-

Supplemental Table 3.2 Cell counts per larva in *gad1b*$^{-/-}$, Tg(*1.4dlx5a-dlx6a:GFP*) cells through development

Total cell counts within the optic tectum. Each count is an individual larva as imaging is terminal.

	4 dpf	**6 dpf**	**8 dpf**	**10 dpf**
1	549	590	575	542
2	449	500	557	533
3	425	622	603	524
4	564	540	532	514
5	610	675	407	501
6	469	520	700	478
7	422	500	746	892
8	573	433	413	261
9	397	534	750	472
10	396	466	636	598
11	588	484	517	575
12	287	458	433	664
13	595	565	522	782
14	417	427	704	749
15	478	724	416	700
16	585	467	756	579
17	533	610	432	503
18	522	731	462	486
19	567	570	656	463
20	677	479	590	600
21	518	488	455	622
22	682	505	542	669
23	487	458	528	412
24	675	524	529	400
25	632	522	428	356
26	449	646	628	631
27	532	464	368	627
28	451	541	461	664
29	439	558	638	688
30	445	465	463	588
31	-	697	628	712
32	-	561	487	444

33	-	680	517	509
34	-	-	485	479
35	-	-	482	-

Supplemental Table 3.3: TUNEL counts in WT and *gad1b*$^{-/-}$ larvae.

Each count is an individual larva.

	WT		***gad1b*$^{-/-}$**	
	6 dpf	**7dpf**	**6 dpf**	**7dpf**
1	32	45	10	26
2	24	36	13	5
3	40	7	6	10
4	34	35	30	13
5	29	64	16	6
6	30	87	20	26
7	30	58	19	25
8	44	30	17	7
9	25	35	15	8
10	15	19	16	26
11	23	52	14	7
12	29	30	12	13
13	35	51	16	10
14	-	43	8	15
15	-	54	-	8
16	-	45	-	5
17	-	53	-	21
18	-	41	-	8
19	-	65	-	11
20	-	62	-	10
21	-	54	-	-
22	-	65	-	-
23	-	42	-	-
24	-	58	-	-
25	-	61	-	-

Supplemental Table 3.4: Ratio of Tg(*vglut2a:GFP*)/Tg*(gad1b:DSRed*)

Each data point is from a signal larva as imaging is terminal.

6dpf WT			**8dpf WT**		
vglut2a:GFP	***gad1b:DSRed***	**Ratio**	***vglut2a:GFP***	***gad1b:DSRed***	**Ratio**
11	40	0.275	25	73	0.34
17	49	0.35	9	35	0.25
15	87	0.17	10	40	0.25
17	81	0.21	11	42	0.26
12	128	0.09	12	48	0.25
14	102	0.14	13	54	0.24
8	63	0.13	9	39	0.23
15	85	0.18	19	47	0.4
15	69	0.22	14	63	0.22
8	47	0.17	22	55	0.40
14	65	0.22	23	82	0.28
11	69	0.16	14	54	0.26
21	65	0.32	15	55	0.27
3	37	0.08	17	49	0.35
12	63	0.19	17	62	0.27
12	77	0.16	15	45	0.33
10	72	0.14	12	43	0.28
7	70	0.10	23	77	0.30
9	60	0.15	27	71	0.38
11	54	0.20	17	77	0.22
15	108	0.14	21	97	0.22
12	85	0.14	10	29	0.34
11	85	0.13	20	134	0.15
18	114	0.16	16	55	0.29
17	90	0.19	18	108	0.17
32	84	0.38	18	60	0.30
25	77	0.32	5	25	-
24	97	0.25	11	10	-
11	70	0.16	-	-	-
15	73	0.2	-	-	-
16	42	0.38	-	-	-
6dpf *gad1b*$^{-/-}$			**8dpf *gad1b*$^{-/-}$**		
vglut2a:GFP	***gad1b:DSRed***	**Ratio**	***vglut2a:GFP***	***gad1b:DSRed***	**Ratio**
18	82	0.22	10	43	0.23

25	67	0.37	3	54	0.06
14	72	0.19	13	42	0.31
19	76	0.25	7	34	0.21
6	40	0.15	8	52	0.15
16	59	0.27	9	47	0.19
14	62	0.23	12	58	0.21
23	82	0.28	8	35	0.23
13	53	0.25	11	57	0.19
20	54	0.37	6	39	0.15
29	92	0.3	8	43	0.19
17	50	0.34	22	106	0.21
15	98	0.15	16	80	0.20
24	77	0.31	13	82	0.16
9	32	0.28	16	91	0.18
19	112	0.17	13	65	0.20
19	105	0.18	13	60	0.22
27	85	0.32	16	84	0.19
19	94	0.20	17	96	0.17
19	97	0.20	9	59	0.15
22	106	0.21	13	53	0.25
23	83	0.28	12	67	0.18
23	83	0.28	12	75	0.16
15	61	0.25	14	72	0.19
7	66	0.11	17	78	0.22
12	94	0.13	17	81	0.21
9	55	0.16	6	36	0.17
10	69	0.15	14	48	0.29
13	54	0.24	14	81	0.17
13	64	0.2	15	97	0.15
13	80	0.16	12	79	0.15
16	89	0.18	16	56	0.29
14	99	0.14	17	69	0.25
8	50	0.16	22	89	0.25
14	91	0.15	21	81	0.26
16	105	0.15	11	54	0.20
14	80	0.18	19	56	0.34
16	66	0.24	13	93	0.14
14	86	0.16	20	84	0.24
12	105	0.11	7	93	0.08

15	78	0.19	17	103	0.17
19	97	0.20	12	62	0.19
17	93	0.18	19	116	0.16
16	86	0.19	17	114	0.15
5	32	0.16	18	91	0.20
5	52	0.10	6	33	0.18
12	69	0.17	18	104	0.17
8	63	0.13	13	107	0.12
10	37	0.27	4	31	0.13
17	106	0.16	17	68	0.25
9	102	0.09	13	74	0.18
6	36	0.17	14	79	0.18
22	113	0.19	12	35	0.34
11	70	0.16	10	68	0.14
19	143	0.13	10	34	0.29
-	-	-	16	66	0.24
-	-	-	17	71	0.24
-	-	-	24	102	0.24
-	-	-	20	74	0.27

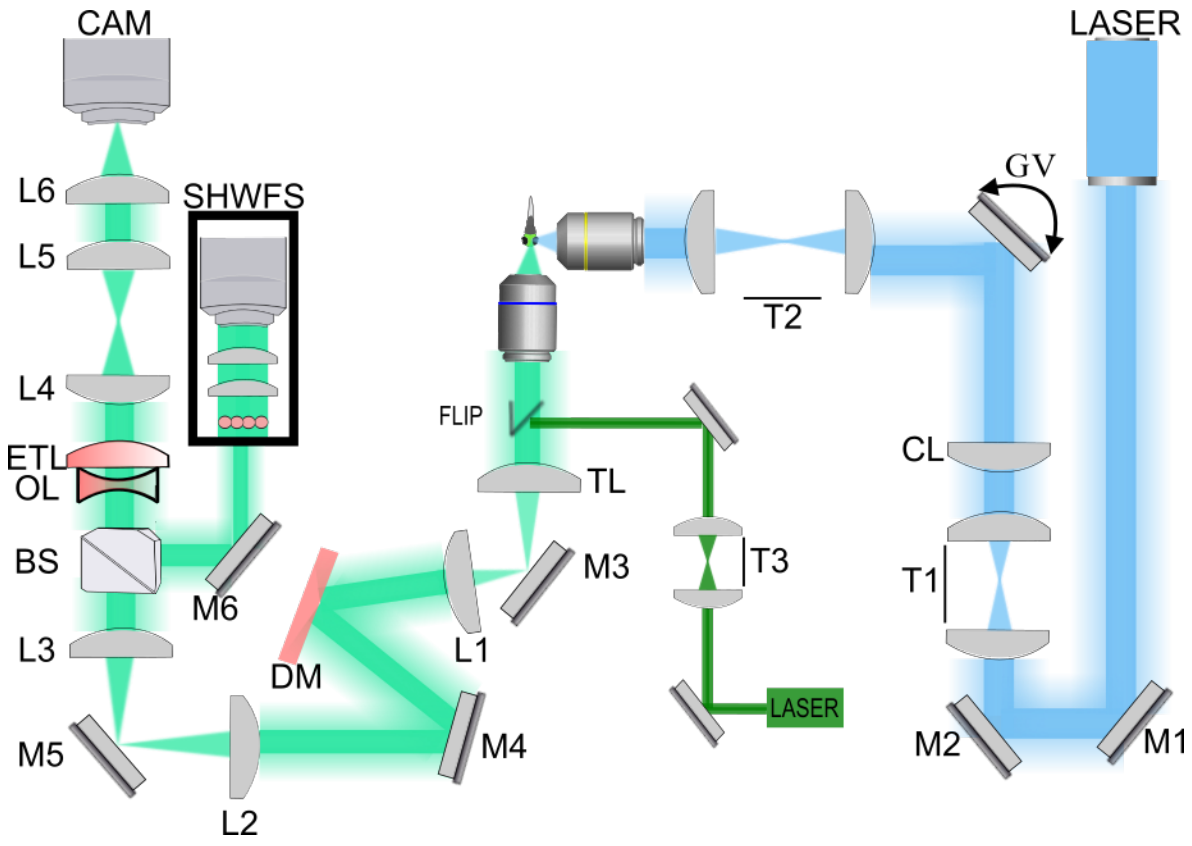

Supplemental Figure 3.1: Schematic of the optical setup.

The illumination objective is a 10× 0.3NA water dipping objective, and the detection objective is a 40× 0.8NA water dipping objective. T1: 3× magnification lens pair (25 mm and 75 mm efl); T2: 5/3 demagnification lens pair (50 mm and 30 mm); TL: Tube lens (180 mm efl); T3: 8× magnification lens pair (25 mm and 200 mm efl). L1-2: Relay lenses (f1=100 mm and f2=200 mm). L3-4: Relay lenses (f3=300 mm and f4=200 mm); L5-6 is a magnifying lens pair (300 mm and 150 mm efl). DM: Deformable Mirror. CL: cylindrical lens (50 mm efl). OL: offset lens (−75 mm efl). ETL: Electrically Tunable Lens. SHWFS: Home built Shack-Hartmann Wavefront Sensor. The green laser is used to calibrate the DM and the SHWFS. The overall magnification of the detection path is 26.67.

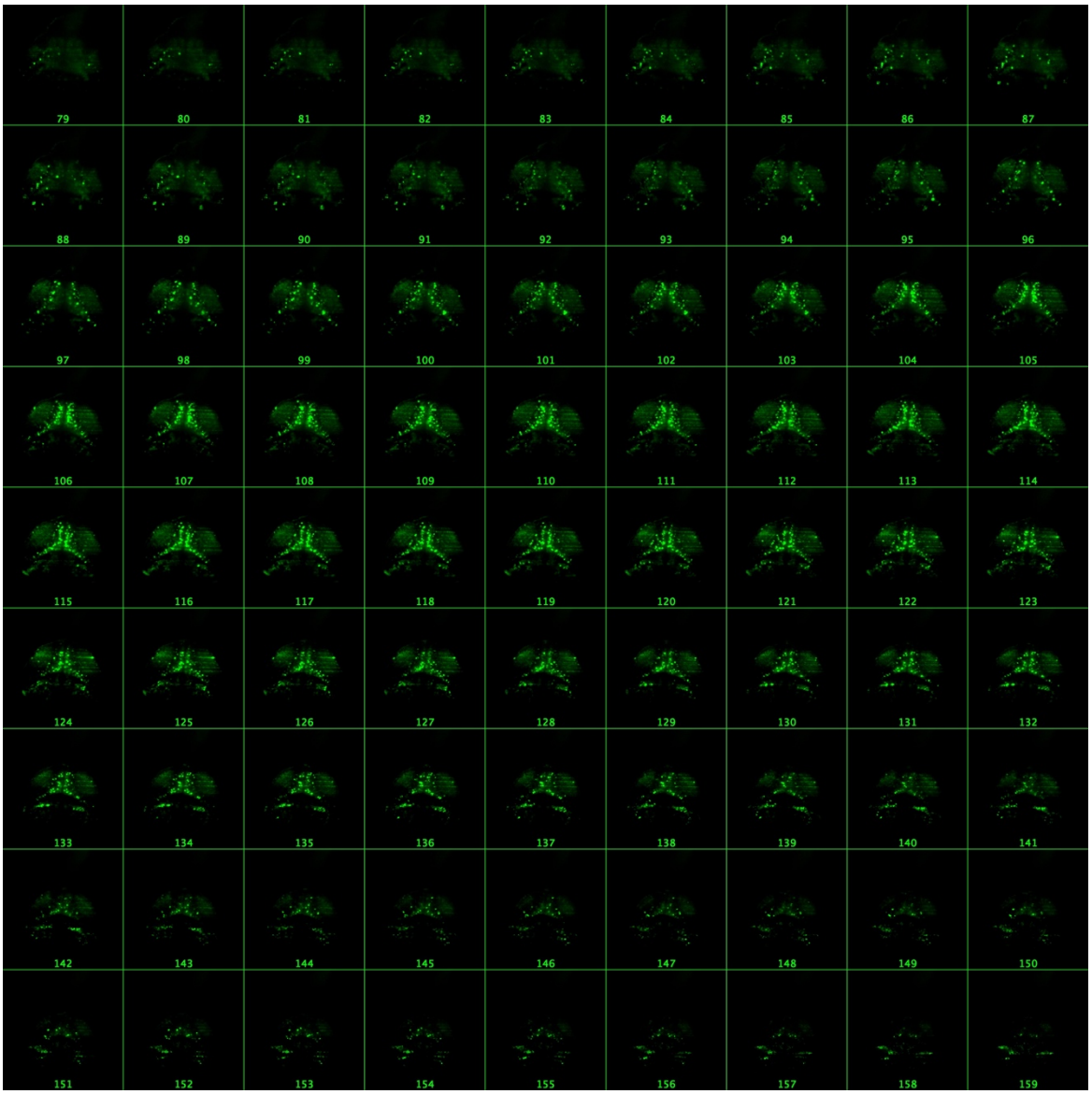

Figure 3.2 Montage of light sheet data Z stack consisting of the optic tectum only.

Light sheet imaging through the entire zebrafish larval brain at brain 6dpTg(*1.4dlx5a-dlx6a:GFP*) and Tg(*gad1b*:DSRed: larvae).

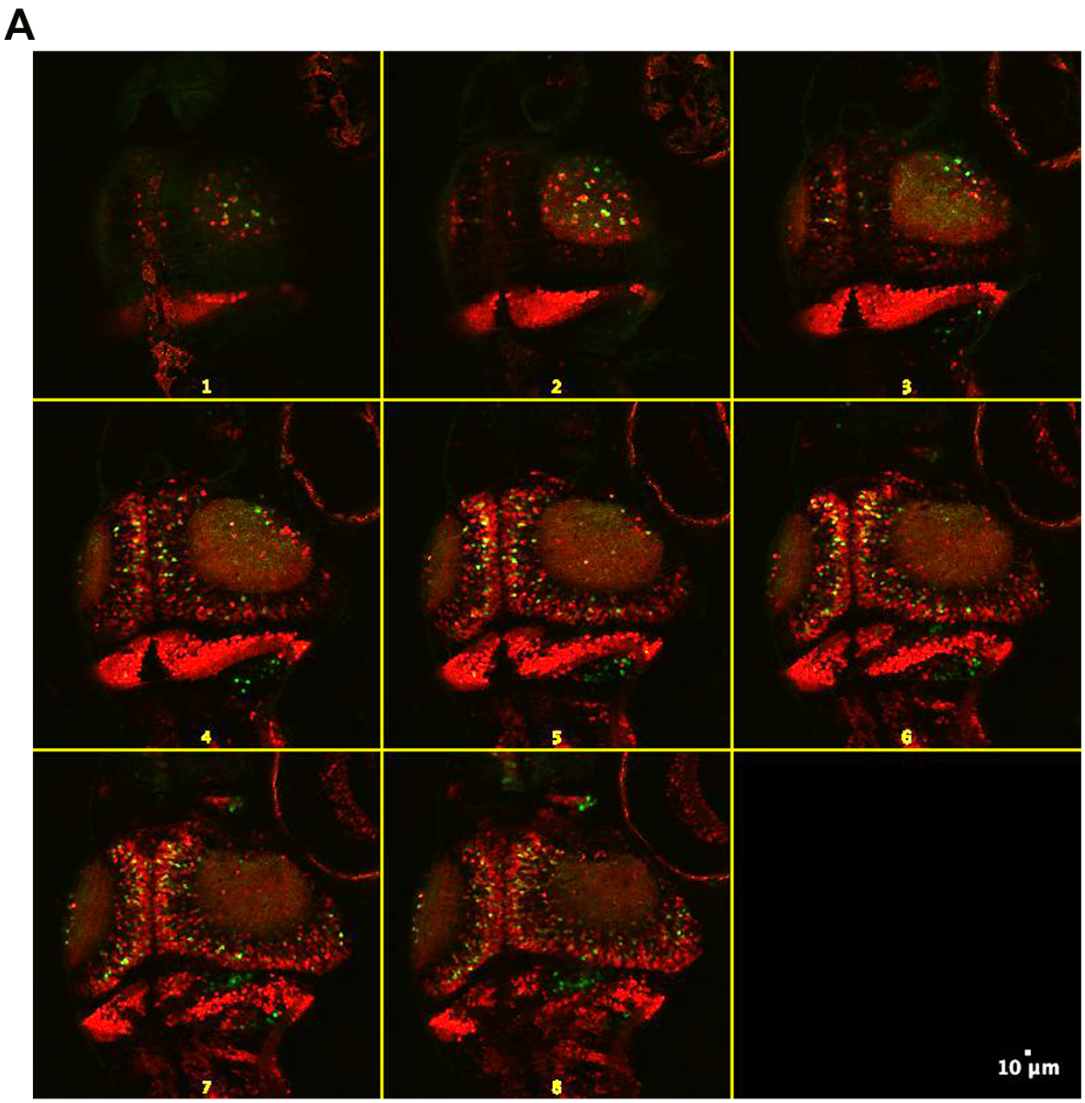

Supplementary Figure 3.3: Confocal montage of Tg(*1.4dlx5a-dlx6a:GFP*) and Tg(*gad1b:DSRed*) larvae.

Stacks were taken, and the slices best representing labeling were chosen for analysis.

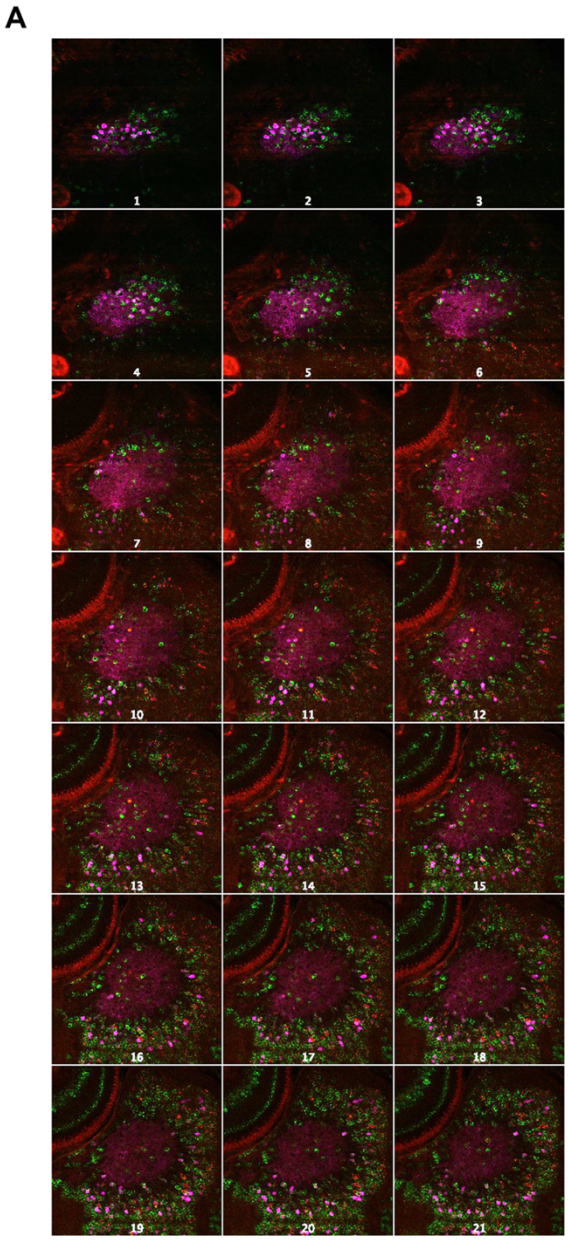

Supplementary Figure 3.4. Montage of HCR in situ data on Tg(*1.4dlx5a-dlxa:GFP*) larvae confocal Z stack.

A z stack was taken of each in situ sample so that the layers best representing labeling could be analyzed in post. *gad1a* (red), *gad1b* (green), and anti-GFP labeling (pink).

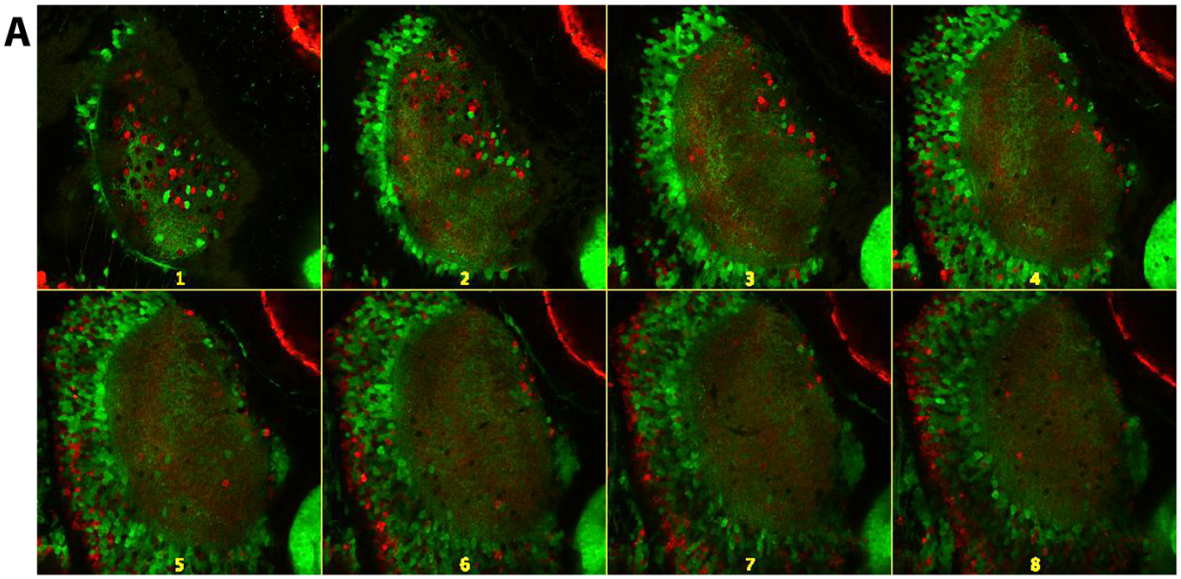

Supplementary Figure 3.5. Montage of v*glut2a:GFP* and *gad1b:DSRed* confocal z stacks.

A) Z stacks were imaged through the brain on confocal so that the best layers for imaging could be chosen for analysis

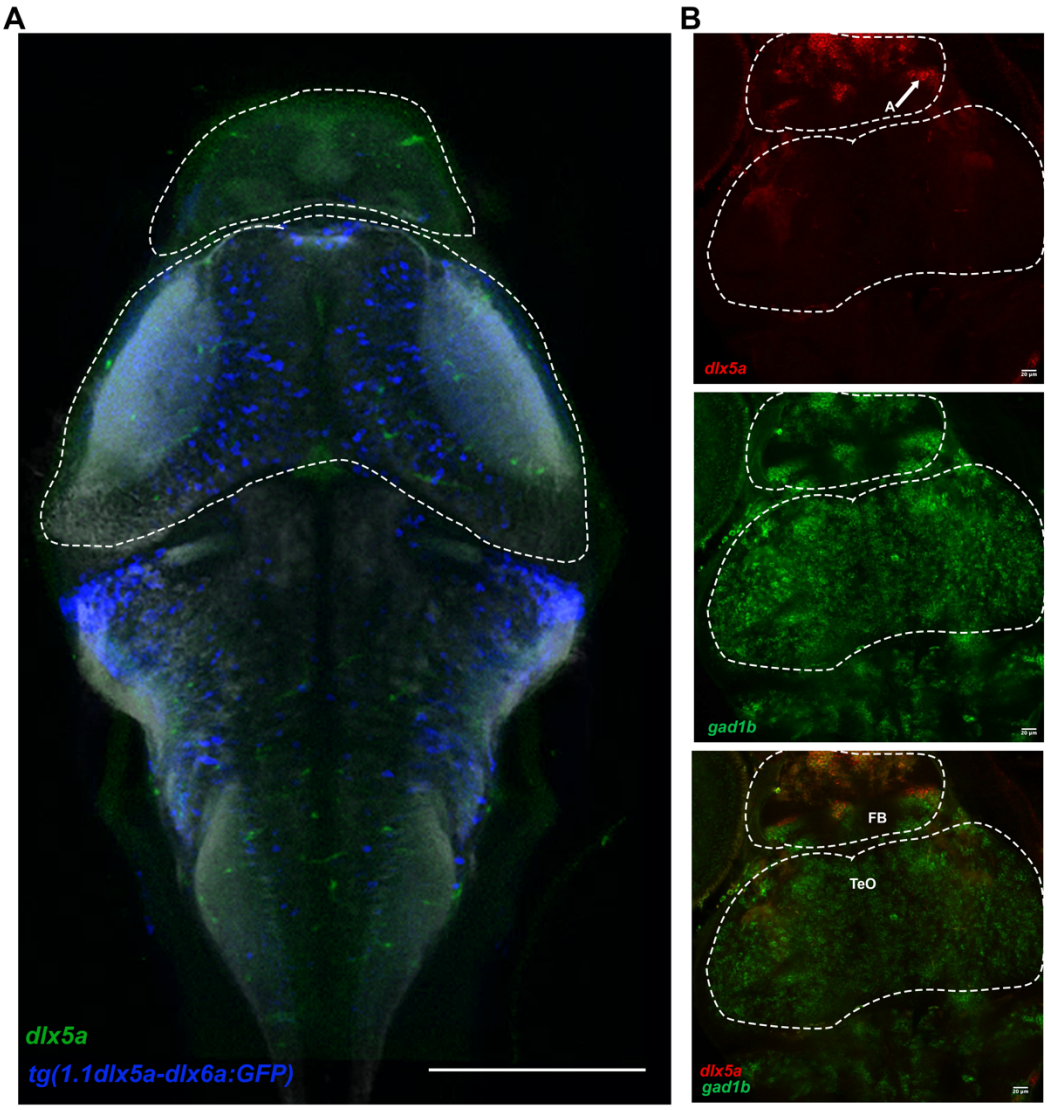

Supplementary Figure 3.6. *dlx5a* expression in the optic tectum.

A). Mapzebrain data of HCR labeling of dlx5 (green) and tg(1.1dlx5a0dlx6a:GFP). B). HCR labeling of dlx 5a in 6dpf WT fish. A represents labeling in the forebrain.

CHAPTER 4

DECREASED GABA LEVELS IMPAIRS THE OPTOMOTOR RESPONSE IN7 DPF ZEBRAFISH

Carly R Duffy, Makenna Otten, Delia Shelton, James D Lauderdale, To Be Submitted To Behavioral Neuroscience

Abstract

Many animals such as insects, birds, fish, and some mammals have a visuomotor reflex called the optomotor response (OMR). This innate response is important for allowing animals to stabilize their visual field when their environment is moving. In zebrafish, assaying for the OMR is a great tool for measuring visual processing associated with motor control. This assay can be used to study how environmental effects or genetic defects alter these abilities. γ-aminobutyric acid (GABA) is the main inhibitory neurotransmitter in the brain and CNS, and it has an important role in maintaining the right balance of excitation to inhibition. GABA is made by the enzyme glutamic acid decarboxylase (GAD). A genome duplication event left zebrafish with the paralogous *gad1a* and *gad1b* null mutants. Both paralogs are viable, which makes zebrafish a unique model for studying the effects of decreased GABA signaling due to a mutation in the *gad* gene since Gad mutations in mice are neonatal lethal. The *gad1b* mutants particularly have decreased GABA levels, increased neural hyperexcitability, and display increased synchronicity of neural activity between the left and right sides of the optic tectum. Overall, this makes *gad1b*$^{-/-}$ larvae great candidates for studying the effects of developing with lower GABA levels and neural excitability on sensory processing. Using the well-established OMR assay on 7dpf larvae, we aim to ask whether decreased levels of GABA affect the innate ability of the *gad1b* $^{-/-}$larvae to appropriately perceive optic flow and subsequently stabilize their receptive field with motor movement.

Introduction

Throughout development, maintaining the excitatory-to-inhibitory balance is necessary for adequate fine-tuning of neural circuitry leading to proper brain development. Variations in the levels of excitatory neurotransmitters such as glutamate or inhibitory neurotransmitters such as γ-aminobutyric acid (GABA) affect this balance and are thought to lead to dysregulation of circuitry refinement (Sohal & Rubenstein, 2019; Zhao et al., 2022).

GABA is made by removing the carboxyl group from glutamate by the enzyme, glutamic acid decarboxylase (GAD)(Martin & Rimvall, 1993). In humans and most vertebrates, there are two GAD genes, GAD1 and GAD2 (Erlander et al., 1991; Kaufman et al., 1991). In mice, mutations in the GAD1 gene are neonatal lethal (Asada et al., 1997; Condie et al., 1997). In zebrafish, however, a genome duplication event resulted in paralogs of the *gad1* gene, *gad1a* and *gad1b* (VanLeuven, 2018). These paralogs allow for the successful generation of *gad1a* and *gad1b* null mutants (Liu et al., n.d.; VanLeuven, 2018), therefore making them a good model for studying how developing with decreased GABA levels affects brain circuitry and visual processing.

Our CRISPR-generated *gad1b* mutants show decreased levels of GABA at the larval stage and increased neural activity due to decreased lateral inhibition, as well as decreased surround inhibition (Liu et al., n.d.; VanLeuven, 2018). Interestingly, along with the increased neural activity, they also show an increase in synchronicity between the left and right sides of the optic tectum (Liu et al., n.d.). However, WT larvae treated with a convulsant Pentylenetetrazol (PTZ), which blocks $GABA_A$ receptors, causing an overall lack of inhibition, do not show increased synchronicity between the left and right sides of the optic tectum, suggesting that the *gad1b* mutants could have altered neural circuitry which would contribute to altered visually

evoked behavior (S.C. Baraban et al., 2005; Liu et al., n.d.). One way of testing for changes in visually evoked behavior is through an assay that tests the optomotor response (OMR).

The optomotor response is an innate response that many insects, fish, and even mammals experience (Neuhauss et al., 1999). This reflexive behavior causes them to begin movement in a specific direction in response to optic flow as they are trying to stabilize their receptive field (Clark, 1981; Easter & Nicola, 1997; Muto et al., 2005) In nature, this serves as a way for the animals to maintain a flight or swim pattern in response to their environment. Larval zebrafish experience this optomotor response when water is flowing past them (Clark, 1981; Easter & Nicola, 1997; Matsuda & Kubo, 2021; Muto et al., 2005). This allows them the instinct to swim against a current when facing upstream, and therefore maintain their position in the water. Optic flow also produces an optokinetic response in zebrafish, but it leads to eye movement instead of motor movement(Easter & Nicola, 1997; Matsuda & Kubo, 2021).

The optomotor response is thought to be mediated by the larvae's visual system, particularly through neurons in the retina. When optic flow is perceived by the photoreceptors in the retina it is communicated to a direction-selective ganglion cell (DSGC) which relays a response based on the direction of movement that is perceived(Lagnado, 1998; Muto et al., 2005; Neuhauss et al., 1999; Robles et al., 2014; Roeser & Baier, 2003). Each type of DSGCs respond strongly to specific direction of movement, but not to others. In zebrafish, there are arborization fields currently numbered 1- 10 that branch from the ganglion cells and innervate various areas in the brain (Baier & Wullimann, 2021). The AF5 arborization field innervates both the optic tectum and the pretectum and is thought to be the arborization that communicates the signal for OMR and OKR (Matsuda & Kubo, 2021). Focusing on OMR, the signal from AF5 goes to the pretectum, and it is then sent to the cerebellum, reticulospinal neurons, and nucleus of the medial

longitudinal fasciculus (nMLFs) which control swimming movement and swimming speed (Matsuda & Kubo, 2021). While AF5 also innervates the optic tectum, prior research has shown that the optic tectum is not required for the OMR as fish can still respond even after the optic tectum is ablated (Roeser & Baier, 2003).

The OMR assay is a well-established and robust manner to measure visual acuity and perception in larvae and adults. In larvae, the assay consists of displaying black and white moving bars horizontally beneath the larvae (LeFauve et al., 2021; Matsuda & Kubo, 2021). They perceive these black-and-white moving bars as a current, flowing against them and they then swim in the same direction as the bars as they try to stabilize their visual field. When the bars are moving at a speed that the larvae can perceive, the fish interpret this as a current flowing against them, which triggers them to swim to maintain their position in the water. As the speed of the bars increases, therefore increasing the flicker rate, the larvae lose the ability to perceive any optic flow, and they no longer swim in response to the stimulus. This assay has been often used in forward genetic screens as well as in studying the effects of environmental toxins or drug treatments on the visual acuity of zebrafish (Muto et al., 2005; Naumann et al., 2016). However, it has not been used as widely to characterize sensory processing issues in reverse genetic mutants.

There was one study that created a dVGAT, an ortholog of the Vesicular GABA Transport (VGAT) gene, mutant in drosophila (Fei et al., 2010). The mutation was homozygous lethal though, so they had to use a rescue and a knockdown to perform behavioral studies. They did not see a defect in the optomotor control of the fruit flies in the knockdown or the mutant with a rescue (Fei et al., 2010). Our mutant line of zebrafish is a better model as GABA signaling is

more directly affected as GABA is genetically reduced in all *gad1b*expressing cells throughout the entirety of development.

As previously discussed, the *gad1b*$^{-/-}$ larvae have decreased levels of GABA which leads to an increase in neural activity. By running these larvae through the OMR assay, we can elucidate the importance of proper GABA signaling, and thus inhibition, on this innate visual ability. After running the *gad1b* mutants through the assay, we found that they do have an altered response. Furthermore, we found that this response can be duplicated by treatment with PTZ, and we can even rescue the OMR ability to an extent by treatment with the anti-epileptic, muscimol. Altogether, this suggests that GABA signaling is required for the visually evoked OMR.

Materials and Methods

Fish rearing and husbandry

WIK (hence referred to as WT) crosses and *gad1b*$^{-/-}$ crosses were set with one male to three female pairings 8 nights before the expected OMR run date for 7 dpf larvae. Eggs are collected in the morning and dark-reared in a 28°C incubator until 7 with egg water being changed out as needed. Fish are transferred into system water the morning of running the OMR and they are allowed to equilibrate to light for approximately 3 hours in the 28˚C fish room. If treatment is occurring, this takes place during those three hours. For the experiment, larvae were placed in a rectangular container with a wall in the middle, allowing for the recording of two genotypes or two repeats at one time. Each side is filled to approximately a 1cm depth with system water. This container sits horizontally on top of a computer monitor (Figure 4.1A). Approximately 15 fish of each genotype were placed on separate sides of the container.

Whole Mount HCR RNA in situ hybridizations and confocal microscopy

HCR in situ hybridizations were performed on 5dpf WIK larvae as described in Chapter 2 Material and Methods. See Table 4.1 for probe and hairpin sets. A Zeiss LSM710 or Zeiss LSM 880 were used at the 20X or 40X objectives.

OMR programs

Regular OMR run

The OMR program runs for approximately 15 minutes. First, a 5-minute acclimation period allows the fish to adjust to the new container. After acclimation, the fish are exposed to a stimulus of black and white moving bars which runs for 45 seconds followed by a 30-second recovery period. The fish are then exposed to the stimulus again, but with the bars moving in the opposite direction and at an increased speed (Figure 4.1B). This sequence then repeats 7 times, each time with the direction of bar movement switching and increasing speed. The whole program is run 3-6 times, switching out the larvae after each run. Speeds were run in this order: 0.8cm/s, 1.6cm/s, 8cm/s, 16cm/s, 32cm/s, 40cm/s, and 64cm/s Videos were recorded with a webcam that is mounted over the monitor (Figure 4.1A). Screenshots were taken in the frame immediately following the stimulus ending. A template of four zones was overlayed using Photoshop and counts of larvae in each zone were done using the 'cell counter' plugin on ImageJ. The percentage of fish found within each zone was calculated for each run using Excel spreadsheets, and results were plotted as individual values and as the mean with SD. A Mann-Whitney multiple t-test was done using the PRISM GraphPad software. The OMR program was written in Python and ran using the software Psycho-Py.

Example Code: https://github.com/cduffy115/OMR-7dpf-larvae.git

All speeds at 1.6cm/s OMR run.

For runs of OMR where every stimulus seed was run at 1.6cm/s, instead of the speed increasing after each 30-second acclimation, the stimulus runs again at 1.6cm/s. 1.6 cm/s was chosen as this is the speed when the *gad1b*$^{-/-}$ mutants have their best response.

OMR ran with decreasing speeds.

For the OMR run with decreasing seeds, the order of the stimulus speeds has been reversed. The stimulus speeds are run in this order: 64cm/s, 40cm/s, 32cm/s, 16cm/s, 8cm/s, 1.6cm/s, and 0.8cm/s.

Interleaved OMR run

For interleaved runs, the program runs for approximately 18 minutes. The assay begins the same as the regular run, still receiving 0.8cm/s as the first speed, then 1.6cm/s, then 8cm/s. The assay then deviates as the next stimulus speed is 1.6cm/s again, followed by the next increase in speed to 16cm/s. These sequences repeat for each increase in speed always followed by 1.6cm/s. Note: The direction of the stimulus speed still switches between every stimulus exposure. Because of this, all 1.6cm/s repeats head in the same direction, and the changing speed stimuli run in the opposite direction to the 1.6cm/s direction.

Treatment with PTZ, GABA, and Muscimol

Treatment of WT fish with PTZ

1mM, 2.5 mM, and 5mM PTZ in egg water were created from a 300mM stock of PTZ. WT larvae were incubated in 20 mL of the PTZ solution for each concentration in a 100mm petri dish for 3 hours in a 28°C fish room. The PTZ solution was decanted safely, and the larvae were rinsed with egg water 3X and then 1X with system water before running the OMR assay to ensure the PTZ was no longer present. Concentrations of PTZ were chosen as these are

subclinical doses where fish do not experience immobility due to seizures. At the dose of 5mm PTZ, larvae do begin experiencing seizure-like events that have a small effect on mobility.

Treatment of fish with GABA

WT and *gad1b*$^{-/-}$ fish were treated with 100µm, 1mM, 25mm, and 100mM GABA in egg water generated from a 1M GABA (SIGMA, Cat#A2129-10G) stock. They were incubated in 20mL of this solution for three hours in 100mm Petri dishes in a 28°C fish room. The fish were rinsed 1X in system water before being run through the OMR.

Treatment of fish with muscimol

WT and *gad1b*$^{-/-}$ fish were treated with 100µM, 200 µM, and 400 µM muscimol in egg water solutions generated from a 100mM muscimol (TOCRIS, Cat#2763-96-4) stock. Fish were incubated for three hours immediately prior to the assay by incubation in 20mL of solution in 100mM Petri dishes in a 28°C fish room. The solution was rinsed out 1X with system water prior to running OMR.

Results

***gad1b* and *gad2* expression in the retina.**

The optomotor response relies upon the visual system for which processing begins at the retina. To fully comprehend the role GABA plays in visual processing and the implications developing with lower levels of GABA would have on its distribution in the retina, we probed for *gad1b* and *gad2* in the retina of 5 dpf WT larvae. *elalvl3* was used as a positive control for the labeling as it marks neural cell bodies (Figure 4.3A). *gad1b* transcripts were detected within the retina in the internuclear layer (INL), likely in amacrine cells, and in the outer plexiform layer, likely in horizontal cells. (Figure 4.2A-B). *gad2* was detected in the INL, likely amacrine

cells, and in a small number of cells in the ganglion cell layer, possibly ganglion cells or displaced amacrine cells (Figure 4.2 A-B). *gad1b* transcripts were also detected in a layer within the ganglion cell layer, separate from *gad2*-expressing cells. We were not able to detect *gad1a,* the paralog of *gad1b*, in the retina (data not shown).

$gad1b^{-/-}$ larvae have a decreased ability to respond to the OMR stimulus.

Since GABA levels are likely decreased in the retina of the *gad1b* mutant larvae, we investigated shifts in visually evoked behavior by running an optomotor response assay, which is a well-established assay in zebrafish that measures a reflexive visuomotor response. In 7dpf WT larvae, results were as expected (Figure 4.1D, Figure 4.3A-B) (Brockerhoff et al., 1995; LeFauve et al., 2021; Muto et al., 2005; Neuhauss, 2003; Roeser & Baier, 2003). Speed 0 represents the acclimation period before larvae are exposed to any stimuli. WT larvae show a random distribution during the acclimation period with only an average of 23±12.2%(SD) of fish already within the response zone right before the first stimulus was run (Figure 4.3A-B, Table S4.1). The first OMR assay speed we exposed the larvae to was 0.8cm/s, at which WT fish showed an average response of 73.8± 13.7% (SD) (Figure 4.3A-B, Table S4.1). The WT larvae then exhibit their greatest ability to respond at the subsequent speeds of 1.6cm/s, 8cm/s, and 16cm/s with an average of 85.8± 10.7%, 83.3 ±8.7%, and 83.1± 16.0% (SD) respectively (Figure 3A-B, Table S1). As stimulus speed increases from here, the WT response begins to decline. At 32cm/s, their average response decreases to 36.9±19.0% (SD) (Figure 4.3A-B Table S4.1). By 40cm/s and 64 cm/s, their response is approaching that of a random distribution with an average of 29.33±12.5%(SD) and 19.9±11.4% (SD)respectively (Figure 4.1D, Figure 3A-B).

In the $gad1b^{-/-}$ larvae, they have the expected random distribution during the acclimation before exposure to any stimulus with an average of 26.8±10.7% (SD) of larvae found in the

response zone (Figure 4.3A-B, Table S4.1). At the first speed of 0.8cm/s, *gad1b*$^{-/-}$ larvae have a response with an average of 57.1±19.9% (SD) of larvae found in the response zone. They then have their strongest response at 1.6cm/s with an average response of 64.9±23.7% (Figure 4.3A-B, Table S4.1). At 8cm/s, the mutants have a 14% decrease in their response with an average response of 50.0±20.3%. (SD) At 16cm/s, the response remains low, at 56.2±26.0% (SD) (Figure 4.3A-B, Table S4.1). There is an apparent increase in response at 16cm/s compared to the mutant's 8cm/s response. Control experiments described later show that this is likely a technical issue where some of the mutants no longer redisperse through the container during re-acclimation, in fact remaining within the response zone. As the stimuli speed increases, the mutant response declines further, approaching a random distribution with an average of 26.1±14.4% (SD) and 37.0±14.5% (SD) at 32cm/s at 40cm/s respectively (Figure 3A-B, Table S1). At the stimulus speed of 64 cm/s, the distribution is random at an average of 17.9 ±11.3% (SD) (Figure 4.3A-B, Table S4.1).

Comparing the WT and the *gad1b*$^{-/-}$ larvae response, there is a significant difference in their percent of response from speeds 0.8cm/s-16cm/s, which are speeds that WT larvae have their strongest response (Figure4.3A-B, Table S4.2). The greatest significant difference between the WT and the mutant larvae response is seen at 8cm/s with the mutant larvae responding approximately 33% less than the WT larvae (Figure 4.3A-B, Table S4.2). At 16cm/s, a difference in response is still observed with the mutants responding an average of 27% less than WT larvae (Figure 4.3A-B).

To gain better insight into how larvae are distributed throughout the whole of the container and not just in the response zone, the analysis was marked with four zones and counts were done in every zone and the mean percent was plotted in a heat map (Figure 4.1E, Figure

4.3C-D). WT larvae have good distribution throughout the container at the end of the first 5-minute acclimation. At the speeds with which a high response is observed for the WT larvae, there is a crisp gradient towards the response zone (Figure 4.3D). The *gad1b*$^{-/-}$ larvae also show a random distribution through all zones at the acclimation time point. At the speeds of an observed response, the mutants have a more diffuse gradient heading towards the response zone, representing that there are more fish found in the middle zones (Figure 4.3D). The heat map also shows a visualization of the *gad1b*$^{-/-}$ larvae that remain on the "right" side response zone due to not redistributing (Figure 4.3D)

***gad1b*$^{-/-}$ fish remain mobile and able to swim the distance of their container.**

Due to the technical issue of certain *gad1b*$^{-/-}$ larvae displaying a lack of redistribution after exposure to faster stimuli during the typical OMR assay runs, we ran multiple controls to test the mobility and responsiveness of the mutant larvae. These involved running the assay with speeds decreasing instead of increasing, running the assay with every stimulus at 1.6cm/s, and running the assay with 1.6cm/s interleaved between every other speed.

To test if the order of stimulus presentation affects the larvae's response, the OMR was run with stimuli speeds decreasing. Running the assay "backwards" in this manner did not affect the WT larvae. The *gad1b*$^{-/-}$ larvae were also unaffected by the reversal of the stimuli speeds (Figure 4.4A)

Second, to test if the *gad1b*$^{-/-}$ larvae remain mobile the entire 15 minutes of the assay as well as able to swim the entire distance of the container, we ran the speed at which *gad1b*$^{-/-}$ larvae displayed their strongest response (1.6cm/s), 7 times in a row, switching directions each time. We found that even at the end of the assay, the *gad1b-/-* larvae were able to respond just as well as at the beginning (Figure 4.4B, Table S4.4). The same is true for WT larvae. This also

demonstrated that the *gad1b* $^{-/-}$ larvae can swim from one end of the container to the other, and they can do so within the 45 seconds that the stimulus runs. This assay also shows that they do not fatigue under these conditions.

Third, to test if the larvae have a typical response no matter which stimuli are played directly prior, we ran the larvae through an interleaved program where the speed of 1.6cm/s is run in between the other stimulus speeds (Figure 4.4 C, Table S4.5-4.6). We found that no speed affected the ability of the *gad1b*$^{-/-}$ larvae to respond at the 1.6cm/s stimulus (Figure 4.4D, Table S4). This manner of interleaving with 1.6cm/s also operated to "force" the larvae to leave the "response zone" due to the alternating directions. Therefore, the results of the changing stimulus speeds were not skewed by larvae that may have never changed positions after their ability to respond was surpassed. (Figure 4.4E, Table S4.5) With this manner of running the experiment, the *gad1b*$^{-/-}$ larvae display an impaired response at 8cm/s, which is further impaired at 16cm/s (Figure 4.4E). Lastly, this again shows that the *gad1b*$^{-/-}$ larvae can swim the full distance of the container and do not fatigue under the conditions of this test.

Treatment with PTZ decreased the OMR of the WT larvae.

To test the effects of reduced GABAergic signaling on the OMR of zebrafish larvae that developed normally, we ran the assay on WT larvae acutely exposed to PTZ at three different subclinical doses. All three doses lead to a decrease in the WT larvae's response (Figure 4.5A, Table S4.7). The highest concentration of 5mM PTZ led to the greatest decrease in the WT fish response at all speeds untreated WT larvae can respond. Their response at this concentration was 10-15% lower than the *gad1b*$^{-/-}$ larvae's ability to respond, and approximately 50% lower than the WT fish response (Figure 4.5A, Table S4.7). The lowest concentration of 1mM PTZ lowered the response of the WT larvae by approximately 10% at 1.6 cm/s, 8 cm/s, and 16 cm/s, which is

approximately a 10-20% higher response than the *gad1b*$^{-/-}$ larvae. (Figure 4.5A, Table S4.7) At 2.5mM PTZ concentration, the WT-treated fish had a response in a range closer to that of the *gad1b*$^{-/-}$ larvae (Figure 4.5A-B). The WT response was lowered by approximately 20%, and this response was approximately 5-10 % higher than the *gad1b*$^{-/-}$ larvae response (Figure 5A-B, Table S6). When specifically looking at 8cm/s, which is where *gad1b*$^{-/-}$ larvae face their greatest deficit in response, we see there is an average response of 73.1% at 1mM PTZ, 62.3%, at 2.5 mM PTZ, 40.4% at 5mM PTZ (Figure 4.5A, Table S4.5). At 2.5mM PTZ, the response is significantly less than WT but is not found to be significantly different from the *gad1b*$^{-/-}$ response (Figure 4.5B, Table S4.7).

When running the PTZ-treated fish through the control assay of every stimulus speed at 1.6cm, the larvae treated with PTZ were able to swim back and forth and remain swimming for the entire duration of the experiment (Figure S4.2). When running through the interleaved experiment, the 2.5mM PTZ-treated WT larvae showed that they were not negatively affected by any stimulus speed (Figure 4.5C). In fact, the 2.5 mM PTZ-treated fish responded during the interleaved run similarly to the *gad1b*$^{-/-}$ larvae. (Figure 4.5C)

GABA treatment increased the OMR ability of *gad1b*$^{-/-}$ larvae.

To further test if the *gad1b*$^{-/-}$ larvae's altered OMR is due to decreased GABA signaling, we exposed the mutants to multiple concentrations of GABA to attempt to rescue GABA signaling. Overall, all concentrations slightly increased the response of the *gad1b*$^{-/-}$ mutants, however, they did not fully recover to the WT larvae's ability (Figure 4.6A-B, Table S4.8). Focusing on the response to the 8cm/s stimulus, the average response was 67.1% at 100µm GABA, 66.0% 1mM GABA, 61.8% at 25mM GABA, and 67.9% at 100mM GABA (Figure 4.6A). All had a response that was improved from the untreated *gad1b*$^{-/-}$ larvae's responses

(Figure 4.6A). The 100mM GABA-treated condition was found to be the best at increasing their response, however, their performance had only a small percentage increase in comparison with the other concentration results. (Figure 4.6A-B), and it only significantly rescued the *gad1b*$^{-/-}$ response at 8cm/s where it was unable to rescue to a response like that of WT larvae (Figure 4.6B). WT fish treated with GABA remained unaffected (Figure 4.6D, Table S4.8)

Muscimol treatment rescued the OMR of *gad1b*$^{-/-}$ larvae.

To investigate if the *gad1b*$^{-/-}$ larvae's response can be fully rescued to the level of a WT response, we treated the fish with the anti-epileptic, muscimol, which is a GABA agonist. All concentrations of muscimol tested were able to increase the response of the mutants, however the lowest concentration tested (100 µM muscimol) had the greatest benefit (Figure 4.7A-B, Table S4.10) Specifically when focusing on the response at 8cm/s, the average response was 83.1% at 100 µM muscimol, 75.5% at 200 µM Muscimol, 75.1% at 400 µM Muscimol (Figure 4.7A, Table S4.10). All three concentrations were rescued to a level no longer significantly different than the WT response at this speed. However, at 16cm/s the responses were 71.3% at 100 µM muscimol, 60.2% at 200 µM Muscimol, and 65.3% at 400 µM Muscimol, which is significantly less than the WT response. (Figure 4.7A). Even for the best-performing treated *gad1b*$^{-/-}$ larvae (100µM muscimol), 8cm/s was the only concentration where they had a significant improvement in response. (Figure 4.7B). Meanwhile, the WT fish were unaffected by the treatment with muscimol at all three concentrations (Figure 4.7C, Table S4.9)

The muscimol-treated *gad1b*$^{-/-}$ larvae also retained their ability to swim back and forth throughout the experiment at all speeds 1.6cm/s (Figure 4.8C.) During the interleaved runs on the muscimol-treated *gad1b*$^{-/-}$ larvae, the mutants performed similarly to the *gad1b*$^{-/-}$ larvae (Figure 4.8A). However, when looking at the interleaved response seen after the stimuli speeds

that even WT larvae can no longer respond, there is an apparent increase in the muscimol-treated *gad1b*$^{-/-}$ larvae's response (n=2), however, more repeats are necessary to confirm any significance as even the responses to changing speeds do not have significance (Figure 4.8B-D)

Discussion

The *gad1b*$^{-/-}$ larvae had a robust phenotype consistently exhibiting a decreased OMR compared to WT at multiple stimuli speeds. Considering that the processing for the OMR is a visual response, the decreased GABA levels in the retina of the mutants are likely a large reason for this discrepancy. *gad1b* and *gad2* are expressed in the INL of the retina in what are likely amacrine cells, which are essential in visual processing as they gate information flow to the ganglion cells. The *gad1b* mutants would have an approximately 50% reduction in GABA levels within the amacrine cells. (Figure 4.2 A-B). *gad1b* is also expressed in what is likely horizontal cells while *gad2* is not, so there is likely a 100% reduction of GABA in the horizontal cells (Figure 4.2). This is critical as horizontal cells are crucial in proper lateral inhibition and center-surround inhibition, therefore affecting which downstream cells receive and interpret the signal. The signal perceived and relayed by the AF5 from the DSGCs to the superficial neurons of the tectum and the pretectum would be receiving information flow from horizontal cells and amacrine cells (Figure 4.2C), which in the *gad1b* mutants, would likely have decreased lateral inhibition and center-surround inhibition leading to an inability to hone a response as there would be an influx of signal to the DSGCs. If multiple DSGCs are responding to the wrong input, then the larvae could be trying to swim in multiple directions at the same time.

Some *gad1b*$^{-/-}$ larvae do not redisperse through the container during their 30-second re-acclimation, causing skewed results due to larvae never leaving the response zone. This raised a

concern that the potential decreased lateral inhibition from the retina causes an influx that leaves the larvae unable to perform any motor function for an extended period.

Therefore, to understand why the mutants were not redispersing and gain more insight into the cause of their impaired response, we performed multiple control runs. We performed a test run with decreasing speeds to assess whether the order of stimulus presentation affected their response. Running the assay in "reverse" showed that greater speeds of the stimulus were not causing any noticeable effects on mutant larvae's mobility. A second control assay was performed where every stimulus speed was that which *gad1b* mutants experienced their least impaired response, 1.6cm/s. This control showed us that the mutants can remain mobile throughout the experiment, and they were able to swim the entire distance of the container in the time allotted to the stimulus presentation. Therefore, we can eliminate any concerns that the mutant larvae may still be able to properly perceive the stimulus, but physically are unable to respond. A third control assay performed was an interleaved experiment where again the stimulus speed 1.6cm/s was run in between each other stimulus speed. This assay showed that after every stimulus speed, the mutant larvae are still able to respond to a stimulus they are consistently able to perceive. This is further evidence that the speed that impairs the mutant's response does not cause a lasting inability to perceive or physically respond. The mutants are simply not redispersing after surpassing their threshold of response.

The interleaved assay also addressed the issue that these sedentary mutant larvae cause by skewing results when the stimulus heads in their direction again. By interleaving 1.6cm/s between every other speed, redistribution of the larvae was essentially forced. This showed us that the apparent increase in response at 16cm/s is due to skewed results, as when looking at the

varying speed responses from the interleaved experiment, the larvae had an impairment in response to the 16 cm/s stimulus that was like the impaired response they have at 8cm/s stimulus.

Next, tests were done to assess if decreased GABA is the cause for the mutants' impaired response. First, WT larvae were treated with three different subclinical doses of PTZ. PTZ is a convulsant that blocks GABA receptors. It was found that treatment with PTZ decreases response to one like *gad1b*$^{-/-}$, but these fish remain mobile and are not triggered into ictal-like events due to the stimulus, suggesting that decreased l GABA signaling is enough to cause a deficit in the OMR.

A recent preprint studying habituation in zebrafish ran an OMR on larvae after exposure to picrotoxin (PTX), a convulsant that has overlapping actions with PTZ. Their dose of this convulsant was purposefully low, with their highest dose used being 10 μm, as they did not want to cause any seizures in the larvae, and their chosen dose was enough to effect habituation. (Lamiré et al., 2023). However, they saw no effect on OMR ability (Lamiré et al., 2023). In a study comparing zebrafish susceptibility to PTX and PTZ, 1mM PTZ was enough to cause Grade I morphological defects in 5dpf larvae after 1 hour of treatment (Bandara et al., 2019). The corresponding dose required to cause this level of defect using PTX was 40μm.(Bandara et al., 2019). In this same study, a dose-response assay found that 1mM PTZ led to a seizure score of 1, while 10μm PTX caused a seizure score of 0.8 (Bandara et al., 2019). Therefore, the dose used in Lamiere, 2023 may not have decreased inhibition enough to cause an OMR deficit. Our OMR assay was performed with multiple doses of PTZ, with 1mM PTZ being the lowest concentration with the least effect on their OMR ability (Figure 4.4). Therefore, the effects on GABA signaling in our studies would be higher than the 10μm PTX effects on GABA signaling. I found that this

manner of treatment with PTZ did decrease the OMR ability of WT larvae, but it did not impair their mobility to respond at lower speeds.

Since decreasing GABA signaling in larvae that developed normally caused an impaired OMR, we questioned whether treating the larvae with GABA would be enough to rescue the response of the mutants. GABA was partially able to rescue the mutants' response, but the response remains significantly less than WT. The inability to fully rescue the response with GABA could be due to inefficiency in the treatment with GABA.as it does not penetrate the blood-brain barrier efficiently or possibly it is being metabolized by cells as it is used in the GABA shunt pathway of the TCA cycle.

To test if the mutants' response can be fully rescued, we treated the mutants with the antiepileptic muscimol, a GABA agonist that is known to efficiently penetrate the blood-brain barrier. We found that muscimol treatment was able to rescue the response to an ability like WT larvae, suggesting that rescuing GABA signaling is enough to return the OMR response (Figure 4.6)

Interestingly, neither GABA nor muscimol had any effect, sedative or beneficial, on the WT larvae. Since treatment with GABA or muscimol did not increase the WT response, perhaps GABA is not the limiting factor in OMR ability. Another idea is that maybe the mutants have an upregulation of GABA receptors making them more sensitive to lower doses of treatments therefore improving their response. On the other side, perhaps the machinery for handling GABA is more robust in the WT fish, and therefore they clear GABA from the synaptic cleft faster than the mutants.

When running the muscimol-treated *gad1b* larvae through the 1.6cm/s interleaved assay, a trend was noticed where these larvae had an increase in their response to the 1.6cm/s stimulus

when run after a speed that cannot be perceived even by the WT larvae (Figure 4.7). *gad1b* mutants did not show this increase in response. Also, muscimol was unable to rescue the response at any other stimulus speed than 8cm/s. There could be more at play in the mutants such as a developmental change in the neural circuitry that could still be contributing to the mutants' deficit in OMR. More investigation into this will be necessary to determine any significance of this observation.

Proper inhibition is important for sensory processing, including visual processing. The results of this study provide evidence that decreased GABA signaling, acute and chronic, can cause a deficit in an innate visually evoked behavior, meaning proper inhibition by GABA is necessary for the efficient OMR response. Furthermore, a developmental defect in neural circuitry due to developing with chronic neural excitability cannot be fully ruled out yet.

Acknowledgements

The authors wish to thank Dr. Heike Kroger, Sneha Mohan, Rida Osman, and Christina Sabine for their helpful discussions on this project. The authors also wish to thank the Young Dawg program at UGA which supported Wade David who helped in running OMR assays. This work was supported by the National Institutes of Health (Grant No. R01NS090645 to JDL, PAK, and F31NS115496 to YL) and the National Science Foundation (Grant No. 1350654 to PAK). The authors also acknowledge the assistance of the Biomedical Microscopy Core at the University of Georgia with imaging using the Zeiss LSM 710 confocal microscope and the Zeiss LSM 880.

Tables

Table 4.1 HCR probe and Amplifier set.

HCR Probe-initiator	Amplifier
elavl3-B2	647
gad1b-B1	488
gad2-B4	546

Figures

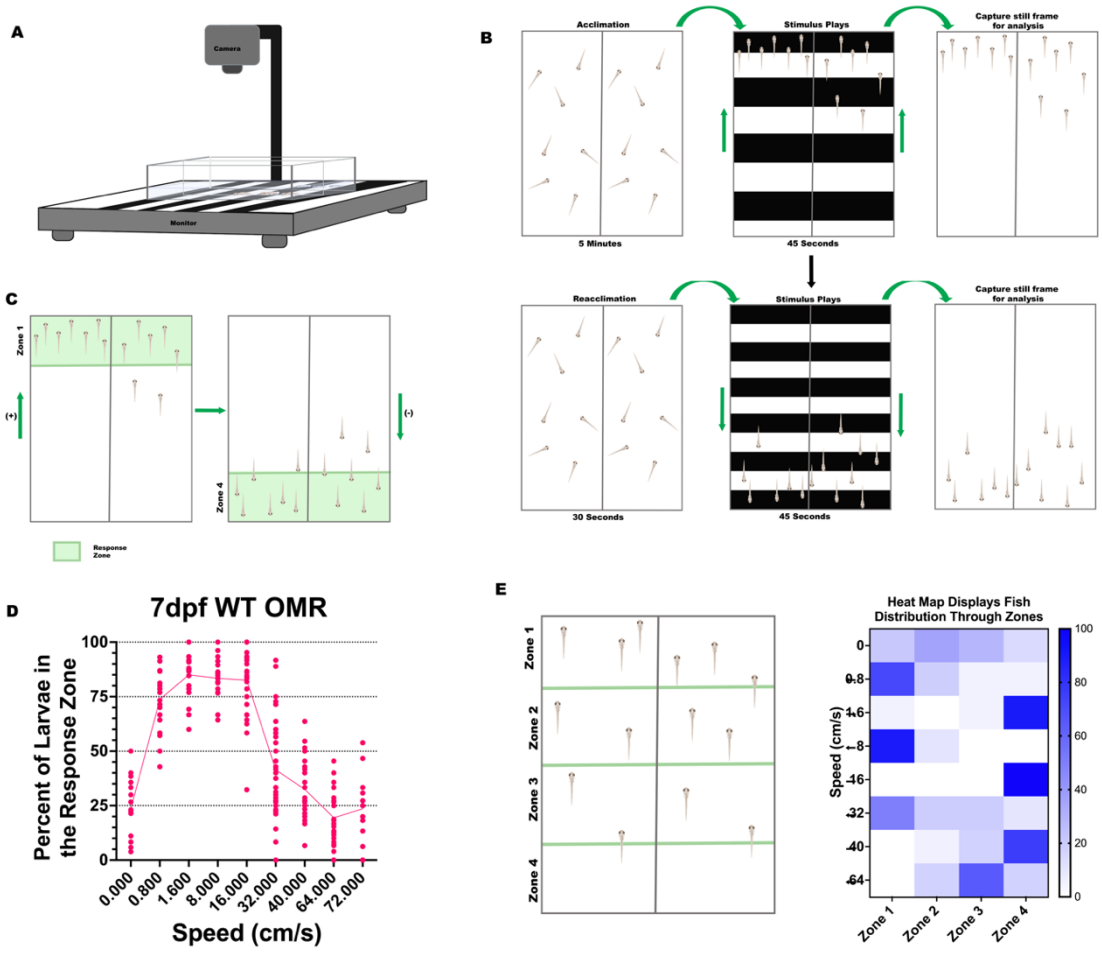

Figure 4.1: Schematic of OMR.

A). Set up of OMR assay showing a clear acrylic container with a middle barrier creating two sides sitting on top of a monitor that plays the OMR program. A camera is mounted above to record videos of the runs. B) Diagram of OMR program starting with a five-minute acclimation where larvae are randomly distributed, followed by a 45-second stimulus heading in the direction

of green arrows. A screen capture is taken of the frame following stimulus cessation. After a 30-second re-acclimation, the stimulus plays again, switching directions and increasing speed. This repeats until the experiment is over. C). Diagram showing he “response zone” based on stimulus direction. D). Graph showing typical response for WT larvae at 7dpf. E). Diagram of zone distribution for whole container analysis (left) and a representative heat map showing larvae distribution through those zones after each speed.

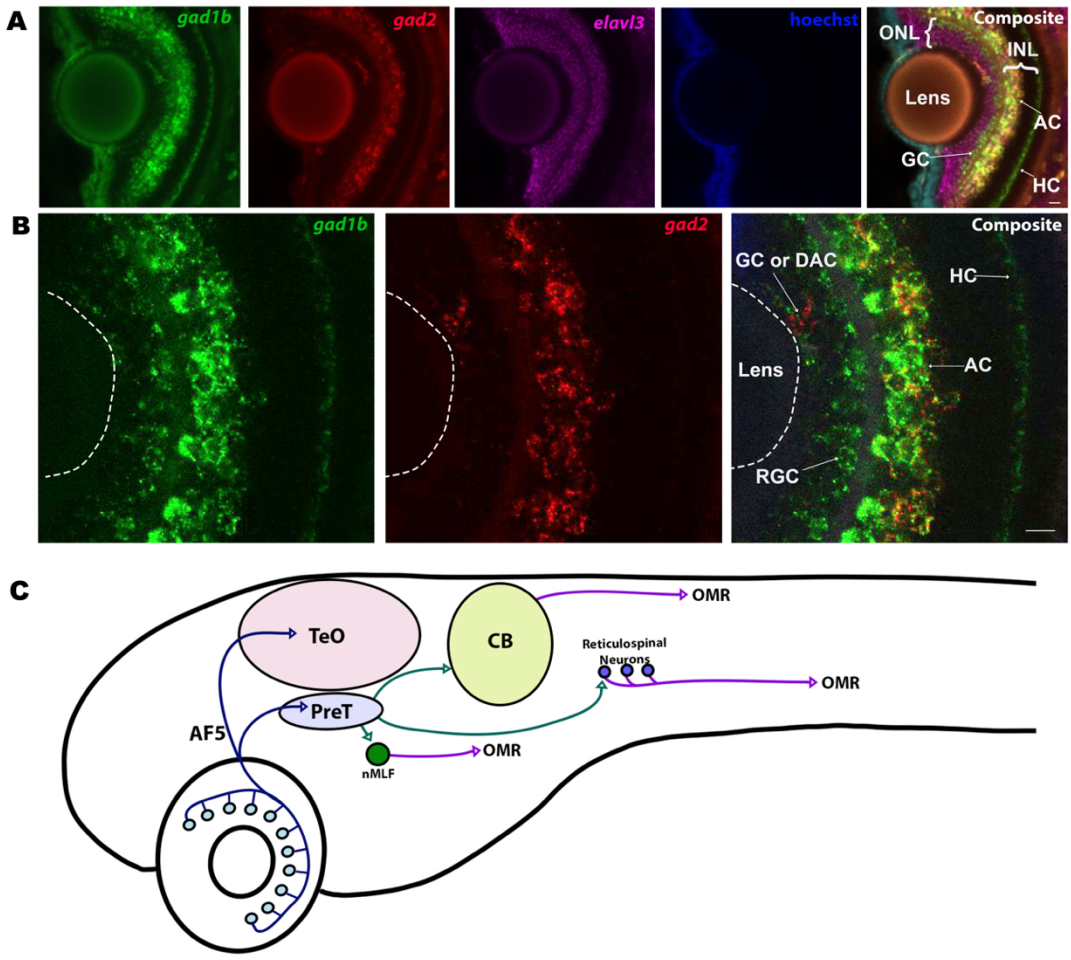

Figure 4.2: *gad1b* and *gad2* expression in the retina and their role in OMR.

A) HCR in situ of *gad1b*, *gad2*, an *elavl3* showing *gad1b* and *gad2* localization in the retina. (AC -amacrine cells HC-Horizontal cells, GC-Ganglion cells, INL-Inner nuclear layer, ONL-outer nuclear layer) B). HCR *in situ* of *gad1b* and *gad2* showing *gad2* expression missing from RGCs and HCs C). Side view of OMR neural processing pathway. (TeO- Optic tectum PreT-Pre tectum, nMLF nucleus of the Medial Longitudinal Fasiculus, OMR-Optomotor Response)

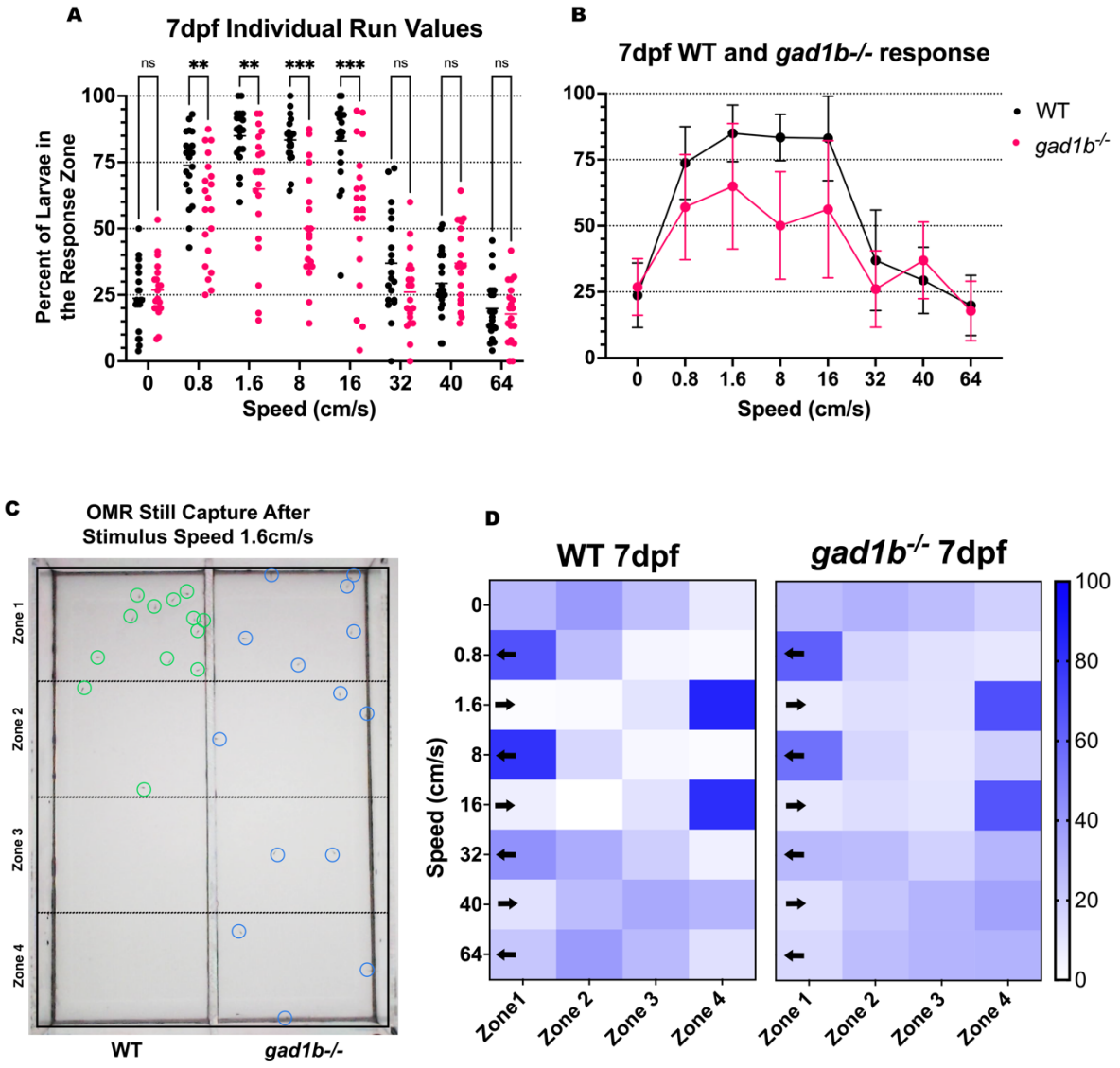

Figure 4.3: *gad1b*$^{-/-}$ fish show decreased response compared to WT from speeds 0.8cm/s to 16 cm/s.

A). Graph of the percentage of responding WT and *gad1b*$^{-/-}$ larvae at each speed with individual run percentages B). Graph of the percentage of responding WT and *gad1b*$^{-/-}$ larvae at each speed as mean with SD. C). Representative still capture of OMR assay results with four zones overlayed. WT on the left with larvae circled in green. *gad1b*$^{-/-}$ fish on the right with larvae circled in blue. D). Heat maps showing the distribution of larvae through the zones at each speed for WT (left) and *gad1b*$^{-/-}$ (right). ns=nonsignificant, **=<0.002, ***=<0.001

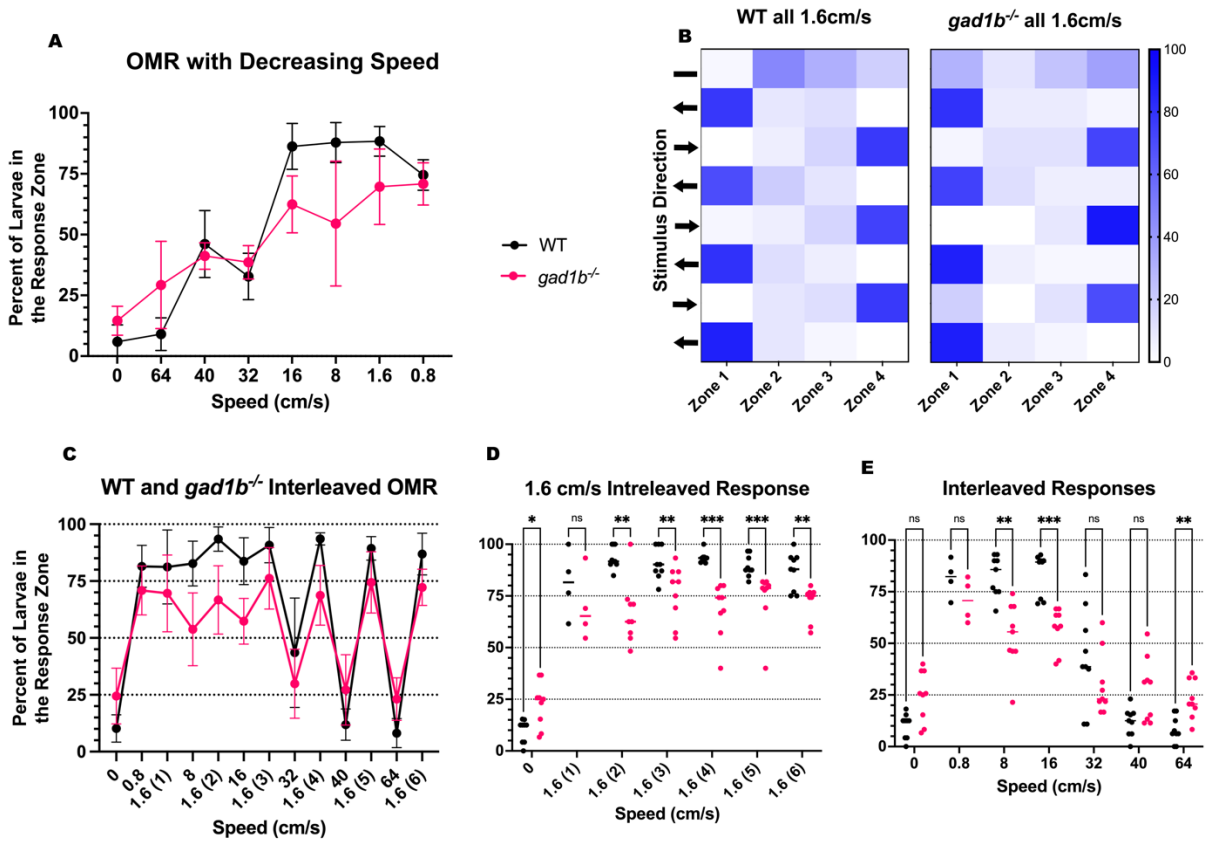

Figure 4.4: *gad1b*$^{-/-}$ fish are still mobile.

A). OMR response ran with stimulus speeds decreasing B). Heat map showing the fish distribution of OMR with stimulus speed all at 1.6cm/s. C). OMR assay ran with 1.6cm/s interleaved between all other speeds. D). Graph showing only the interleaved strongest speed responses. E). Graph showing only the interleaved increasing speed responses ns=non-significant, **=<0.002, ***=<0.001

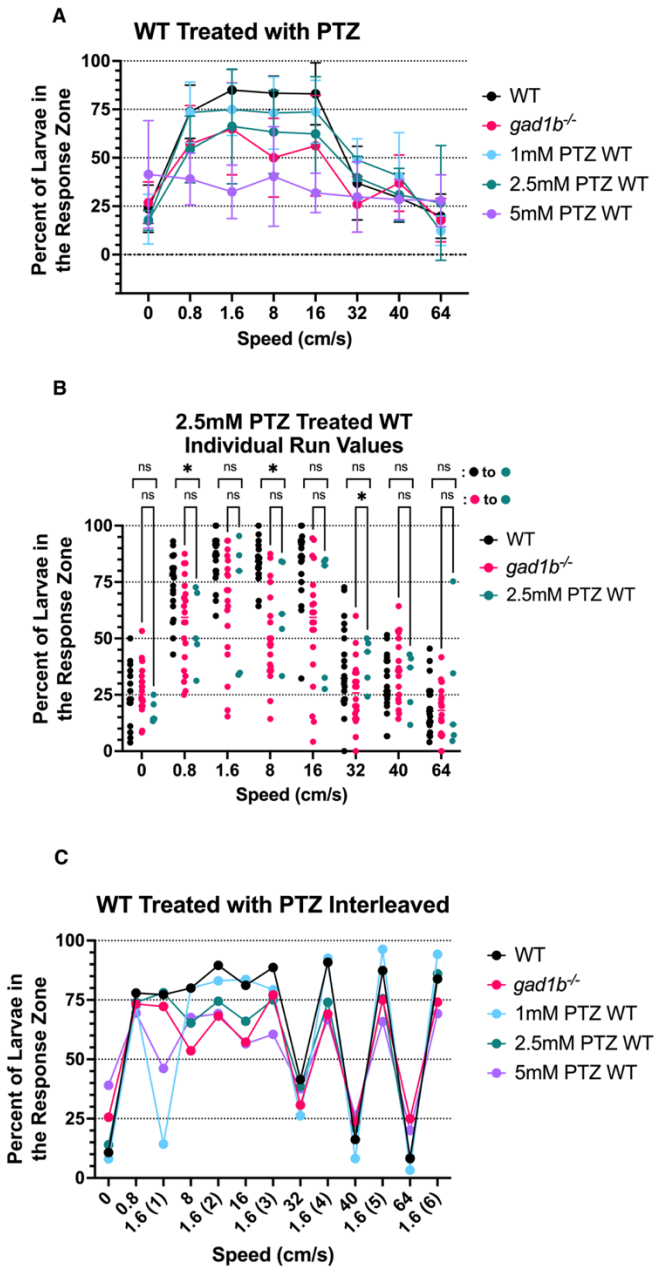

Figure 4.5: PTZ decreases WT fish response.

A). OMR response of WT treated with 1mM, 2.5mM, and 5mM PTZ. B). Induvial responses of 2.5mM PTZ treatment (blue) which is similar to *gad1b*$^{-/-}$. C). Interleaved responses of WT fish treated with PTZ. ns=non-significant *=<0.033

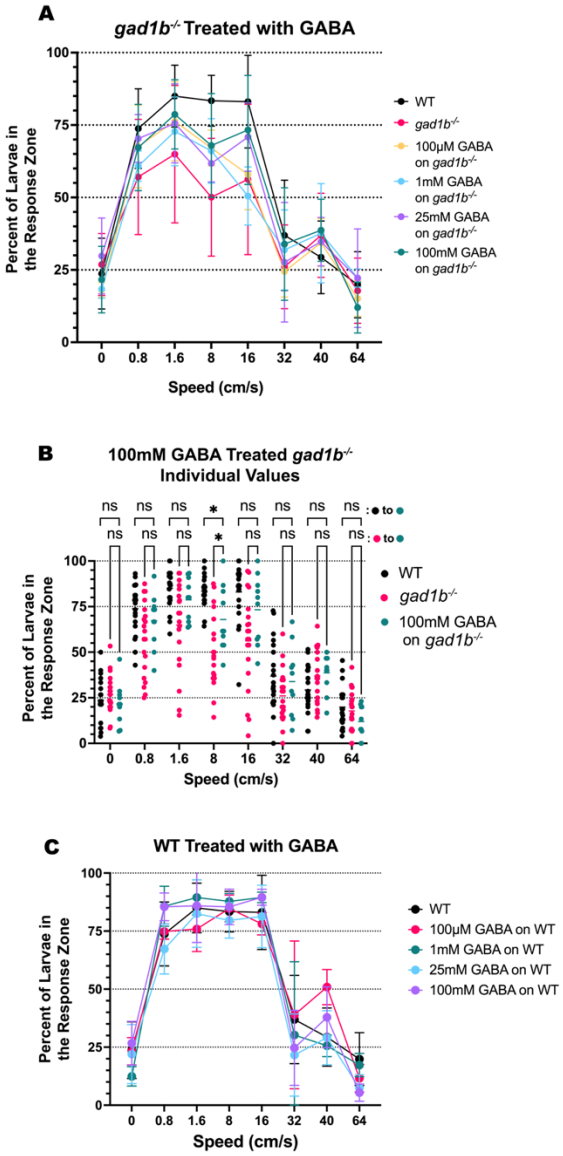

Figure 4.6: GABA increases but does not rescue the OMR of *gad1b*$^{-/-}$ fish at 8cm/s

A). Graph of GABA-treated *gad1b*$^{-/-}$ larvae responses at all speeds as mean with SD. B). Individual runs with 100mM GABA-treated *gad1b*$^{-/-}$ larvae. D) WT treated with GABA responses. ns=nonsignificant, *=<0.033

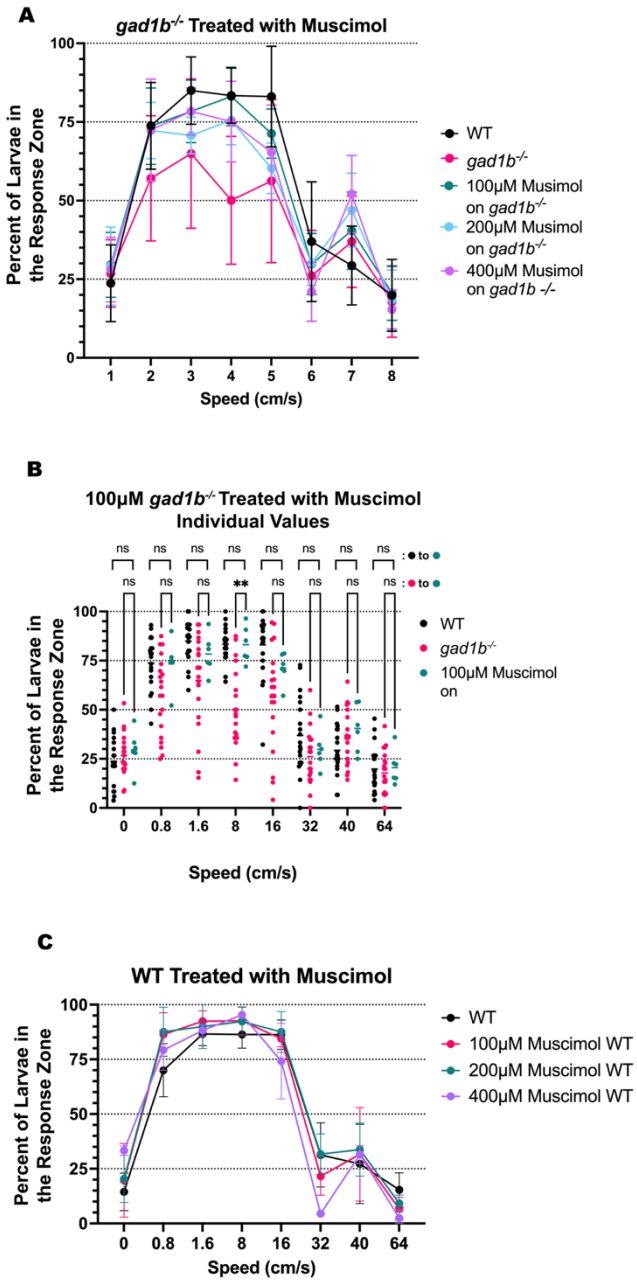

Figure 4.7: Muscimol rescues the ability of gad1b$^{-/-}$ fish to respond at 8cm/s

A). Response of *gad1b*$^{-/-}$ larvae treated with muscimol. B*). gad1b*$^{-/-}$ treated with 100µm muscimol response as individual values. C). WT fish treated with muscimol OMR results. ns=non-significant, **=<0.002

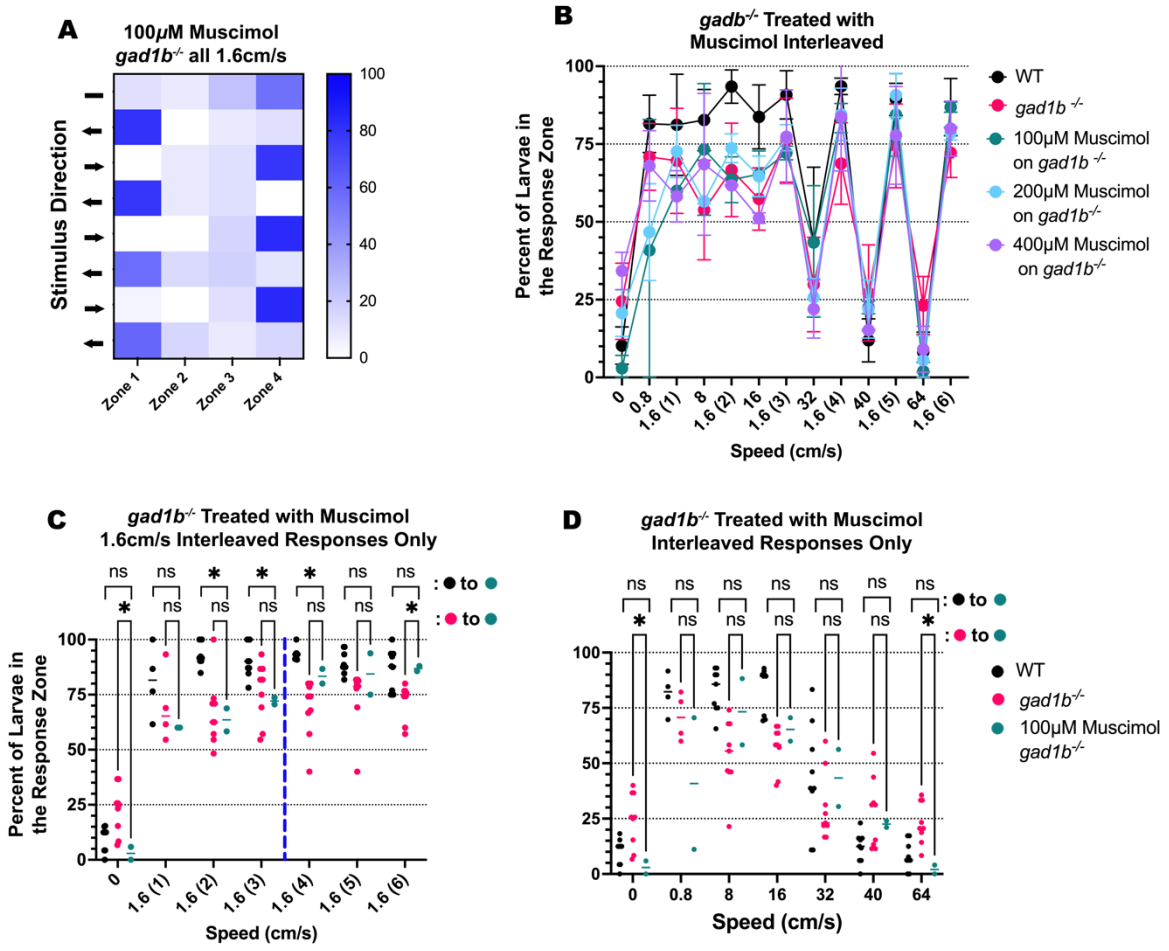

Figure 4.8: *gad1b*$^{-/-}$ larvae treated with muscimol control runs

A) Only the 1.6cms/s interleaved response of the 100µm muscimol treated *gad1b*$^{-/-}$ larvae with mean with SD B). Interleaved responses of *gad1b*$^{-/-}$ larvae treated with muscimol as mean with SD. C). Individual values of 1.6cm/s interleaved responses. Blue line indicates demarcation between when WT larvae still display an OMR and when they do no longer display an OMR D). Individual values from changing speed interleaved reponses. ns=non-significant *=<0.033

References

Asada, H., Kawamura, Y., Maruyama, K., Kume, H., Ding, R.-G., Kanbara, N., Kuzume, H., Sanbo, M., Yagi, T. & Obata, K. (1997). Cleft palate and decreased brain γ-aminobutyric acid in mice lacking the 67-kDa isoform of glutamic acid decarboxylase. *Proceedings of the National Academy of Sciences*, *94*(12), 6496–6499. https://doi.org/10.1073/pnas.94.12.6496

Baier, H. & Wullimann, M. F. (2021). Anatomy and function of retinorecipient arborization fields in zebrafish. *Journal of Comparative Neurology*, *529*(15), 3454–3476. https://doi.org/10.1002/cne.25204

Bandara, S. B., Carty, D. R., Singh, V., Harvey, D. J., Vasylieva, N., Pressly, B., Wulff, H. & Lein, P. J. (2019). Susceptibility of larval zebrafish to the seizurogenic activity of GABA type A receptor antagonists. *NeuroToxicology*, *76*, 220–234. https://doi.org/10.1016/j.neuro.2019.12.001

Baraban, S. C., Taylor, M. R., Castro, P. A. & Baier, H. (2005). Pentylenetetrazole induced changes in zebrafish behavior, neural activity and c-fos expression. *Neuroscience*, *131*(3), 759–768. https://doi.org/10.1016/j.neuroscience.2004.11.031

Brockerhoff, S. E., Hurley, J. B., Janssen-Bienhold, U., Neuhauss, S. C., Driever, W. & Dowling, J. E. (1995). A behavioral screen for isolating zebrafish mutants with visual system defects. *Proceedings of the National Academy of Sciences*, *92*(23), 10545–10549. https://doi.org/10.1073/pnas.92.23.10545

Clark, D. T. (1981). *Visual Responses inDeveloping Zebrafish*.

Condie, B. G., Bain, G., Gottlieb, D. I. & Capecchi, M. R. (1997). Cleft palate in mice with a targeted mutation in the γ-aminobutyric acid-producing enzyme glutamic acid decarboxylase 67. *Proceedings of the National Academy of Sciences*, *94*(21), 11451–11455. https://doi.org/10.1073/pnas.94.21.11451

Easter, S. S. & Nicola, G. N. (1997). The Development of Eye Movements in the Zebrafish (Danio rerio). *Developmental Psychobiology*.

Erlander, M. G., Tillakaratne, N. J. K., Feldblum, S., Patel, N. & Tobin, A. J. (1991). Two genes encode distinct glutamate decarboxylases. *Neuron*, *7*(1), 91–100. https://doi.org/10.1016/0896-6273(91)90077-d

Fei, H., Chow, D. M., Chen, A., Romero-Calderón, R., Ong, W. S., Ackerson, L. C., Maidment, N. T., Simpson, J. H., Frye, M. A. & Krantz, D. E. (2010). Mutation of the Drosophila vesicular GABA transporter disrupts visual figure detection. *Journal of Experimental Biology*, *213*(10), 1717–1730. https://doi.org/10.1242/jeb.036053

Kaufman, D. L., Houser, C. R. & Tobin, A. J. (1991). Two Forms of the γ-Aminobutyric Acid Synthetic Enzyme Glutamate Decarboxylase Have Distinct Intraneuronal Distributions and Cofactor Interactions. *Journal of Neurochemistry*, *56*(2), 720–723. https://doi.org/10.1111/j.1471-4159.1991.tb08211.x

Lagnado, L. (1998). Retinal processing: Amacrine cells keep it short and sweet. *Current Biology*, *8*(17), R598–R600. https://doi.org/10.1016/s0960-9822(98)70385-9

Lamiré, L.-A., Haesemeyer, M., Engert, F., Granato, M. & Randlett, O. (2023). Functional and pharmacological analyses of visual habituation learning in larval zebrafish. *Neuroscience*.

LeFauve, M. K., Rowe, C. J., Crowley-Perry, M., Wiegand, J. L., Shapiro, A. G. & Connaughton, V. P. (2021). Using a variant of the optomotor response as a visual defect detection assay in zebrafish. *Journal of Biological Methods*, *8*(1), e144. https://doi.org/10.14440/jbm.2021.341

Liu, Y., Chen, Y., Duffy, C. R., VanLeuven, A. J., Byers, J. B., Schriever, H. C., Ball, R. E., Carpenter, J. M., Gunderson, C. E., Filipov, N. M., Ma, P., Kner, P. A. & Lauderdale3, and J. D. (n.d.). *Decreased GABA levels during development results in increased connectivity in the larval zebrafish tectum*.

Martin, D. L. & Rimvall, K. (1993). Regulation of γ-Aminobutyric Acid Synthesis in the Brain. *Journal of Neurochemistry*, *60*(2), 395–407. https://doi.org/10.1111/j.1471-4159.1993.tb03165.x

Matsuda, K. & Kubo, F. (2021). Circuit Organization Underlying Optic Flow Processing in Zebrafish. *Frontiers in Neural Circuits*, *15*, 709048. https://doi.org/10.3389/fncir.2021.709048

Muto, A., Orger, M. B., Wehman, A. M., Smear, M. C., Kay, J. N., Page-McCaw, P. S., Gahtan, E., Xiao, T., Nevin, L. M., Gosse, N. J., Staub, W., Finger-Baier, K. & Baier, H. (2005). Forward Genetic Analysis of Visual Behavior in Zebrafish. *PLoS Genetics*, *1*(5), e66. https://doi.org/10.1371/journal.pgen.0010066

Naumann, E. A., Fitzgerald, J. E., Dunn, T. W., Rihel, J., Sompolinsky, H. & Engert, F. (2016). From Whole-Brain Data to Functional Circuit Models: The Zebrafish Optomotor Response. *Cell*, *167*(4), 947-960.e20. https://doi.org/10.1016/j.cell.2016.10.019

Neuhauss, S. C. F. (2003). Behavioral genetic approaches to visual system development and function in zebrafish. *Journal of Neurobiology*, *54*(1), 148–160. https://doi.org/10.1002/neu.10165

Neuhauss, S. C. F., Biehlmaier, O., Seeliger, M. W., Das, T., Kohler, K., Harris, W. A. & Baier, H. (1999). Genetic Disorders of Vision Revealed by a Behavioral Screen of 400 Essential Loci in Zebrafish. *The Journal of Neuroscience*, *19*(19), 8603–8615. https://doi.org/10.1523/jneurosci.19-19-08603.1999

Robles, E., Laurell, E. & Baier, H. (2014). The Retinal Projectome Reveals Brain-Area-Specific Visual Representations Generated by Ganglion Cell Diversity. *Current Biology*, *24*(18), 2085–2096. https://doi.org/10.1016/j.cub.2014.07.080

Roeser, T. & Baier, H. (2003). Visuomotor Behaviors in Larval Zebrafish after GFP-Guided Laser Ablation of the Optic Tectum. *The Journal of Neuroscience*, *23*(9), 3726–3734. https://doi.org/10.1523/jneurosci.23-09-03726.2003

Sohal, V. S. & Rubenstein, J. L. R. (2019). Excitation-inhibition balance as a framework for investigating mechanisms in neuropsychiatric disorders. *Molecular Psychiatry*, *24*(9), 1248–1257. https://doi.org/10.1038/s41380-019-0426-0

VanLeuven, A. J. (2018). *UNDERSTANDING THE ROLE OF THE GAD GENES IN NEURAL DEVELOPMENT AND NERVOUS SYSTEM FUNCTION IN ZEBRAFISH*.

Zhao, H., Mao, X., Zhu, C., Zou, X., Peng, F., Yang, W., Li, B., Li, G., Ge, T. & Cui, R. (2022). GABAergic System Dysfunction in Autism Spectrum Disorders. *Frontiers in Cell and Developmental Biology*, *9*, 781327. https://doi.org/10.3389/fcell.2021.781327

Supplementary Tables and Figures

Supplemental Table 4.1: Means and SDs of the responses from the no treatment runs of WT and *gad1b*$^{-/-}$

Speed	WT mean response	SD	*gad1b*$^{-/-}$ mean response	SD
No stimulus	23.70	12.21	26.83	10.70
0.8cm/s	73.77	13.75	57.08	19.88
1.6cm/s	84.98	10.689	64.94	23.73
8m/s	83.39	8.75	50.08	20.33
16cm/s	83.06	16.00	56.24	25.95
32cm/s	36.93	19.03	26.06	14.45
40cm/s	29.34	12.53	36.94	14.53
64cm/s	19.86	11.40	17.81	11.26

Supplemental Table 4.2 Means and SDs of the changing speed stimuli responses of the interleaved OMR runs of WT and *gad1b*$^{-/-}$

Speed	WT mean interleaved response	SD	*gad1b*$^{-/-}$ mean interleaved response	SD
No stimulus	10.23	5. 98	24.46	12.26
0.8cm/s	81.49	9.21	70.89	10.73
8m/s	82.70	9.83	53.79	15.99
16cm/s	83.73	10.29	57.34	10.01
32cm/s	43.51	24.06	29.85	15.18
40cm/s	11.91	6.91	27.17	15.44
64cm/s	8.16	6.40	23.14	9.33

Supplemental Table 4.3 **Means and SDs of the 1.6cm/s responses of the interleaved OMR runs of WT and *gad1b*$^{-/-}$**

	WT average interleaved response	SD	*gad1b*$^{-/-}$ average interleaved response	SD
1	81.17	16.25	69.60	16.88
2	93.46	5.36	66.69	15.01
3	90.81	7.75	76.25	13.50
4	93.54	2.6	68.74	13.11
5	89.35	5.16	74.39	13.46
6	86.86	9.17	72.21	7.95

Supplemental Table 4.4: **Means and SDs of the responses from the all 1.6cm/s OMR runs of WT and *gad1b*$^{-/-}$**

Speed	WT	SD	*gad1b*$^{-/-}$	SD
No stimulus	5.887042	6.934901	14.54545	5.95874
→	9.019886	6.710078	29.26085	17.93236
←	46.09155	13.78219	41.17939	5.435488
→	32.7364	9.544268	38.5884	6.841918
←	86.26547	9.445993	62.40828	11.71247
→	87.86238	8.220248	54.5	25.68398
←	88.35575	6.096406	69.67983	15.53305
→	74.51109	6.265987	70.84034	8.702518

Supplemental Table 4.5: Means and SDs of the responses from the WT PTZ treatment OMR runs

Speed	1mM PTZ treated WT	SD	2.5mM PTZ treated WT	SD	5mM PTZ treated WT	
No stimulus	18.27	12.83	17.58	5.08	41.45	27.79
0.8cm/s	73.43	15.67	54.32	17.24	39.03	13.35
1.6cm/s	74.98	13.42	66.20	29.60	32.43	13.83
8m/s	73.13	18.63	63.32	21.50	40.37	25.73
16cm/s	73.80	16.24	62.34	29.53	31.87	10.14
32cm/s	48.92	10.90	39.74	10.98	29.78	18.10
40cm/s	40.54	22.46	30.91	13.61	28.44	10.42
64cm/s	12.35	7.65	26.69	29.67	27.84	13.36

Supplemental Table 4.6: Means and SDs of the responses from the WT GABA treatment OMR runs

Speed	100μM GABA on WT	SD	1mM GABA on WT	SD	25mM GABA on WT	SD	100mM GABA on WT	SD
No stimulus	23.22	5.87	12.41	4.17	22.01	12.74	26.67	9.43
0.8cm/s	74.83	3.31	85.70	8.59	67.27	10.76	85.45	5.96
1.6cm/s	75.89	9.70	89.48	7.60	82.52	14.52	85.91	15.81
8m/s	84.75	5.74	87.77	3.41	79.62	7.64	85.42	7.62
16cm/s	78.10	4.72	89.50	2.25	81.30	13.43	89.58	3.44
32cm/s	38.91	31.82	30.19	31.59	21.590	17.68	24.70	16.14
40cm/s	50.88	7.58	25.59	4.65	29.08	11.63	37.86	13.11
64cm/s	11.57	5.97	17.28	5.04	7.40	5.72	5.42	3.70

Supplemental Table 4.7 Means and SDs of the responses from the *gad1b*$^{-/-}$ GABA treatment OMR runs

Speed	100μM GABA on *gad1b*$^{-/-}$	SD	1mM GABA on *gad1b*$^{-/-}$	SD	25mM GABA on *gad1b*$^{-/-}$	SD	100mM GABA on *gad1b*$^{-/-}$	SD
No stimulus	18.07	2.57	18.37	3.14	29.81	13.09	21.64	11.51
0.8cm/s	67.60	14.27	60.81	5.22	70.35	8.24	67.24	14.91
1.6cm/s	76.30	13.64	72.80	11.88	75.57	13.64	78.67	11.95
8m/s	67.08	6.14	66.05	11.14	61.75	6.42	67.94	17.91
16cm/s	57.93	12.14	50.49	10.04	70.86	11.80	73.29	18.81
32cm/s	24.45	8.85	31.88	13.80	27.63	20.63	33.91	19.42
40cm/s	34.40	8.22	37.64	17.14	34.72	8.347	38.67	10.71
64cm/s	15.12	6.18	22.21	3.14	22.13	17.01	11.99	8.79

Supplemental Table 4.8: Means and SDs of the responses from the WT Muscimol treatment OMR runs

Speed	100μM Muscimol on WT	SD	200μM Muscimol on WT	SD	400μM Muscimol on WT	SD
No stimulus	19.67	16.82	20.37	10.75	33.30	2.096
0.8cm/s	86.34	9.96	87.61	11.20	79.22	9.18
1.6cm/s	92.42	4.74	90.00	10.08	88.18	2.57
8m/s	92.59	6.23	92.32	6.65	95.35	0.15
16cm/s	84.40	3.63	87.54	9.31	74.13	17.30
32cm/s	21.57	8.69	31.69	9.16	4.45	0.14
40cm/s	31.61	21.32	33.74	12.15	31.47	4.10
64cm/s	6.68	5.22	9.15	3.87	2.50	3.54

Supplemental Table 4.9: Means and SDs of the responses from the *gad1b*$^{-/-}$ muscimol treatment OMR runs

Speed	100μM Muscimol on *gad1b*$^{-/-}$	SD	200μM Muscimol on *gad1b*$^{-/-}$	SD	400μM Muscimol *on* *gad1b*$^{-/-}$	SD
No stimulus	29.58	10.31	29.14	12.42	28.05	10.26
0.8cm/s	73.65	12.16	72.27	8.96	72.42	16.18
1.6cm/s	78.37	9.923	70.68	5.83	78.35	7.50
8m/s	83.11	9.31	75.54	7.78	75.12	12.82
16cm/s	71.30	7.83	60.25	8.03	65.34	15.04
32cm/s	29.85	9.70	30.09	7.04	20.97	9.38
40cm/s	40.42	12.28	46.95	11.72	52.05	12.29
64cm/s	20.58	8.66	18.43	9.51	15.41	6.18

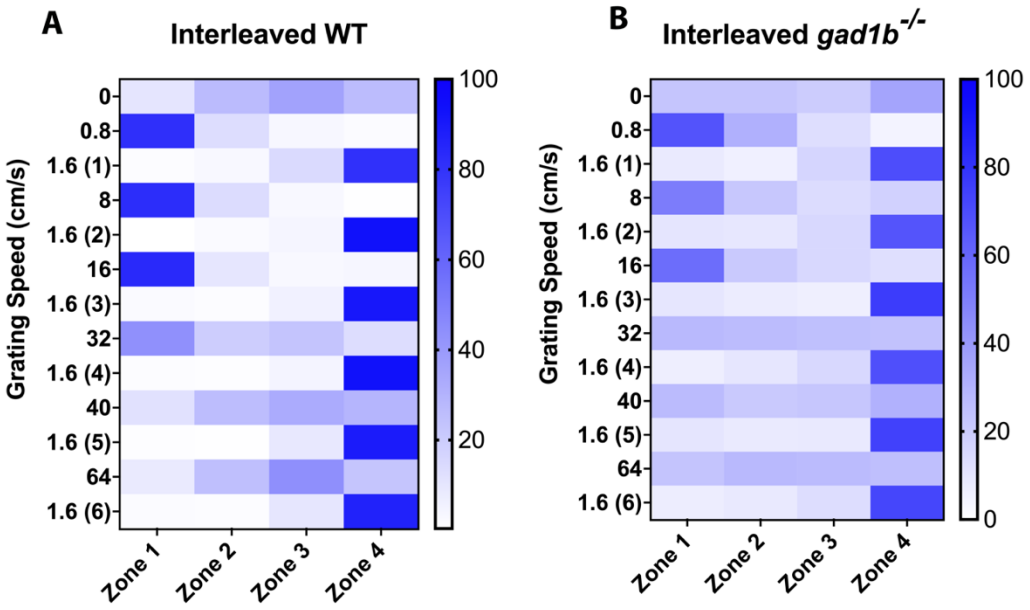

Supplementary Figure 4.1: Distribution of larvae through the container during the interleaved control runs. A). WT distribution. B). *gad1b*$^{-/-}$ ditribution

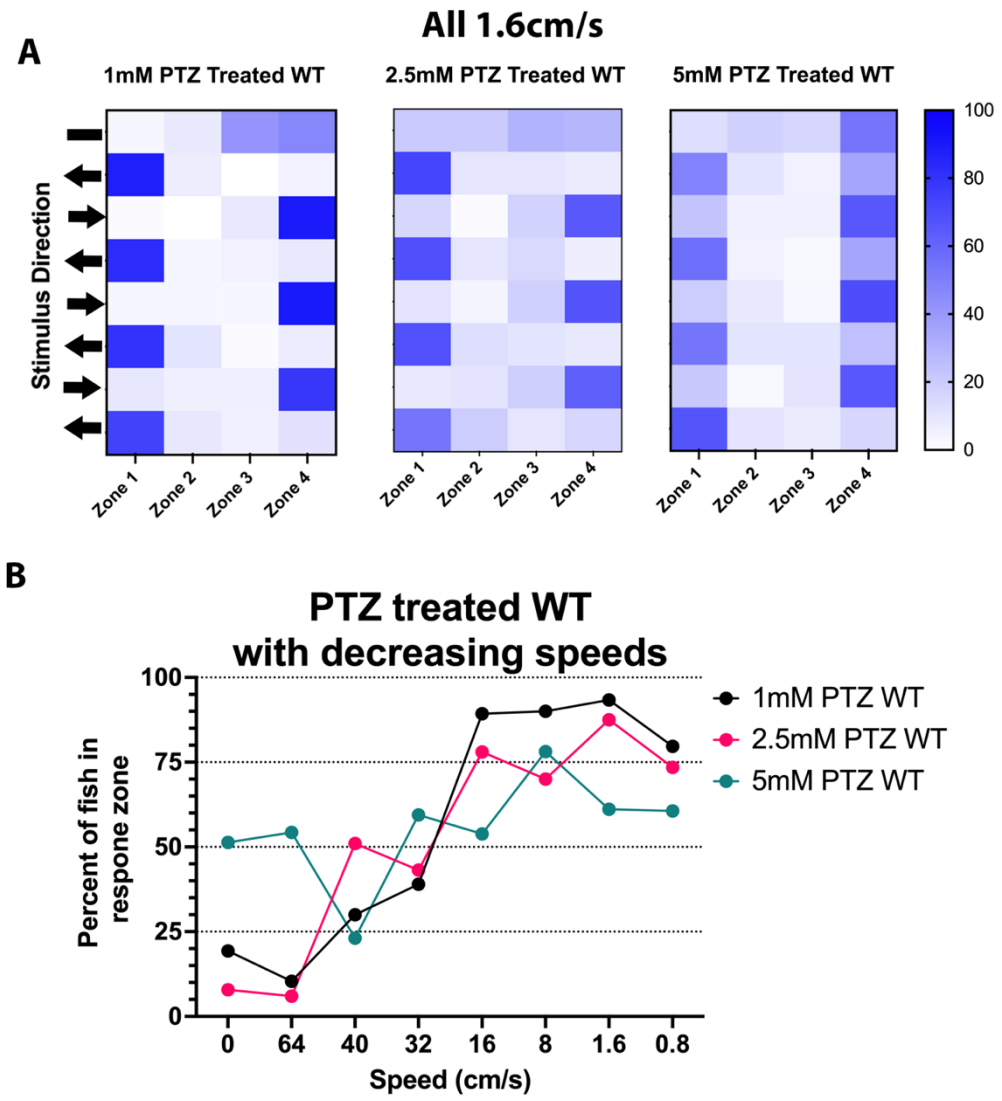

Supplementary Figure 4.2. PTZ Treated WT Control Runs. A). Assay ran with all speed 1.6cm/s. B). Assay ran with peeds decreasing

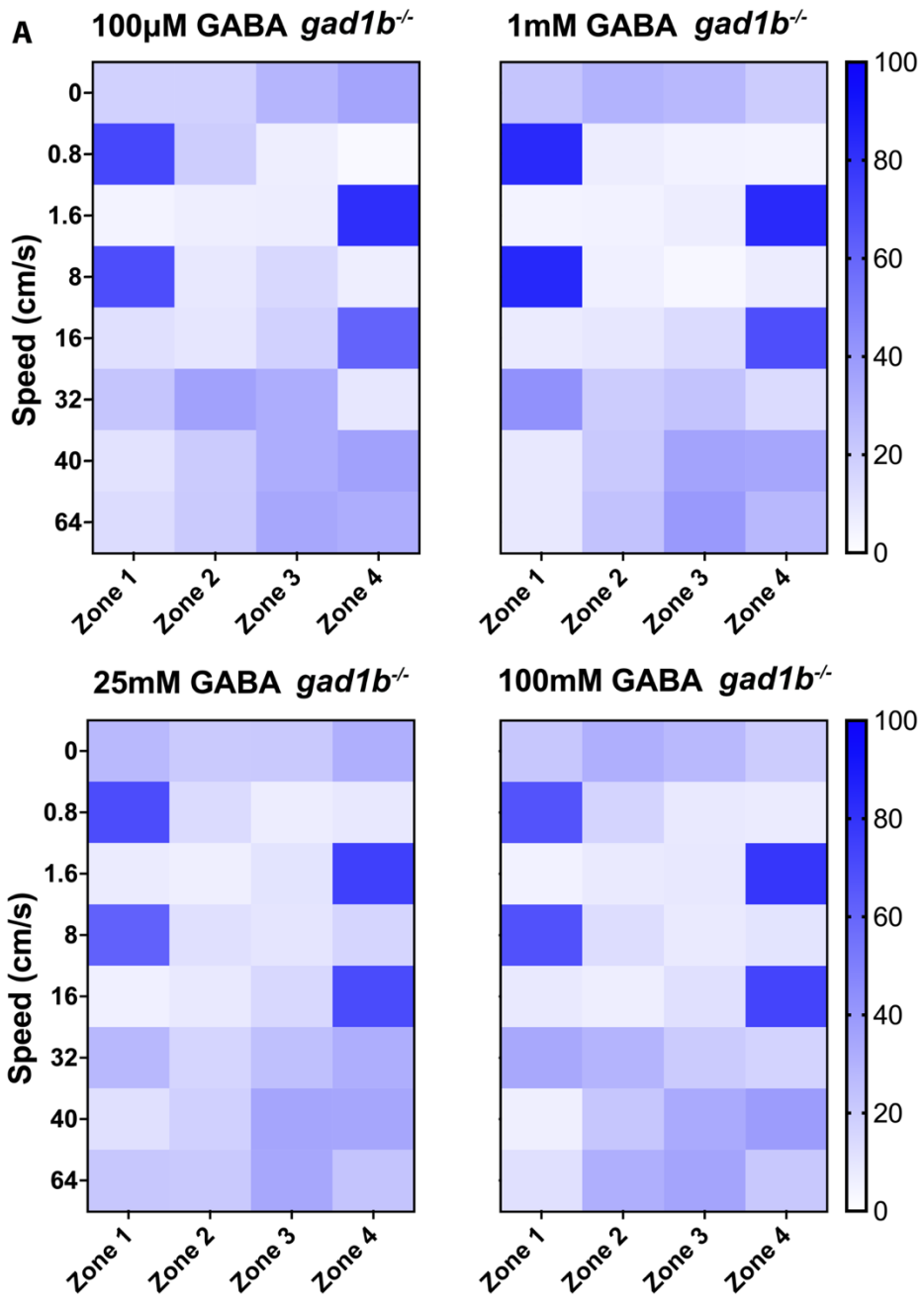

Supplementary Figure 4.3. Distribution through the container for GABA treated *gad1b*$^{-/-}$ larvae. Heat map showing distribution through the four zones

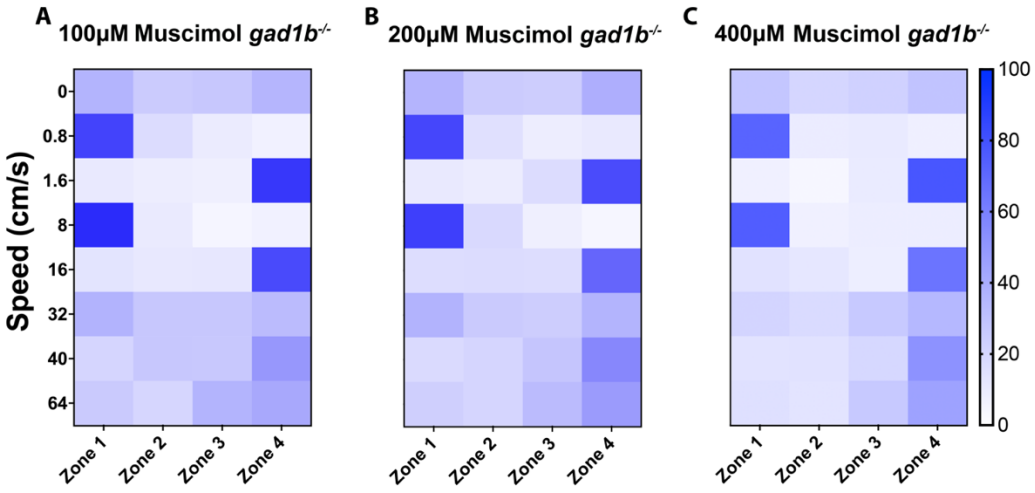

Supplementary Figure 4.4 Distribution through the container for GABA treated *gad1b*$^{-/-}$ larvae. Heat map showing distribution through the four zones

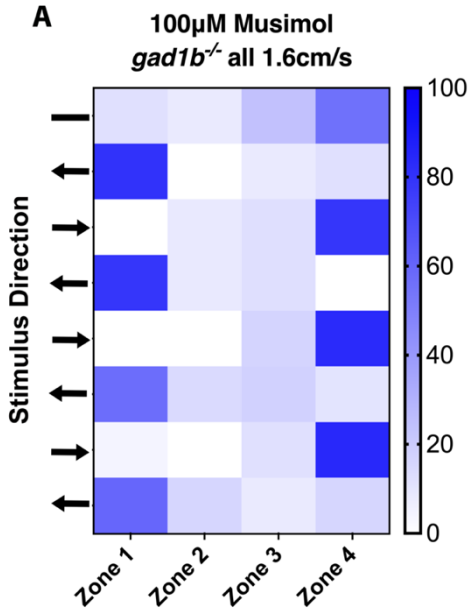

Supplementary Figure 4.5. Muscimol treated *gad1b*$^{-/-}$ larvae distribution during control run of all speeds 1.6cm/s. Heat map showing distribution through the four zones

CHAPTER 5

CONCLUSIONS

In my studies presented in this dissertation, I have contributed evidence on the importance of GABA signaling for proper brain development. Studying the excitatory-inhibitory balance is of high interest for understanding developmental neurological disorders, but there are few model organisms that are viable with null mutations that lead to an interrupted balance. Despite the importance of GAD in generating GABA, there have not been many studies looking into how a mutation in GAD, affects the E/I balance and brain development. This is mostly because GAD mutations in mice are limited to knockdowns and conditional knockouts due to the neonatal lethality of the GAD1 mutation (Asada et al., 1996, 1997; Condie et al., 1997). The *gad1b* zebrafish mutant developed in our lab provides a great model for studying changes in neural activity and subsequently the effects on the developing brain (Liu et al., n.d.; VanLeuven, 2018). In my project, I used two main methods to show the importance of GABA signaling in developing zebrafish. One was through imaging experiments and the other was through behavioral experiments.

Imaging

My lab previously identified our CRISPR generated *gad1b* mutants as a good model for studying neural hyperactivity due to HPLC data showing decreased GABA levels and electrophysiology detecting ictal-like events (Liu et al., n.d.; VanLeuven, 2018). Through work performing live calcium imaging and light sheet microscopy of the optic tectum, we have been

able to visualize an increase in neural activity and illuminate its propagation pattern through the tectum. We found that there is a decrease in lateral inhibition leading to a broader path of neural propagation. By masking this data with the layers of the optic tectum, we found there is an increase in synchronicity between the left and right sides of the brain within the mutants, which is not seen in WT larvae treated with a convulsant. This is very interesting as it suggests there is increased neural circuitry.

Currently, our work only focuses on one plane of view, so we are missing the larger scope of the pattern of propagation of neural activity through the whole tectum. It would be fascinating to see what is occurring on a 3-dimensional level. Our collaborators are working on fast volumetric imaging, and they have been able to use our line of WT fish expressing Tg(*elavl3:gcamp5G*), the Kner lab was able to image a video of neural activity taking place through the 3-D optic tectum. This kind of work will be central for capturing whole brain data of neural activity and further illuminating ways a genetic mutation alters the pattern of neural propagation. Currently, they are working to increase the speed of their imaging in hopes imaging will be fast enough to capture alterations in neural activity between the wild-type larvae and mutants such as our *gad1b*$^{-/-}$ line.

Additionally, I have contributed evidence that the increased neural hyperactivity we observed through calcium imaging in our mutants can alter the ratio of excitatory and inhibitory cells within the brain. It is assumed that interrupting the balance of excitatory and inhibitory neurotransmitters can cause dysregulation of synaptic pruning and neural circuitry refinement (Chechik et al., 1998; Jill, 2020; Paolicelli et al., 2011). Much of the work looking into this has been done in knockdowns or mutants that indirectly affect the balance. The results of my studies are consistent with this idea and are some of the first studies looking at a *gad* mutation that

directly alters the E/I balance by decreasing GABA signaling due to decreased GABA. My data is of the first to show there is a change in the number of neurons between mutants and wild type.

Due to convention, many labs do not continue investigations in larvae past 5 dpf when studying the brain in zebrafish. There are multiple reasons for this. One is that it is harder to image older larval zebrafish due to pigment production. The use of 1-phenyl 2-thiourea (PTU) is required to image larvae in a background that produces pigment. However, PTU can be challenging as it easily comes out of solution and is unstable in light. While there are strains of larvae that produce less pigment, they are not always a feasible option. The *nacre* line of zebrafish has a mutation in the tyrosinase pathway causing inhibition of melanocyte production. For our studies, the use of this background with the *gad1b* mutants was not achievable as the gene resides on the same chromosome as *gad1b*. Another line of zebrafish with decreased pigment is the albino line. These larvae are great for imaging as they do not produce melanocytes in the epithelium or within the retina. However, I found their viability to be decreased, and, therefore, crossing these larvae with a mutant line plus transgenes was a trying task that I was not able to accomplish in a timely manner. Therefore, my best choice was treatment with PTU. Though frustrating, I found that with consistent refreshing of the PTU and proper storage of the solution, I was able to keep the pigment level low enough to image out to 10dpf. With the careful use of PTU, I was able to image the mutants at 8dpf and 10 dpf and found there was a difference in the number of neurons at these ages, which others may have missed by imaging at too early of a time point.

I have been able to visualize detailed transcript localization of the *gad1a* and *gad1b* paralogs in the zebrafish optic tectum. Our lab identified the paralogs, *gad1b* and *gad1a,* and revealed that *gad1a* was expressed in cells in the neuron separate from *gad1b* and *gad2* at 1 dpf.

gad1a also had a distinct expression pattern at 3dpf. However, penetrance into the deeper layers of whole embryos at 3dpf onward did not provide enough resolution to probe for specific colocalization of the three genes. I brought to our lab the more sensitive detection method of HCR in situ hybridizations, which uses small 20 bp probe sets and an initiator complex that amplifies fluorophore numbers at the spot of transcripts. This technique penetrated 5 and 6 dpf whole zebrafish larvae efficiently, producing detailed labeling of expression within the brain. Further investigations will be able to generate a quantitative level of coexpression between *gad1a* and *gad1b*, *gad2* expressing cells.

I have produced in our lab a way to decrease lipofuscin autofluorescence from blood cells in the zebrafish based on ways this was decreased in other organisms (Cheng et al., 2014; King & Newmark, 2013). The autofluorescence from blood cells was very frustrating particularly when performing TUNEL, when only around 30 cells are detectable. The autofluorescence from the blood cells would drown out this signal as well as cause confusion when trying to count TUNEL. Treatment with CuSO4 worked to decrease the autofluorescence without blocking the fluorophore signal. I was able to use this method for fluorescent HCR in situ hybridizations as well as generating better results.

Behavior

The optomotor response assay has been essential in identifying mutants with visual deficits, but its full potential hasn't been realized yet, as it is not yet being widely used to test for sensory processing issues in reverse genetic mutants. Given the importance of GABA in visual processing, the OMR assay makes for a great method for confirming visual processing deficits. By running the larvae through the OMR assay, I have been one of the first to gather evidence that GABA signaling is needed for proper OMR ability.

Prior tests investigating OMR with lowered GABA have been performed, without such findings. However, these prior studies had their limitations. One test was done using treatment with convulsant picrotoxin (PTX), but they saw no effect on the OMR ability. Their dose of this convulsant was purposefully low and they never observed any spontaneous seizures in the larvae they ran through the experiment (Lamiré et al., 2023)s. This dose may not have decreased inhibition enough to cause an OMR deficit. I performed the OMR assay with multiple subclinical doses of PTZ that still visually increased the activity of the larvae. I found that this manner of treatment with PTZ did decrease the OMR ability of WT larvae, but it did not impair their mobility. Additionally, there was a dose-response in OMR impairment. The higher doses impaired the OMR more so than the lower doses.

Another lab working with drosophila created a dVGAT, an ortholog of the Vesicular GABA Transport (VGAT) gene, mutant(Fei et al., 2010). The mutation was homozygous lethal though, so they had to use a rescue and a knockdown to perform behavioral studies. They did not see a defect in the optomotor control of the fruit flies (Fei et al., 2010). Our mutant line of zebrafish is a better model as GABA signaling is more directly affected as *GABA* is genetically reduced in all *gad1b* expressing cells throughout all of development.

I believe that my evidence showing an interrupted E/I balance can lead to altered visually evoked behavior, is a step towards studying sensory processing issues that are associated with neurological disorders, particularly autism spectrum disorder (ASD). Zebrafish is becoming a popular model of choice in studying autism and the neural circuitry that could be associated with ASD (Tayanloo-Beik et al., 2022), and I believe that the OMR assay would be a good assay for studying these zebrafish models. There is growing evidence that low-level visual perception is a common deficit in individuals diagnosed with ASD and that issues with visual perception could

be a cause behind core deficits such as social cognition dysfunction (Maaswinkel & Li, 2003; Zaidel et al., 2015). A recent study found children with ASD may have deficits in recognizing illusory shapes asthey exhibit delayed neural processing of the illusion (Gori et al., 2016). This ability to recognize an illusory shape involves a processing ability like that of the OMR as it requires the image to be perceived in one part of the brain and quickly processed in another.

Combining behavioral studies with imaging, it is possible to record calcium imaging while exposing fish to an OMR stimulus (Marvin et al., 2019; Vladimirov et al., 2014). Currently, this has only been used to show brain activity when exposed to the stimulus in WT fish or used to validate imaging tools that turn on with neural stimulation like GCaMP6s (Vladimirov et al., 2014) or the iGABASnFR (Marvin et al., 2019). This manner of imaging has not yet been used to study changes in the neural propagation of neural circuitry. It would be fascinating to perform this assay on the *gad1b* mutant zebrafish and other mutant fish being used as a model for neurological disorders, particularly ASD, and unveil what changes in neural circuitry have occurred that affect sensory processing.

References

Asada, H., Kawamura, Y., Maruyama, K., Kume, H., Ding, R., Ji, F. Y., Kanbara, N., Kuzume, H., Sanbo, M., Yagi, T. & Obata, K. (1996). Mice Lacking the 65 kDa Isoform of Glutamic Acid Decarboxylase (GAD65) Maintain Normal Levels of GAD67 and GABA in Their Brains but Are Susceptible to Seizures. *Biochemical and Biophysical Research Communications*, *229*(3), 891–895. https://doi.org/10.1006/bbrc.1996.1898

Asada, H., Kawamura, Y., Maruyama, K., Kume, H., Ding, R.-G., Kanbara, N., Kuzume, H., Sanbo, M., Yagi, T. & Obata, K. (1997). Cleft palate and decreased brain γ-aminobutyric acid in mice lacking the 67-kDa isoform of glutamic acid decarboxylase. *Proceedings of the National Academy of Sciences*, *94*(12), 6496–6499. https://doi.org/10.1073/pnas.94.12.6496

Chechik, G., Meilijson, I. & Ruppin, E. (1998). Synaptic Pruning in Development: A Computational Account. *Neural Computation*, *10*(7), 1759–1777. https://doi.org/10.1162/089976698300017124

Cheng, C. N., Li, Y., Marra, A. N., Verdun, V. & Wingert, R. A. (2014). Flat Mount Preparation for Observation and Analysis of Zebrafish Embryo Specimens Stained by Whole Mount In situ Hybridization. *Journal of Visualized Experiments : JoVE*, *89*, 51604. https://doi.org/10.3791/51604

Condie, B. G., Bain, G., Gottlieb, D. I. & Capecchi, M. R. (1997). Cleft palate in mice with a targeted mutation in the γ-aminobutyric acid-producing enzyme glutamic acid decarboxylase 67. *Proceedings of the National Academy of Sciences*, *94*(21), 11451–11455. https://doi.org/10.1073/pnas.94.21.11451

Fei, H., Chow, D. M., Chen, A., Romero-Calderón, R., Ong, W. S., Ackerson, L. C., Maidment, N. T., Simpson, J. H., Frye, M. A. & Krantz, D. E. (2010). Mutation of the Drosophila vesicular GABA transporter disrupts visual figure detection. *Journal of Experimental Biology*, *213*(10), 1717–1730. https://doi.org/10.1242/jeb.036053

Gori, S., Molteni, M. & Facoetti, A. (2016). Visual Illusions: An Interesting Tool to Investigate Developmental Dyslexia and Autism Spectrum Disorder. *Frontiers in Human Neuroscience*, *10*, 175. https://doi.org/10.3389/fnhum.2016.00175

Jill, S. (2020). Core Concept: How synaptic pruning shapes neural wiring during development and, possibly, in disease. *Proceedings of the National Academy of Sciences*, *117*(28), 16096. https://doi.org/10.1073/pnas.2010281117

King, R. S. & Newmark, P. A. (2013). In situ hybridization protocol for enhanced detection of gene expression in the planarian Schmidtea mediterranea. *BMC Developmental Biology*.

Lamiré, L.-A., Haesemeyer, M., Engert, F., Granato, M. & Randlett, O. (2023). Functional and pharmacological analyses of visual habituation learning in larval zebrafish. *Neuroscience*.

Liu, Y., Chen, Y., Duffy, C. R., VanLeuven, A. J., Byers, J. B., Schriever, H. C., Ball, R. E., Carpenter, J. M., Gunderson, C. E., Filipov, N. M., Ma, P., Kner, P. A. & Lauderdale3, and J. D. (n.d.). *Decreased GABA levels during development results in increased connectivity in the larval zebrafish tectum*.

Maaswinkel, H. & Li, L. (2003). Spatio-temporal frequency characteristics of the optomotor response in zebrafish. *Vision Research*, *43*(1), 21–30. https://doi.org/10.1016/s0042-6989(02)00395-4

Marvin, J. S., Shimoda, Y., Magloire, V., Leite, M., Kawashima, T., Jensen, T. P., Kolb, I., Knott, E. L., Novak, O., Podgorski, K., Leidenheimer, N. J., Rusakov, D. A., Ahrens, M. B., Kullmann, D. M. & Looger, L. L. (2019). A genetically encoded fluorescent sensor for in vivo imaging of GABA. *Nature Methods*, *16*(8), 763–770. https://doi.org/10.1038/s41592-019-0471-2

Paolicelli, R. C., Bolasco, G., Pagani, F., Maggi, L., Scianni, M., Panzanelli, P., Giustetto, M., Ferreira, T. A., Guiducci, E., Dumas, L., Ragozzino, D. & Gross, C. T. (2011). *Synaptic Pruning by Microglia Is Necessary for Normal Brain Development*.

Tayanloo-Beik, A., Hamidpour, S. K., Abedi, M., Shojaei, H., Tavirani, M. R., Namazi, N., Larijani, B. & Arjmand, B. (2022). Zebrafish Modeling of Autism Spectrum Disorders, Current Status and Future Prospective. *Frontiers in Psychiatry*, *13*, 911770. https://doi.org/10.3389/fpsyt.2022.911770

VanLeuven, A. J. (2018). *UNDERSTANDING THE ROLE OF THE GAD GENES IN NEURAL DEVELOPMENT AND NERVOUS SYSTEM FUNCTION IN ZEBRAFISH*.

Vladimirov, N., Mu, Y., Kawashima, T., Bennett, D. V., Yang, C.-T., Looger, L. L., Keller, P. J., Freeman, J. & Ahrens, M. B. (2014). Light-sheet functional imaging in fictively behaving zebrafish. *Nature Methods*, *11*(9), 883–884. https://doi.org/10.1038/nmeth.3040

Zaidel, A., Goin-Kochel, R. P. & Angelaki, D. E. (2015). Self-motion perception in autism is compromised by visual noise but integrated optimally across multiple senses. *Proceedings of the National Academy of Sciences*, *112*(20), 6461–6466. https://doi.org/10.1073/pnas.1506582112